NASA CR-137971

(NASA-CR-137971) PRELIMINARY DESIGN-LIFT/CRUISE FAN RESEARCH AND TECHNOLOGY AIRPLANE FLIGHT CONTROL SYSTEM Final Report (Boeing Aerospace Co., Seattle, Wash.) 106 p HC A06/MF A01. CSCL 01C G3/08

N77-11064

Unclas 56143

PRELIMINARY DESIGN-LIFT/CRUISE FAN RESEARCH AND TECHNOLOGY AIRPLANE FLIGHT CONTROL SYSTEM

By Philip Gotlieb, George E. Lewis and Leo J. Little

Final Report

November 1976

Prepared under Contract No. NAS2-9177

by

MILITARY AIRPLANE DEVELOPMENT ORGANIZATION

BOEING AEROSPACE COMPANY

SEATTLE, WASHINGTON

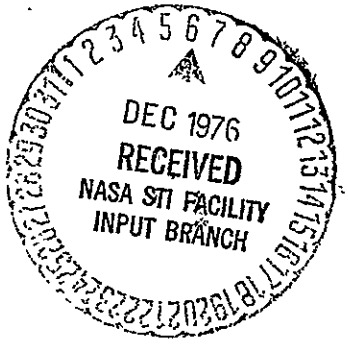

for

AMES RESEARCH CENTER

NATIONAL AERONAUTICS AND SPACE ADMINISTRATION

1 Report No	2 Government Accession No	3 Recipient's Catalog No
NASA CR-137971		

4. Title and Subtitle	5 Report Date
Preliminary Design-Lift/Cruise Fan Research and Technology Airplane Flight Control System	November 1976
	6 Performing Organization Code
7. Author(s)	8 Performing Organization Report No
Philip Gotlieb, George E. Lewis, Leo J. Little	D180-20216-1
	10 Work Unit No
9 Performing Organization Name and Address	11. Contract or Grant No
Boeing Aerospace Company Boeing Military Airplane Development Organization P. O. Box 3999 Seattle, WA 98124	NAS2-9177
	13 Type of Report and Period Covered
12 Sponsoring Agency Name and Address	Final Report
National Aeronautics and Space Administration Washington, D.C. 20546	14. Sponsoring Agency Code

15 Supplementary Notes

Technical Monitor, Richard F. Vomaske
Ames Research Center, Moffett Field, CA 94035

16 Abstract

This report presents the preliminary design of a stability augmentation system for a NASA V/STOL research and technology airplane. This stability augmentation system is postulated as the simplest system that meets handling qualities levels for research & technology missions flown by NASA test pilots.

The airplane studied in this report is a T-39 fitted with tilting lift/cruise fan nacelles and a nose fan. The propulsion system features a shaft interconnecting the three variable pitch fans and three power plants. The mathematical modeling is based on pre-wind tunnel test estimated data. The selected stability augmentation system uses variable gains scheduled with airspeed. Failure analysis of the system illustrates the benign effect of engine failure. Airplane rate sensor failure must be solved with redundancy.

17 Key Words (Suggested by Author(s))	18 Distribution Statement
V/STOL Lift Fan Flight Control Systems	

19 Security Classif. (of this report)	20 Security Classif. (of this page)	21 No. of Pages	22 Price*
Unclassified	Unclassified		

*For sale by the National Technical Information Service, Springfield, Virginia 22151

TABLE OF CONTENTS

1.0 INTRODUCTION

A tilt nacelle lift/cruise fan research and technology aircraft (RTA) has been proposed for V/STOL research. See Figure 1.1. The purpose of this report is to present results of a design study for the RTA flight control system.

The aircraft selected is a modified T-39 fitted with tilting nacelles, a shaft interconnected propulsion system, a modified forward fuselage housing a lift fan and a new variable incidence "T"-tail. The study uses estimated aerodynamic and propulsion data that includes both induced aerodynamic and propulsion data that includes both power effects and gyroscopic moments peculiar to a tilt fan VTOL aircraft.

It is emphasized that the results presented herein should be considered preliminary inasmuch as a piloted simulation is necessary to properly evaluate handling characteristics in determining the overall suitability of a particular stability augmentation system design. A wind tunnel investigation with the VTOL aircraft model should also be conducted to verify the aerodynamic characteristics used in this study.

1.1 Objective

The study objective is to design a flight control system for a tilt nacelle lift/cruise fan aircraft. A prime goal for the control system is simplicity. That is, a minimum number of control system elements and a minimum of gain changes.

1.2 Analysis Procedure

The analysis methodology is to examine the effect of augmentation on the unaugmented aircraft stability characteristics. Five discrete analysis conditions, representing the transition from hover to forward flight, are used. These conditions are presented in Table1.1,in terms of the aircraft trim and fan thrust values.

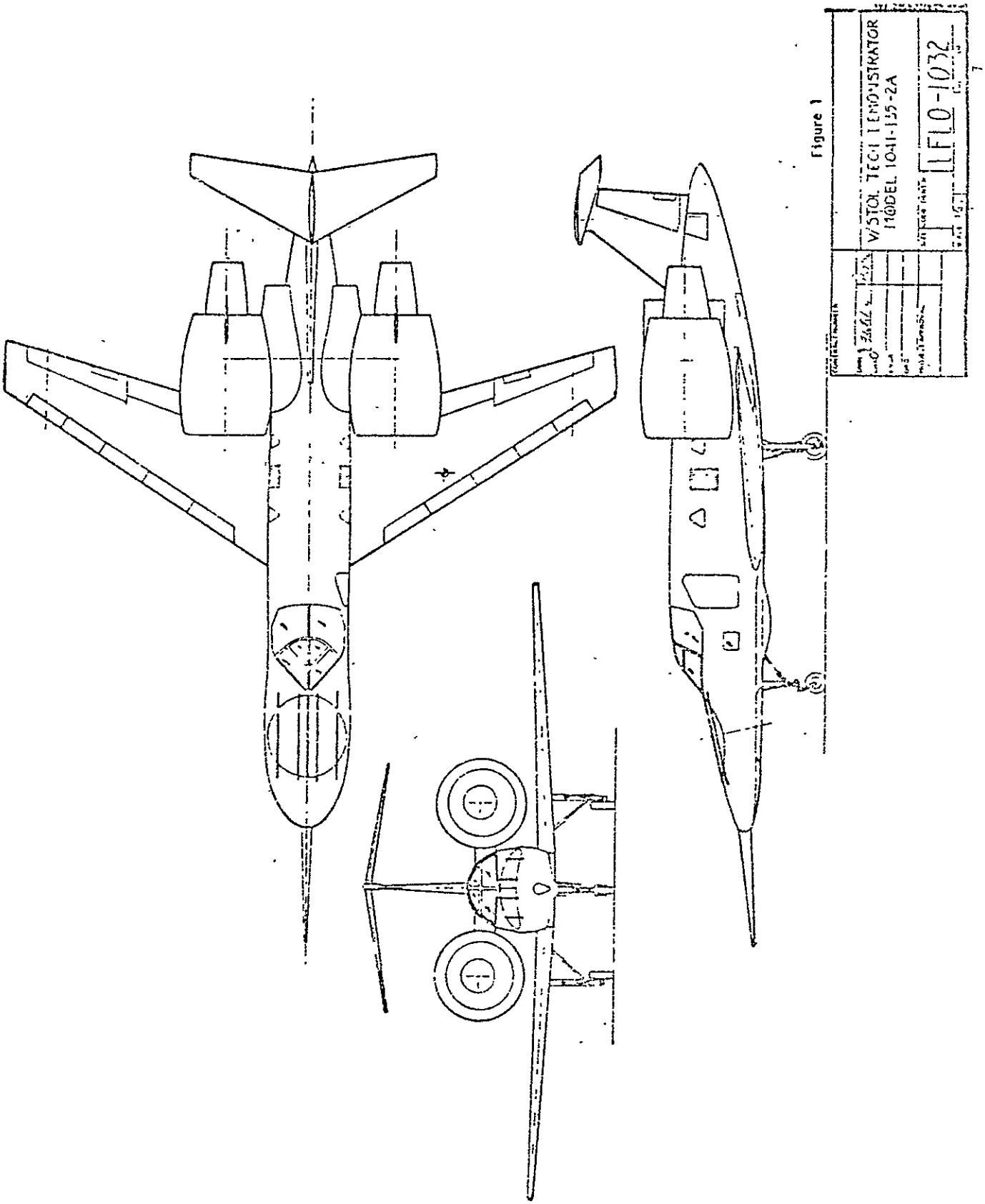
Figure 1
V/STOL TECH DEMONSTRATOR
MODEL 1041-155-2A
LF10-1032

FIGURE 1.1

Table 1

MODEL 1041-135-2

CHARACTERISTICS OF THE SELECTED TRIM POINTS

GROSS WEIGHT = 11,340 KILOGRAMS

(25,000 LBS)

AIRSPEED KM/HR (KNOTS)	α (DEG)	NACELLE TILT- (DEG)	NOSE FAN GROSS THRUST- NEWTONS (LBS)	L/C FAN GROSS THRUST- NEWTONS (LBS)	$\frac{V}{V_J}$ L/C FAN	$\frac{V}{V_J}$ NOSE FAN	$\frac{\partial \epsilon}{\partial \alpha}$
0	0	97	33,630 (7,560)	38,790 (8, 720)	0	0	-
90 (50 KNOTS)	7	68	29,090) (6,540)	35,580 (8,000)	0.21	0.23	0.76
165 (90)	9	40	17,750 (3,990)	28,160 (6,330)	0.43	0.54	0.69
220 (120)	10	10	7,250 (1630)	27,220 (6120)	0.58	1.12	0.58
370 (200)	5	0	0	15,120 (3400)	1.30	———	0.49

TABLE 1.1

The analysis is performed using a mathematical model representing the aircraft and augmentation system for linearized small disturbances. Estimated linear aerodynamic and propulsion data were used.

The three criteria used in evaluating the control system are the stability characteristics, handling and response and the effect of system component failure such as rate/attitude sensor and fan control lockup. The system performance is compared to the NASA guidelines for RTA dynamic stability (Reference 19).

The study flow is schematically represented in Figure 1.2.

The aerodynamic derivatives, including induced effects and control terms, as well as model mass-inertia properties and gyroscopic coupling terms are also computed for formation of the state model equations at each of the selected airspeeds.

Decoupling of the lateral and longitudinal modes is employed to simplify the analysis. The state model analysis technique used provides both system eigenvalues and eigenvectors and time history response to an arbitrary forcing function.

The solution was obtained on a Nova minicomputer using a Boeing program for state variable model analysis of control systems. The program architecture permits real-time operator control over execution of the program for rapid analysis of the effect of control system gain changes.

1.3 Conclusions

A flight control system is defined which accomplishes the objectives of this study. Autmentation on, the airplane meets NASA Level 1 guidelines for dynamic stability (Reference 19). Augmentation off, the airplane fails to meet Level 2 requirements. This suggests sufficient redundancy be provided to make loss of augmentation an unlikely event.

STUDY OUTLINE

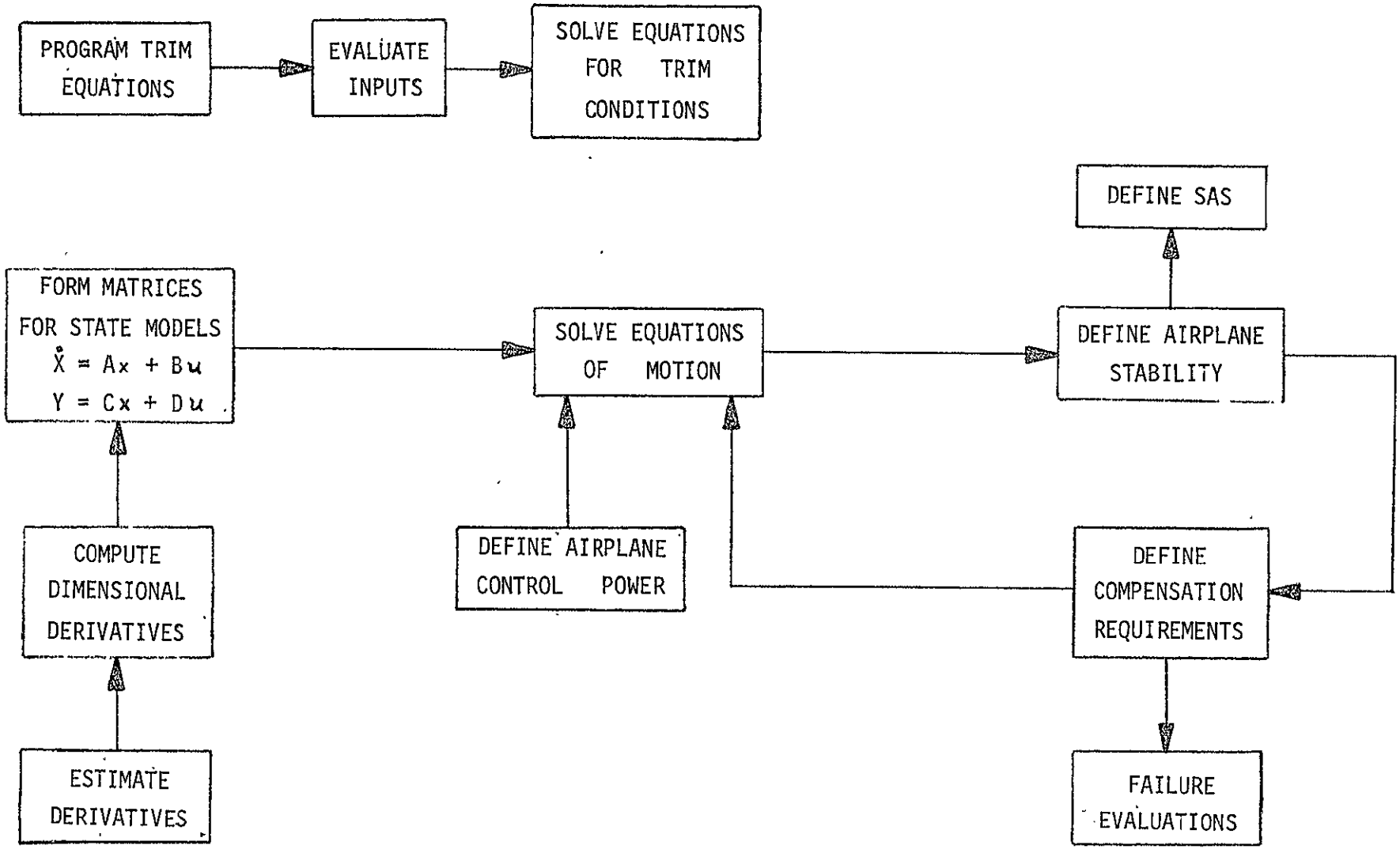

FIGURE 1.2

The control system was designed as an attitude system in pitch and roll and as a rate system in yaw. System feedback of attitudes and rates to both the aerodynamic control surfaces and fan thrust modulation are used according to the flight regime and stability requirements. At the lower speeds, only thrust modulation is effective whereas at the high end of flight transition control is almost completely by aerodynamic means. Consequently, the control system gains are scheduled with airspeed. Details of the gain schedule are shown in Section 4.

Airplane handling qualities are judged satisfactory, although improved performance could be achieved by adding complication to the system. For example, the airplane exhibits a roll-off of bank angle in response to a lateral control input. Adding a lead-lag network would eliminate most of the roll-off. Whether such complication is necessary can only be determined after an evaluation on a full flight simulator with a pilot in the system. For now, the compensation network is omitted from the system.

The configuration exhibits little coupling between the longitudinal and lateral-directional modes. Therefore, a classical separation between the modes was utilized during control system design.

Sensor redundancy is required for the rate gyros in order to maintain Level 2 operation with sensor failure at the lower speeds. Failure of any fan control mechanism (pitch and roll) does result in some degradation in performance, but Level 2 minimums are not violated. The effect of an engine failure is minimal at any speed due to the propulsion system shaft interconnect.

2.0 DYNAMIC MODEL

2.1 Airplane Description

The airplane modeled in this report is the Boeing Model 1041-135-2A. The airplane is a VTOL modification of the North American T-39. The propulsion system is three 1.57 meter (62 inch) variable pitch fans driven by three Allison XT-701 engines. The airplane has the following reference characteristics:

Gross Weight	11,340	Kgs	(25,000 lbs)
Center of Gravity	WL 241.30	M	(95.0 in)
	FS 649.22	M	(255.6 in)
Wing Area	31.77	M^2	(342 ft^2)
Wing Reference Chord	2.56	M	(100.6 in)
Wing Span	13.56	M	(44.5 ft)
Roll Inertia	30,200	$Kg-M^2$	(22,240 $Slug-Ft^2$)
Pitch Inertia	126,000	$Kg-M^2$	(92,960 $Slug-Ft^2$)
Yaw Inertia	142,300	$Kg-M^2$	(104,960 $Slug-Ft^2$)
Cross Product	10,400	$Kg-M^2$	(7,675 $Slug-Ft^2$)

The airplane aerodynamic controls are supplemented with thrust modulation to permit control of the VTOL at hover and in the lower speed range of the transition, where the aerodynamic controls are ineffective. The aerodynamic controls are the rudder, ailerons and stabilizer. The stabilizer has been modified from the T-39 into a "T"-tail arrangement that has a large incidence range to cope with the downwash angles encountered in V/STOL flight.

The action of the V/STOL controls is illustrated in Figure 2.1. Control about both the roll and pitch axes is achieved through differential thrust obtained by modulating the fan blade angles. Control about the yaw axis

V/STOL CONTROL ACTION

FIGURE 2.1

is by thrust deflection by yaw vanes located in the fan exits. Height control is accomplished by increase or decrease of thrust on all three fans simultaneously. Airspeed is controlled by adjusting pitch attitude or by nacelle tilt.

Details of control power and stick sensitivities are described in Section 3.0. The overall system architecture is shown on Figure 2.2. The figure illustrates the relationship between the crew station controls and the control system elements of blade angle, yaw vane, nacelle tilt, and the aerodynamic controls. The height and speed control are open loop systems. The pitch and roll control are attitude command systems and the yaw control is a rate command system. There is an interconnect between the nacelle tilt angle and the stabilizer and fan blade pitch to relieve the pilot of most of the large longitudinal trim variations that occur as the nacelle is tilted.

Figure 2.3 shows the fan and engine number system that has been adapted for this report. The left lift cruise fan is designated as number 1 and the nose fan is number 3. The number 1 engine drives number 1 fan and the number 3 engine is mounted in the aft cabin. The interconnecting shaft as well as the gear box arrangements are shown on the inboard profile (Figure 2.4). The number 3 engine exhaust is split in a "Y" duct running laterally through the side of the fuselage. The reaction forces of the two engine exhaust of the "Y" duct are equal and opposite and produce no moment about the center of gravity. A later model of the RTA has been drawn with a single exhaust at the bottom of the body. This configuration change was made too late to incorporate into this report. No significant effect is anticipated on the dynamic stability, however.

The shaft interconnect gives the airplane engine failure safety. The shafts and gear boxes sum and distribute engine power to the 3 fans.

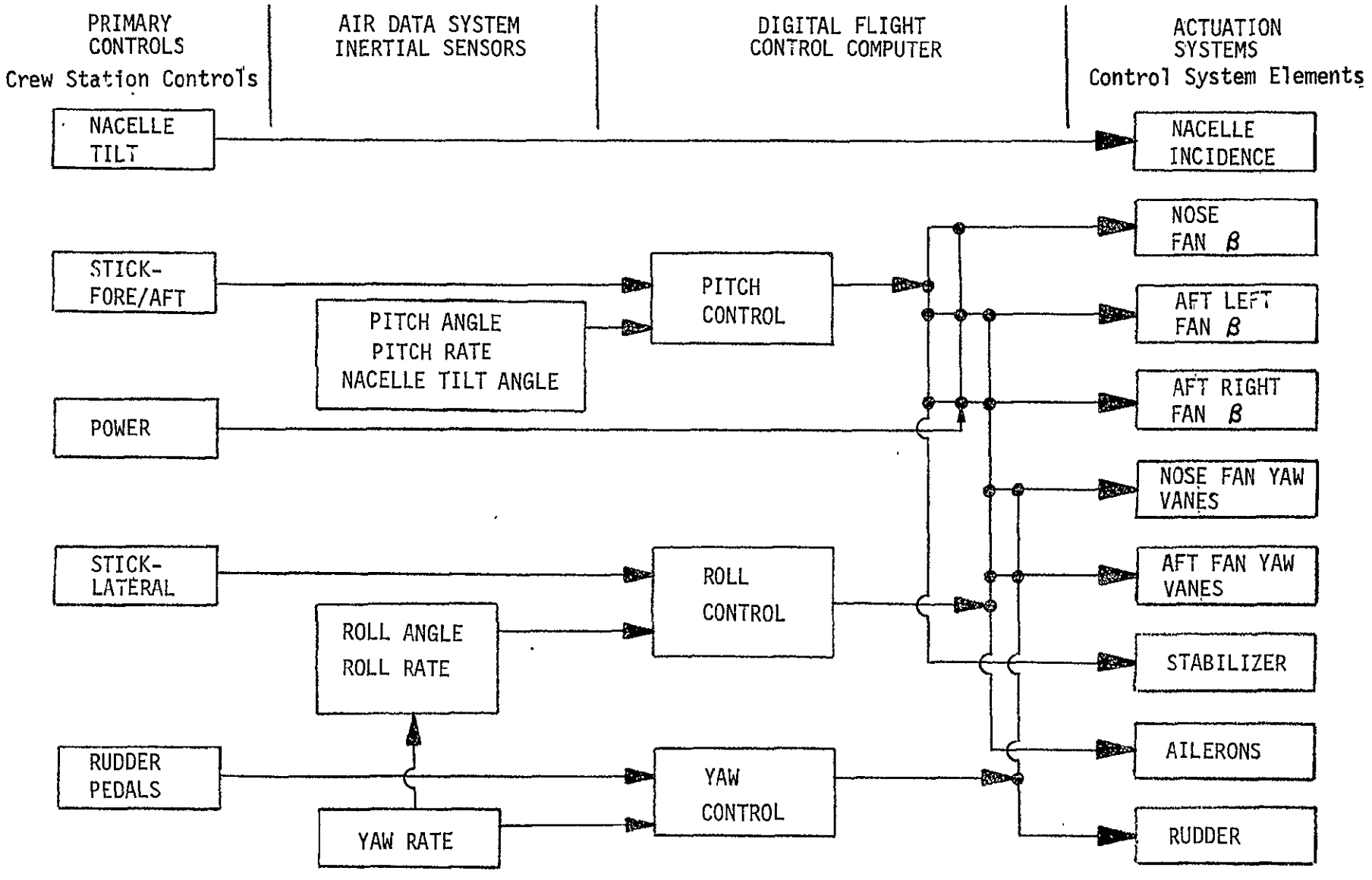

SYSTEM ARCHITECTURE

FIGURE 2.2

FIGURE 2.3

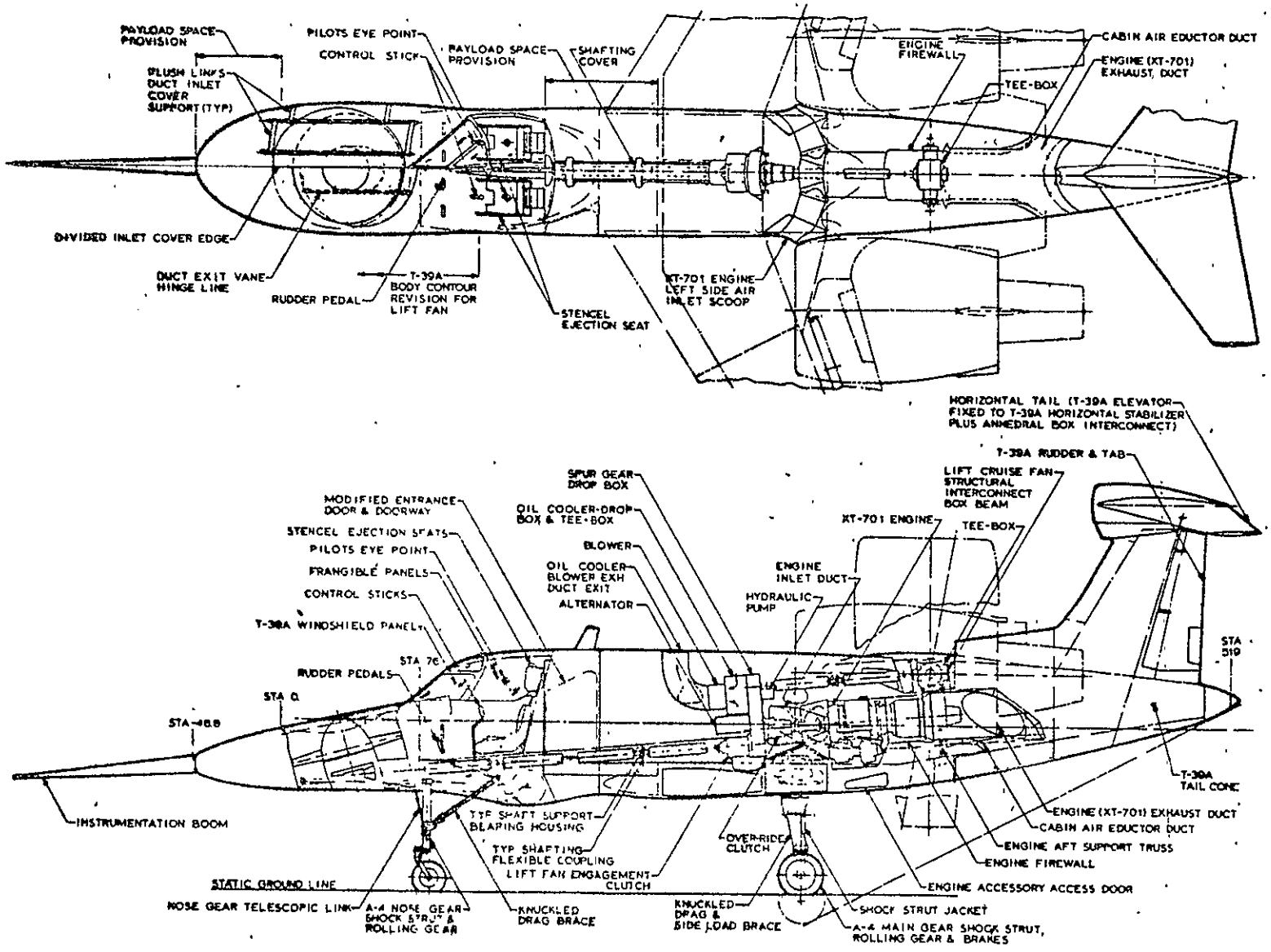

INBOARD PROFILE

FIGURE 2.4

Failure of an engine reduces the maximum power that can be applied to the fans, but there is essentially no moment upset associated with engine failure. Propulsion system performance used in this study is shown in Section 3.6

2.2 Equations of Motion

The airplane mathematical model used in this study is a perturbation model. Perturbation theory assumes that the dynamic forces and moments acting on the airplane can be represented with force and moment derivatives evaluated at the discrete airspeeds selected for study.

A special application of matrix algebra is used to formulate the equations of motion. The equations are cast so that each class of term is carried in its own matrix. The formulation is shown in Figure 2.5. The forces and moments are segregated into five different classes. These classes are:

- Mass Properties
- Aerodynamic
- Inlet momentum
- Gyroscopic
- Induced power effects

Terms for flight controls are carried separately as shown. The control terms are discussed in Section 3.5. This methodology was adopted to allow complete visibility of individual terms. Unusual behavior can be easily traced to a specific term. The definition of the terms in each matrix is shown on Figures 2.6 through 2.11.

An example of the application of the matrix equation of motion formulation technique is given by examining the single term, pitch damping (M_q). The airplane net pitch rate damping is composed of 4 terms expressed mathematically below:

$$M_q = M_q \text{ aero} + M_q \text{ induced} + M_q \text{ momentum} + M_q \text{ gyroscopic}$$

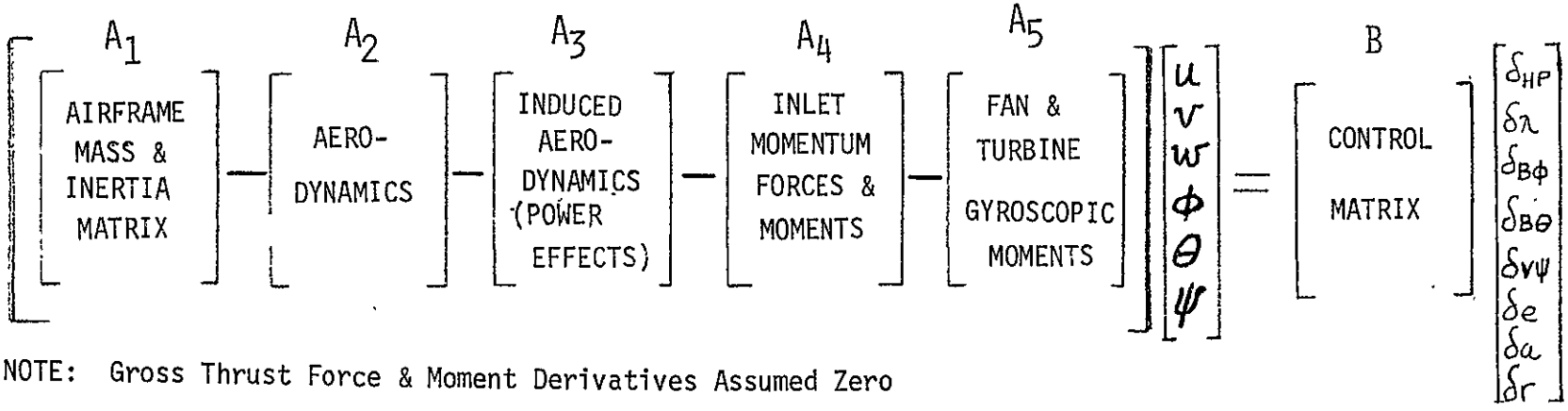

NOTE: Gross Thrust Force & Moment Derivatives Assumed Zero

EQUATIONS OF MOTION IN MATRIX FORM

FIGURE 2.5

MASS PROPERTIES [A₁]

FIGURE 2.6

$$
\begin{bmatrix} X \\ Y \\ Z \\ L \\ M \\ N \end{bmatrix} =
\begin{bmatrix}
\rho VS\left(-C_D - C_{D_u}\right) & & \frac{\rho}{2}VS\left(-C_{D_\alpha} + C_L\right) & & -\frac{\rho}{4}VScC_{D_q}\Delta & \\
 & \frac{\rho}{2}VSC_{Y_\beta} & & \frac{\rho}{4}VSbC_{Y_p}\Delta & & \frac{\rho}{4}VSbC_{Y_r}\Delta \\
\rho VS\left(-C_L - C_{L_u}\right) & & \frac{\rho}{2}VS\left(-C_{L_\alpha} - C_D\right) & & -\frac{\rho}{4}VScC_{L_q}\Delta & \\
 & & -\frac{\rho}{4}ScC_{L_{\dot\alpha}}\Delta & & & \\
 & \frac{\rho}{2}VSbC_{\ell_\beta} & & \frac{\rho}{4}VSb^2C_{\ell_p}\Delta & & \frac{\rho}{4}VSb^2C_{\ell_r}\Delta \\
\rho U_c SC_{m_u} & & \frac{\rho}{2}VSc\left[C_{m_{\dot\alpha}}C_{L_\alpha} - C_{L_{\alpha_h}}\bar{V}\eta\left(1-\epsilon_\alpha\right)\right] & & \frac{\rho}{4}VSc^2C_{m_q}\Delta & \\
 & & +\frac{\rho}{4}Sc^2C_{m_{\dot\alpha}}\Delta & & & \\
 & \frac{\rho}{2}VSbC_{n_\beta} & & \frac{\rho}{4}VSb^2C_{n_p}\Delta & & \frac{\rho}{4}VSb^2C_{n_r}\Delta
\end{bmatrix}
\begin{matrix} u \\ v \\ ur \\ \Phi \\ \theta \\ \Psi \end{matrix}
\times
\begin{bmatrix} u \\ v \\ w \\ \Phi \\ \theta \\ \Psi \end{bmatrix}
$$

AERODYNAMIC TERMS $[A_2]$

(BODY AXIS)

FIGURE 2.7

u
v
w
p
q
r
X
Y
Z
L
M
N
=
$-C_{L_{\alpha_v}} \bar{V} S_v \frac{\rho}{2}\left(1-\frac{\partial\sigma}{\partial\beta}\right)\left[K_{\sigma_{V/V_J}}-1\right]$
$-C_{m_\alpha}\lambda\left(\frac{2F_1+F_3}{V_J}\right)$
$\left[Y_v\right]\ell_{z_{fin}}$
$\frac{\rho}{2} S \bar{c} \bar{r}_h \omega\left[4K_{\epsilon_{\alpha_h}}\left(\frac{V}{V_J}\right)^2 + 3K_{\epsilon_{\alpha_h}}\left(\frac{V}{V_J}\right)\right] C_{L_{\alpha_h}}$
$\left[C_{L_{\alpha_h}} \bar{r}_h S \bar{c} V \frac{\rho}{2} - 2C_{L_{\alpha_h}} \bar{r}_h S \bar{c}^2 V \frac{k_f \rho}{\bar{c}\ 4}\left\{\left[K_{L^2_{\epsilon_\alpha}}\left(\frac{V}{V_J}\right)^2 + K_{L_{\epsilon_\alpha}}\left(\frac{V}{V_J}\right)\right] - \epsilon_\alpha\right\}\right.$
$\left[Y_r\right]\ell_{x_{fin}}$
INDUCED EFFECTS
$[A_3]$
X
u
v
w
p
q
r

FIGURE 2.8

$$
\begin{bmatrix} X \\ Y \\ Z \\ L \\ M \\ N \end{bmatrix} =
\begin{bmatrix}
u & v & w & p & q & r \\
-\sum_{1}^{3}\left(\frac{\omega_a}{g}\right)_n & & & & -2\left(\frac{\omega_a}{g}\right)_1 \ell_{z_1} & \\
 & & & & -\left(\frac{\omega_a}{g}\right)_3 \ell_{z_3} & \ell_{y_1}\left(\frac{\omega_{a_1}-\omega_{a_2}}{g}\right)_1 \\
 & -\sum_{1}^{3}\left(\frac{\omega_a}{g}\right)_n & & 2\left(\frac{\omega_a}{g}\right)_1 \ell_{z_1} & & -\left(\frac{\omega_a}{g}\right)_3 \ell_{x_3} \\
 & & & + \left(\frac{\omega_a}{g}\right)_3 \ell_{z_3} & & -\left(\frac{\omega_{a_1}+\omega_{a_2}}{g}\right)\ell_{x_1} \\
 & & -\sum_{1}^{3}\left(\frac{\omega_a}{g}\right)_n & \ell_{y_1}\left(\frac{\omega_{a_1}-\omega_{a_2}}{g}\right) & \left(\frac{\omega_a}{g}\right)_3 \ell_{x_3} & \\
 & & & & + \left(\frac{\omega_{a_1}+\omega_{a_2}}{g}\right)\ell_{x_1} & \\
 & \left(\frac{\omega_a}{g}\right)_3 \ell_{z_3} & \left(\frac{-\omega_{a_1}+\omega_{a_2}}{g}\right)\ell_{y_1} & -\left(\frac{\omega_{a_1}+\omega_{a_2}}{g}\right)\ell_{y_1}^2 & \left(\frac{\omega_{a_1}-\omega_{a_2}}{g}\right)\ell_{x_1}\ell_{y_1} & -\left(\frac{\omega_a}{g}\right)_3 \ell_{x_3}\ell_{z_3} \\
 & +\left(\frac{\omega_{a_1}+\omega_{a_2}}{g}\right)\ell_{z_1} & & -\left(\frac{\omega_{a_1}+\omega_{a_2}}{g}\right)\ell_{z_1}^2 & & -\left(\frac{\omega_{a_1}+\omega_{a_2}}{g}\right)\ell_{x_1}\ell_{x_3} \\
 & & & -\left(\frac{\omega_a}{g}\right)_3 \ell_{z_3}^2 & -\ell_{z_3}^2\left(\frac{\omega_a}{g}\right)_3 - \ell_{x_3}^2\left(\frac{\omega_a}{g}\right)_3 & \\
-\left(\frac{\omega_a}{g}\right)_3 \ell_{z_3} & & \left(\frac{\omega_{a_1}+\omega_{a_2}}{g}\right)\ell_{x_1} & -\ell_{y_1}\ell_{x_1}\left(\frac{\omega_{a_1}-\omega_{a_2}}{g}\right) & -\ell_{z_1}^2\left(\frac{\omega_{a_1}+\omega_{a_2}}{g}\right) & \ell_{z_1}\ell_{y_1}\left(\frac{\omega_{a_1}-\omega_{a_2}}{g}\right) \\
-2\left(\frac{\omega_a}{g}\right)_1 \ell_{z_1} & & +\left(\frac{\omega_a}{g}\right)_3 \ell_{x_3} & & -\ell_{x_1}^2\left(\frac{\omega_{a_1}+\omega_{a_2}}{g}\right) & \\
 & & & & & -\left(\frac{\omega_{a_1}+\omega_{a_2}}{g}\right)\ell_{y_1}^2 \\
\left(\frac{\omega_{a_1}-\omega_{a_2}}{g}\right)\ell_{y_1} & -\left(\frac{\omega_a}{g}\right)_3 \ell_{x_3} & & \left(\frac{\omega_a}{g}\right)_3 \ell_{z_3}\ell_{x_3} & \left(\frac{\omega_{a_1}-\omega_{a_2}}{g}\right)\ell_{z_1}\ell_{y_1} & -\left(\frac{\omega_a}{g}\right)_3 \ell_{x_3}^2 \\
 & -\left(\frac{\omega_{a_1}+\omega_{a_2}}{g}\right)\ell_{x_1} & & +\left(\frac{\omega_{a_1}+\omega_{a_2}}{g}\right)\ell_{z_1}\ell_{x_1} & & -\left(\frac{\omega_{a_1}+\omega_{a_2}}{g}\right)\ell_{x_1}^2
\end{bmatrix}
\times
\begin{bmatrix} u \\ v \\ w \\ p \\ q \\ r \end{bmatrix}
$$

INLET MOMENTUM TERMS $[A_4]$

FIGURE 2.9

	I KG-M² (SLUG-FT²)	Ω RAD/SEC (RPM)	H KG-M/SEC (SLUG-FT²/SEC)
FAN	19.405 (14.3)	-366.45 (-3500)	-7130.96 (-5240)
TURBINE	1.099 (0.81)	1235.46 (11,800)	1357.78 (1000)
COMPRESSOR	1.615 (1.19)	1570.50 (15,000)	2536.36 (1870)

$i_3 = 15^\circ$

FIGURE 2.10

$$
\begin{bmatrix} X \\ Y \\ Z \\ L \\ M \\ N \end{bmatrix} = \begin{bmatrix}
\delta_{HP} & \delta_\lambda & \delta_{B\theta} & \delta_{B\phi} & \delta_{V\psi} & \delta_a & \delta_s & \delta_r \\
F_{\delta_B}(2\cos\lambda + \sin i) & -2F_2 \sin\lambda_0 & & & & & & \\
 & & & & & C_{Y_{\delta_a}} \frac{\rho}{2} V^2 S & & C_{Y_{\delta_r}} \frac{\rho}{2} V^2 S \\
-F_{\delta_B}(2\sin\lambda + \cos i) & -2F_2 \cos\lambda_0 & & & & & \frac{\rho}{2} V^2 S \left(-C_{L_{\delta_s}}\right) & \\
 & & & -2F_{2_{\delta_{B\phi}}}\left(l_{z_2} \sin\delta_{V_2} + l_{Y_2} \sin\lambda_2 \cos\delta_{V_2}\right) & -2F_2 l_{z_2} + 2F_3 l_{z_3} \cos i_3 & \frac{\rho}{2} V^2 S b \left(C_{l_{\delta_a}} - C_{n_{\delta_a}} \alpha\right) & & \frac{\rho}{2} V^2 S b \left(C_{l_{\delta_r}} - C_{n_{\delta_r}} \alpha\right) \\
F_{\delta_B}(2 l_{eff_2} + l_{eff_3}) & 2F_2\left(\frac{\partial l_{eff_2}}{\partial \lambda}\right) & 2F_{2_{B\phi}} l_{s_2} \cos\delta_{V_2} - l_{s_3} \cos\delta_{V_3} & & & & \frac{\rho}{2} V^2 S \bar{c} C_{m_{\delta_s}} & \\
 & & & 2F_{2_{\delta_{B\phi}}}\left(l_{x_2} \sin\delta_{V_2} - l_{Y_2} \cos\lambda_2 \cos\delta_{V_2}\right) & 2F_2 l_{x_2} - 2F_3 l_{x_3} \cos i & \frac{\rho}{2} V^2 S b \left(C_{n_{\delta_a}} + C_{l_{\delta_a}} \alpha\right) & & \frac{\rho}{2} V^2 S b \left(C_{n_{\delta_r}} + C_{l_{\delta_r}} \alpha\right)
\end{bmatrix} \times \begin{bmatrix} \delta_{HP} \\ \delta_\lambda \\ \delta_{B\theta} \\ \delta_{B\phi} \\ \delta_{V\psi} \\ \delta_a \\ \delta_s \\ \delta_r \end{bmatrix}
$$

CONTROL MATRIX $[B]$

FIGURE 2.11

The terms are summed and the damping moment is computed in the following fashion:

$$[A]_{total} = [A]_1 + [A]_2 + [A]_3 + \ldots$$

$$[M] = [A] \times [q]$$

The same formulation is used for the airplane control elements. The propulsive terms are carried independent of the aerodynamic terms. This is necessary to facilitate the mathematics of SAS design. Details of the control matrix are shown in Section 3.5.

A body axis system was used. A graphical representation is shown on Figure 2.12. The sign conventions for moment arms, control deflections, speeds, attitudes and rate are shown on Figure 2.13. A tabular list of the moment arms used to represent the propulsion system is shown on Table 2.14. To illustrate the complex nature of the reaction points of the propulsive and momentum forces, Figure 2.15 is also shown.

BODY AXIS COORDINATE SYSTEM

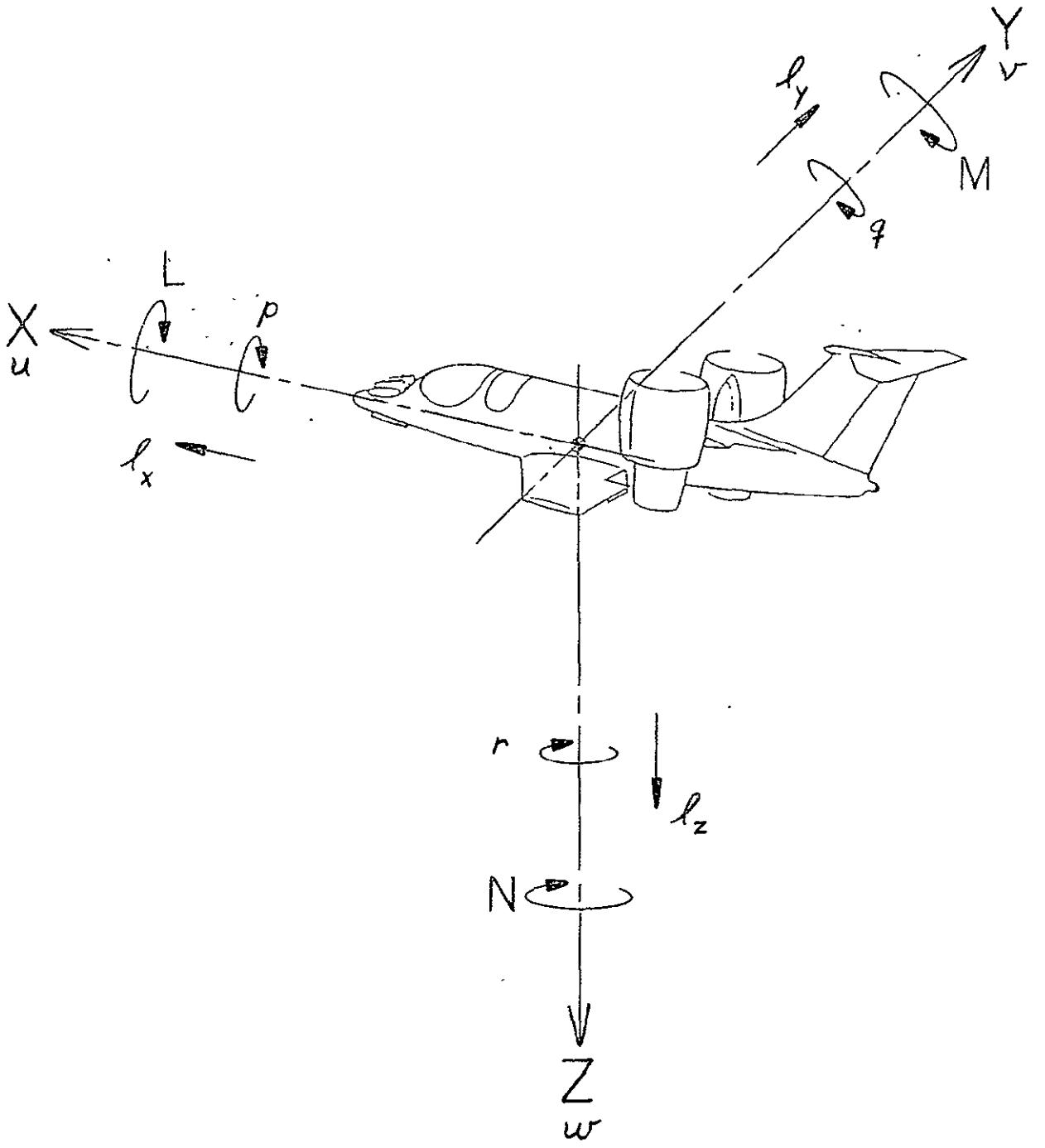

FIGURE 2.12

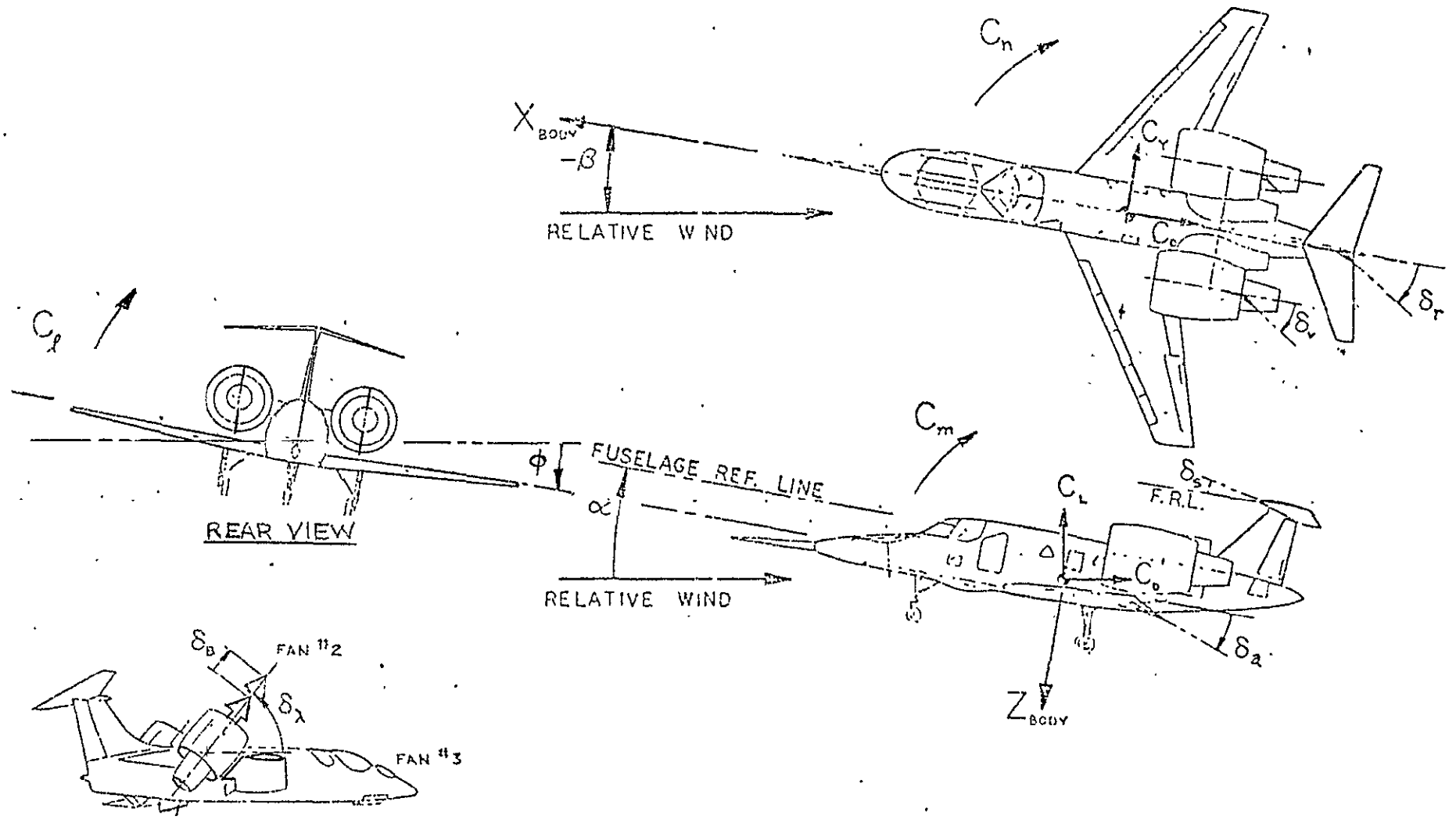

SIGN CONVENTION

FIGURE 2.13

MOMENT ARMS OF MODEL 1041-135-2A

FORCE VECTOR			RIGHT LIFT/CRUISE FAN MOMENT ARM ~ METERS (FT.) ~					3 ENGINE MOMENT ARM ~ METER (FT.)	NOSE FAN ARM ~ METER (FT.)
NACELLE TILT ($\lambda°$)			0	20	50	70	90		
GROSS THRUST	YAW VANE MOMENT ARMS	ℓ_x	-3.264 (-10.708)	-3.209 (-10.527)	-2.937 (-9.637)	-2.662 (-8.734)	-2.349 (-7.708)	N.A.	5.419 (17.780)
	ROLL MOMENT ARMS	ℓ_y	1.880 (6.167)	←		→	1.880 (6.167)	N.A.	0
	YAW VANE MOMENT ARMS	ℓ_z	-0.833 (-2.733)	-0.520 (-1.707)	-0.133 (-0.435)	0.026 (0.086)	0.081 (0.267)	N.A.	0.792 (2.600)
	PITCH MOMENT ARMS	ℓ_{eff}	-0.833 (-2.733)	-1.600 (-5.250)	-2.337 (-7.667)	-2.464 (-8.083)	-2.351 (-7.713)	0	5.477 (17.969)
INLET MOMENTUM (GEOMETRIC)		ℓ_x	-0.724 (-2.375)	-0.822 (-2.697)	-1.305 (-4.280)	-1.781 (-5.842)	-2.349 (-7.708)	2.432 (7.980)	5.656 (18.555)
		ℓ_y	1.880 (6.167)	←		→	1.880 (6.167)	0.280 (0.917)	0
		ℓ_z	-0.833 (-2.733)	-1.389 (-4.557)	-2.078 (-6.819)	-2.361 (-7.745)	-2.459 (-8.067)	-1.016 (-3.333)	-0.089 (-0.292)

ENGR.	LITTLE	9/8/76			
CHECK	L.G.L.	9/8/76			
APR.					
APR.					

MOMENT ARM VARIATION WITH NACELLE ROTATION

1041-135-2A

TABLE 2.14

24

D1 5007 2070 ORIG. 6/73

J15-047

3.50
31.20
40.00
B.L. 0.00
222.66
213.36
95.76
92.50
76.54
29.10
STA. 255.26
96.80 (TYP)
32.80
3.20 (TYP)
85.00 (TYP)
14.00 (TYP)
W.L. 95.00
UP
FWD
OUTBD
FAN INLET
PIVOT POINT
FAN EXIT PLANE
ENGINE TAIL PIPE
3RD. ENGINE INLET
3RD. ENGINE OUTLET
C.G. REF: 0.30 A/C W & 4.035 C
DWG. NO. REF: LFLO-1026 (3/19/70)
LFLO-1027 (3/19/70)
PROPULSION SYSTEM LOCATION
OF 1041-135-2A
AT λ=90°
FIG 2.15

FIGURE 2.15

3.0 FORCE AND MOMENTS DEFINITION

3.1 Aerodynamic Data

This section defines the power off aerodynamic data used in this study. Fan inlet momentum forces and moments, and induced power effects are given in Sections 3.2 and 3.3. Figure 3.1 is a tabulation of the aerodynamic derivatives and Figure 3.2 shows lift and drag coefficients as a function of airplane angle of attack. The data presented has been estimated using the techniques and data in Reference 1. The coefficients are based on the reference geometry given in Section 2.1 (Airplane Description). The airplane is conventional except for the size of the lift-cruise nacelles. The nacelles will have a stabilizing effect (both longitudinally and directionally) on the airplane. However, the effect of the nacelles on the empennage is expected to be destabilizing. Lacking wind tunnel data, the stabilizing effect of the nacelles was assumed to cancel their destabilizing effect on the empennage.

A center of gravity located at 30% of the mean aerodynamic chord is used throughout the report. The static longitudinal stability margin is estimated to be 10 % with the airplane in the low speed conventional configuration (nacelle tilt = 0 degrees). The addition of power effects tends to make the airplane unstable and the mathematical modeling used in this report reflects the general trend. The relative magnitude of the aerodynamic forces on the airplane is illustrated by Figure 3.3. The figure shows that the wing supports 74% of the airplane weight at 220 km/hr, for an angle of attack = 10 degrees.

3.2 Inlet Momentum Forces and Moments

Fan inlet momentum produces significant forces and moments at low airspeeds. These forces and moments resist both angular and linear motion to produce an effective damping.

STABILITY & CONTROL DERIVATIVES

WING/BODY/TAIL (PER RAD.)

LATERAL/DIRECTIONAL

$C_{Y_\beta} = .0957 C_L^{2.2} - .7947$

$C_{Y_p} = -.455 C_L + .009$

$C_{Y_r} = .3968$

$C_{\ell_\beta} = -.135 C_L - .05346$

$C_{\ell_p} = -.01423 C_L^2 - .40615$

$C_{\ell_r} = .3 C_L + .0005$

$C_{n_\beta} = .01948 C_L^2 + .06246$

$C_{n_p}^{\star} = .00868 C_L^2 + .303 C_L + .2204$

$C_{n_r} = -.01 C_L^2 - .2256$

LONGITUDINAL

$C_{L_\alpha} = 4.65$

$C_{L_{\dot\alpha}} = 1.81$

$C_{L_q} = 5.63$

$C_{m_\alpha} = -.465$

$C_{m_{\dot\alpha}} = -4.39$

$C_{m_q} = -10.28$

★ NOTE: REEVALUATED TO MATCH TYPICAL LEAR JET CONVENTIONAL FLIGHT DYNAMIC CHARACTERISTICS. (VALUE USED, $0.02 \times C_L$)

CONTROLS

$C_{Y_{\delta_a}}$ = NEGLIGIBLE

$C_{Y_{\delta_r}} = .226$

$C_{\ell_{\delta_a}} = .081$

$C_{\ell_{\delta_r}} = .0272$

$C_{n_{\delta_a}} = -.0141 C_L$

$C_{n_{\delta_r}} = -.0816$

$C_{L_{\delta_s}} = .764$

$C_{m_{\delta_s}} = -1.848$

FIGURE 3.1

LIFT & DRAG

FLAPS DOWN

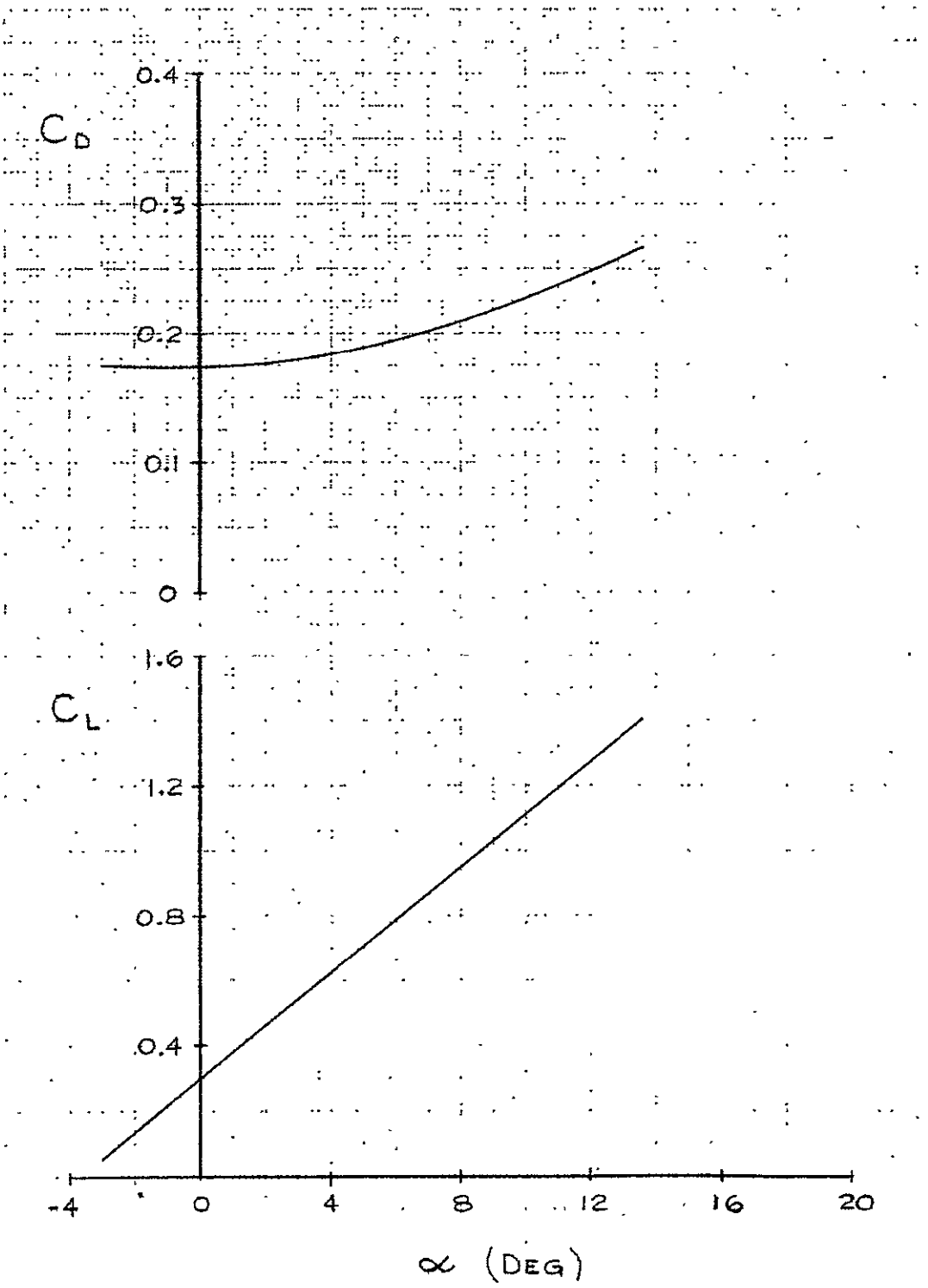

REF: NASA CR 137750

FIGURE 3.2

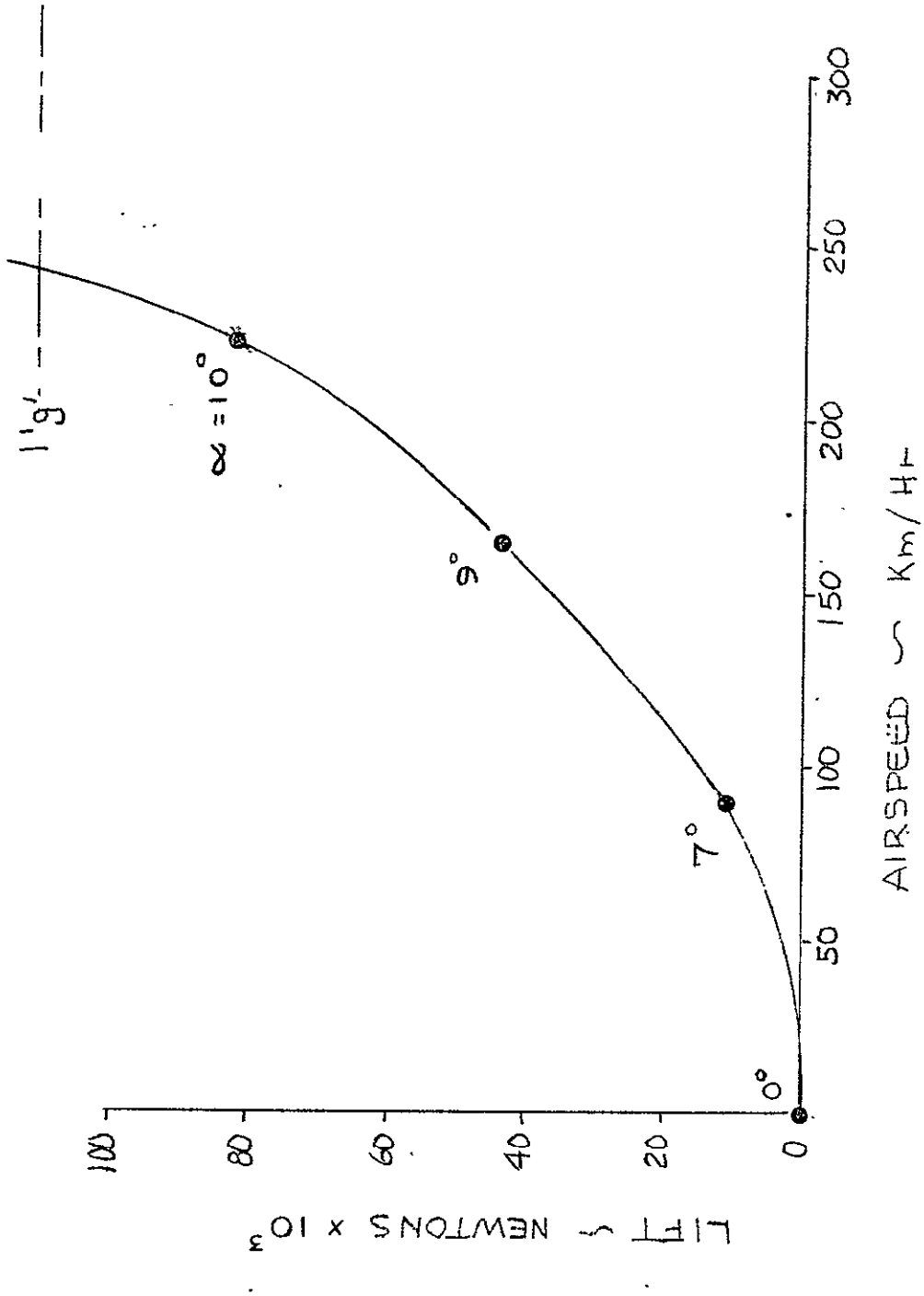

WING LIFT

FIGURE 3.3

In this report special consideration was given to defining an empirical relationship that accounts for the moment data trends exhibited by similar configurations. The results of this effort are shown in Figures 3.4 and 3.5. These figures are used to estimate an incremental moment arm as a function of fan thrust, airspeed and tilt angle. The data indicates that the momentum moment arm is also associated with the type of inlet (i.e., deep, shallow, scarfed...etc.) consequently data is given for both the nose fan and the lift cruise fans. The data in references 7, 8, 9, and 10 were used to determine the empirical relationships.

Figure 3.6 shows the geometry used to estimate the inlet momentum and moments. The figure defines the sign convention.

A tabulation of the inlet momentum derivatives used in this report is given in Figure 2.8. The relative damping of the momentum data is illustrated in Figure 3.8. The momentum roll damping term L_p due to fan inlet momentum is compared to the aerodynamic roll damping term. Both types of roll damping are shown as a function of airspeed.

3.3 Power Effects

The power effects are defined as the aerodynamic forces and moments resulting from the fan exhaust induced flow fields on the wings, horizontal tail and vertical fin. The analysis procedure is to postulate the total aerodynamic effect based on empirical comparisons with existing VTOLs and to then determine the individual derivative associated with a particular state variable. The detailed derivation of the terms is discussed in the following paragraphs.

The induced lift on the wing was estimated by evaluating the wind tunnel test data for several comparable VTOL configurations and selecting a

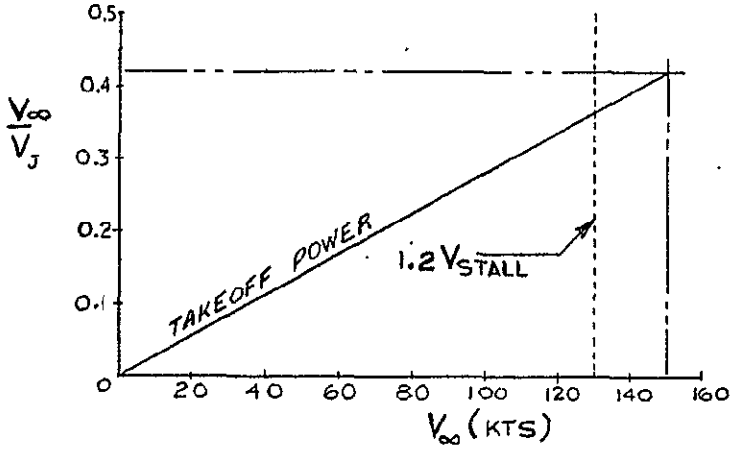

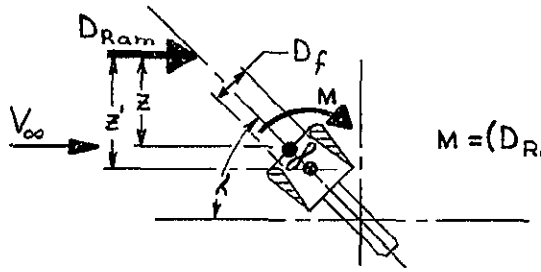

SYM.	REF.	DISC LOADING	$\lambda°$
⊙	TND 2498	1.1 PSF	80
⊡	TND 995	1.02	90
—	DATCOM SEC. 9.3	1.01	90, 70, 40

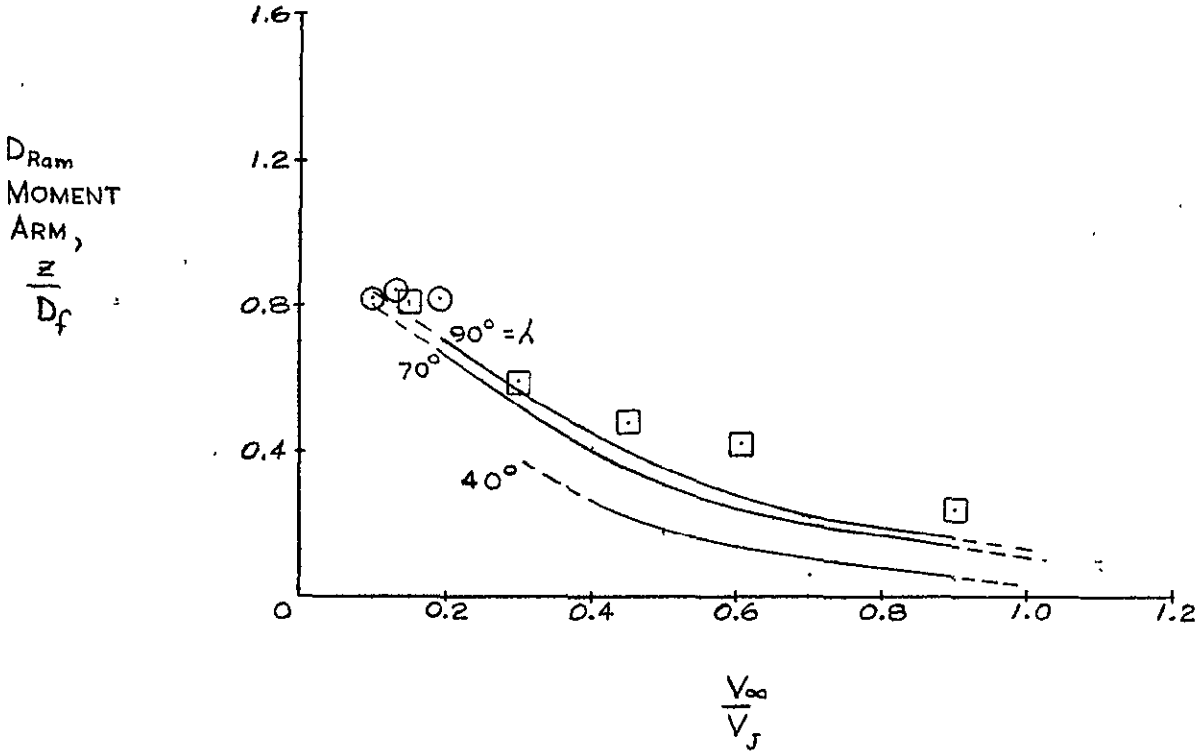

7/6/76

CALC	L. LITTLE	7-1-76		
CHECK		7/6/76		
APR				
REVISED		7/6/76		
DATE		7-5-76		

RAM DRAG MOMENT ARM

1041-135-2

FIGURE 3.4

PAGE 31

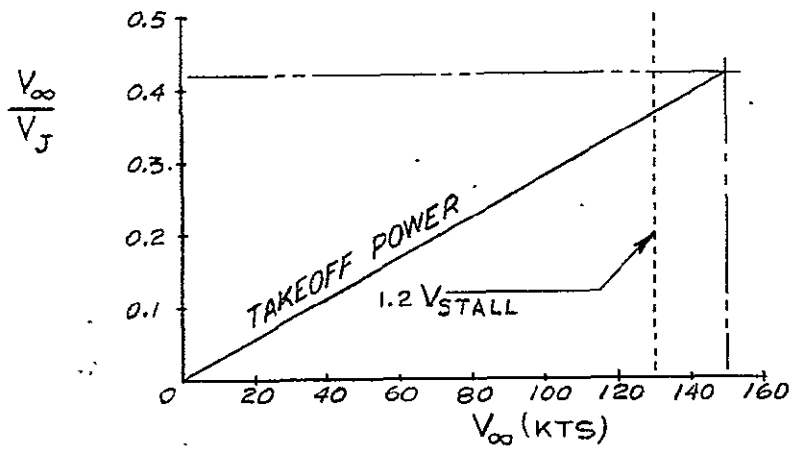

RAM DRAG MOMENT ARM EVALUATION

REF: TND-775

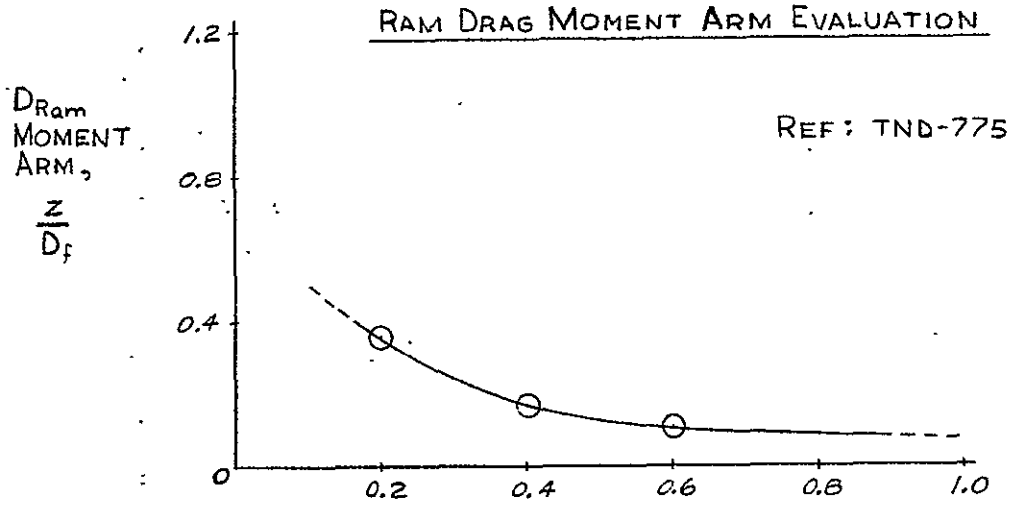

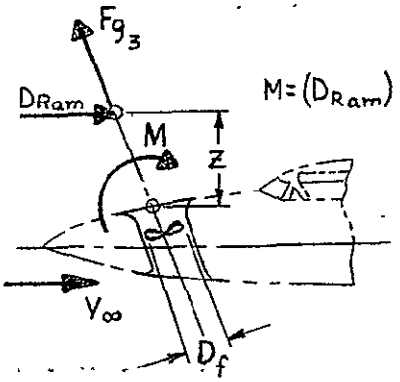

$M = (D_{Ram})\, z$

8/13/76

CALC	L. LITTLE	8/13/76	REVISED	DATE	NOSE FAN RAM-DRAG MOMENT ARM EVALUATION	MODEL 1041-135-2A
CHECK						FIGURE 3.5
APR						
APR						PAGE 32

DEFINITION OF MOMENTUM TERMS

BODY AXIS (DEFINITION & SIGN CONVENTION):

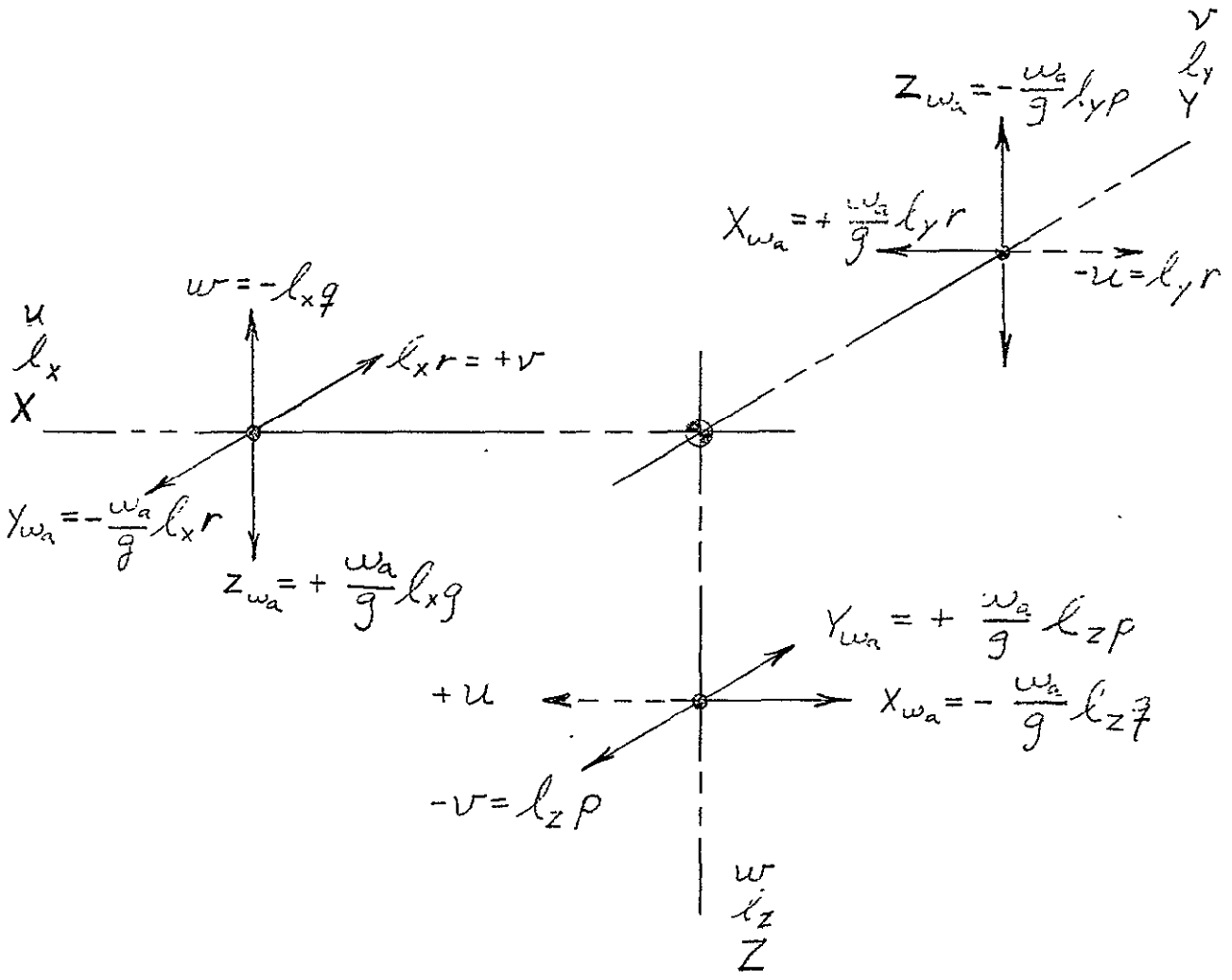

FIGURE 3.6.

DAMPING COMPARISON

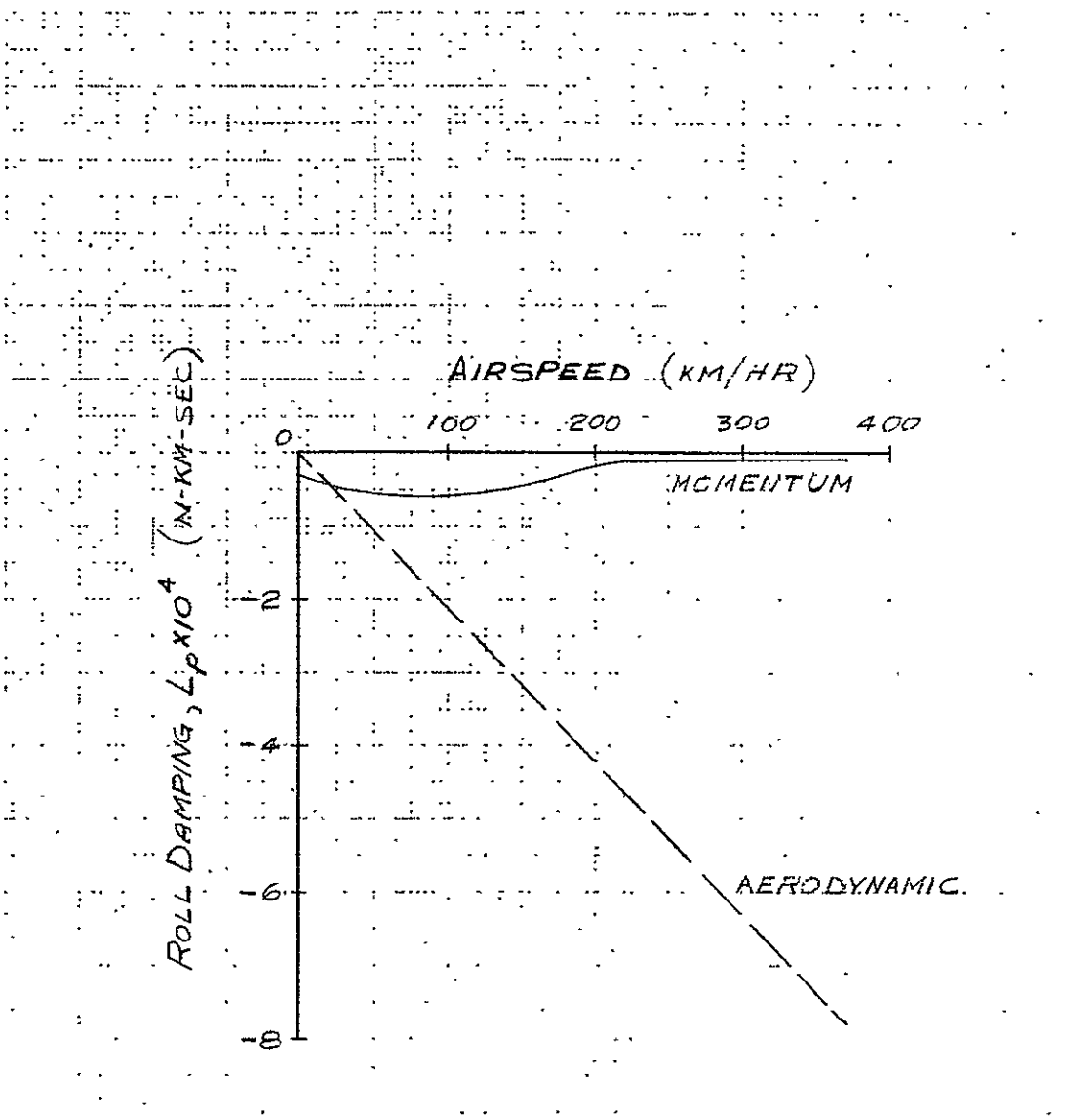

FIGURE 3.8

representative data trend. The selected data is shown on Figure 3.9. References 7, 8, 9, 10 were used. The induced lift is predicted to be a function of airspeed, jet velocity and nacelle tilt angle. The effect of angle of attack is small and has been neglected.

The induced pitching moment is composed of two terms. The first is the moment on the wing-body (tail off). The second is the moment induced by the change in flow field at the horizontal tail. The wing-body pitching moment is small and is neglected. The more significant power effects on the tail have been estimated. The change in flow field at the tail generates variations in tail angle of attack. The changes in flow field with variations in power setting, flight speed and tilt angle are represented.

A schematic of the flow field is illustrated on Figure 3.10. The illustration shows that a decay in the tail stability contribution takes place at the power settings and nacelle tilt angles are representative of VTOL flight because the tail angle of attack derivative is attentuated by power effects.

The power effects on the pitching moment were predicted by extrapolating the wind tunnel data of Reference 7. The results of this effort are a prediction for downwash angle (ε) and the rate of change of downwash with wing angle of attack ($\frac{\partial \varepsilon}{\partial \alpha}$) (See Figure 3.11). From this, the tail lift is determined by applying the simple relationships:

$$\alpha_h = \alpha_w - \varepsilon + i_h$$
$$\partial \alpha_h / \partial \alpha_w = (1 - \varepsilon_\alpha)$$

This mathematic representation was then used to predict the power effects on the longitudinal derivatives of the flow field at the tail, M_α, $M_{\dot{\alpha}}$, and M_q.

$$\frac{\Delta L}{T_S} = \left(\frac{V}{V_J}\right) \text{Cos } \lambda^\circ$$

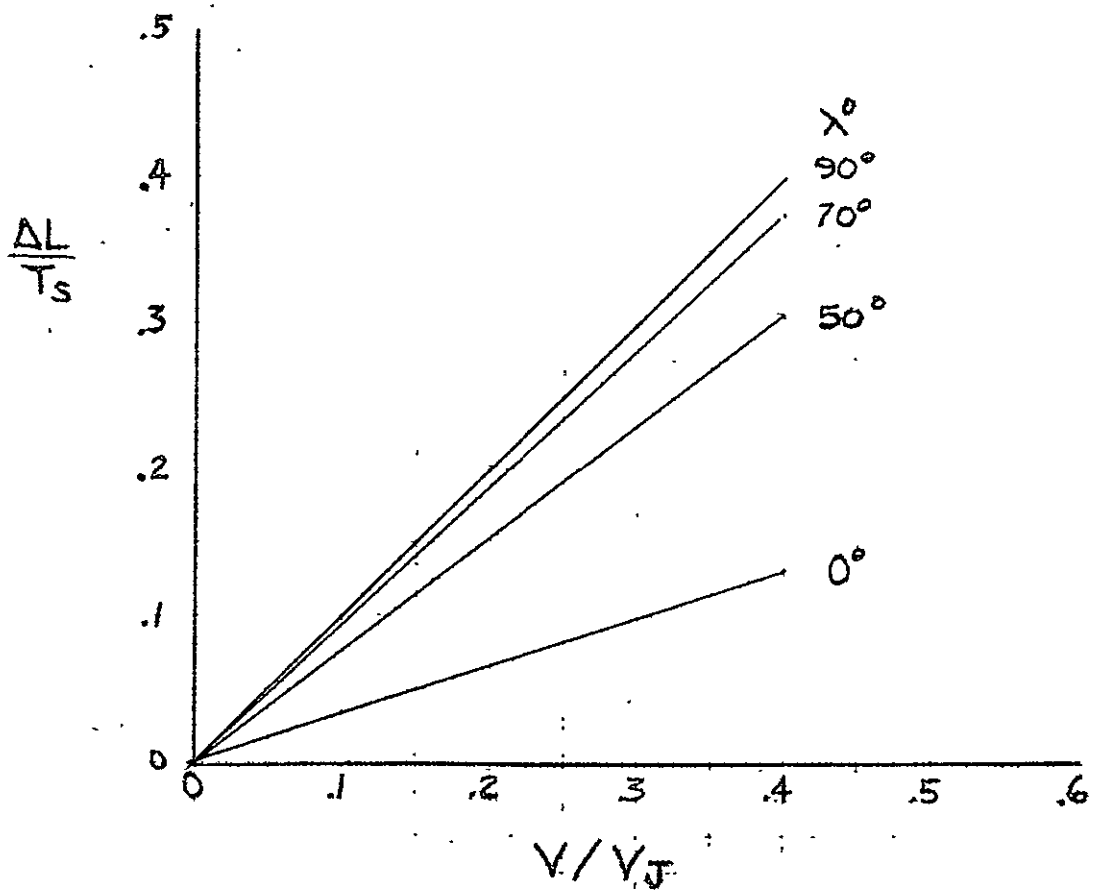

CALC	PG	6-30-76	REVISED	DATE
CHECK				
APR				
APR				

ESTIMATED INDUCED LIFT
MODEL 1041-135-2A

FIGURE 3.9

PAGE 36

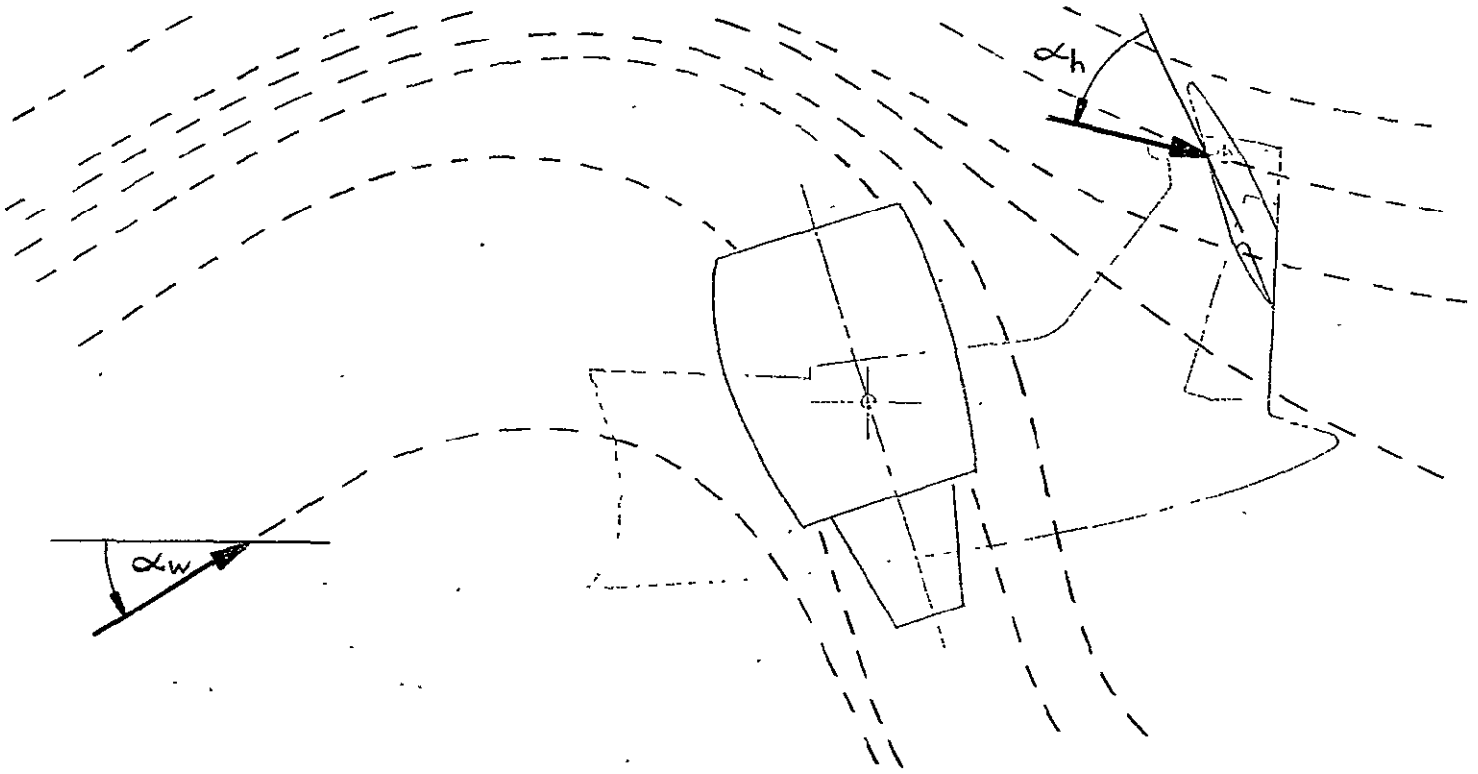

LARGE EFFECT IN V/STOL MODE AT FOLLOWING CONDITIONS:

- SMALL (V/V_T)
- LARGE NACELLE TILT ANGLE
- LARGE POWERSETTING

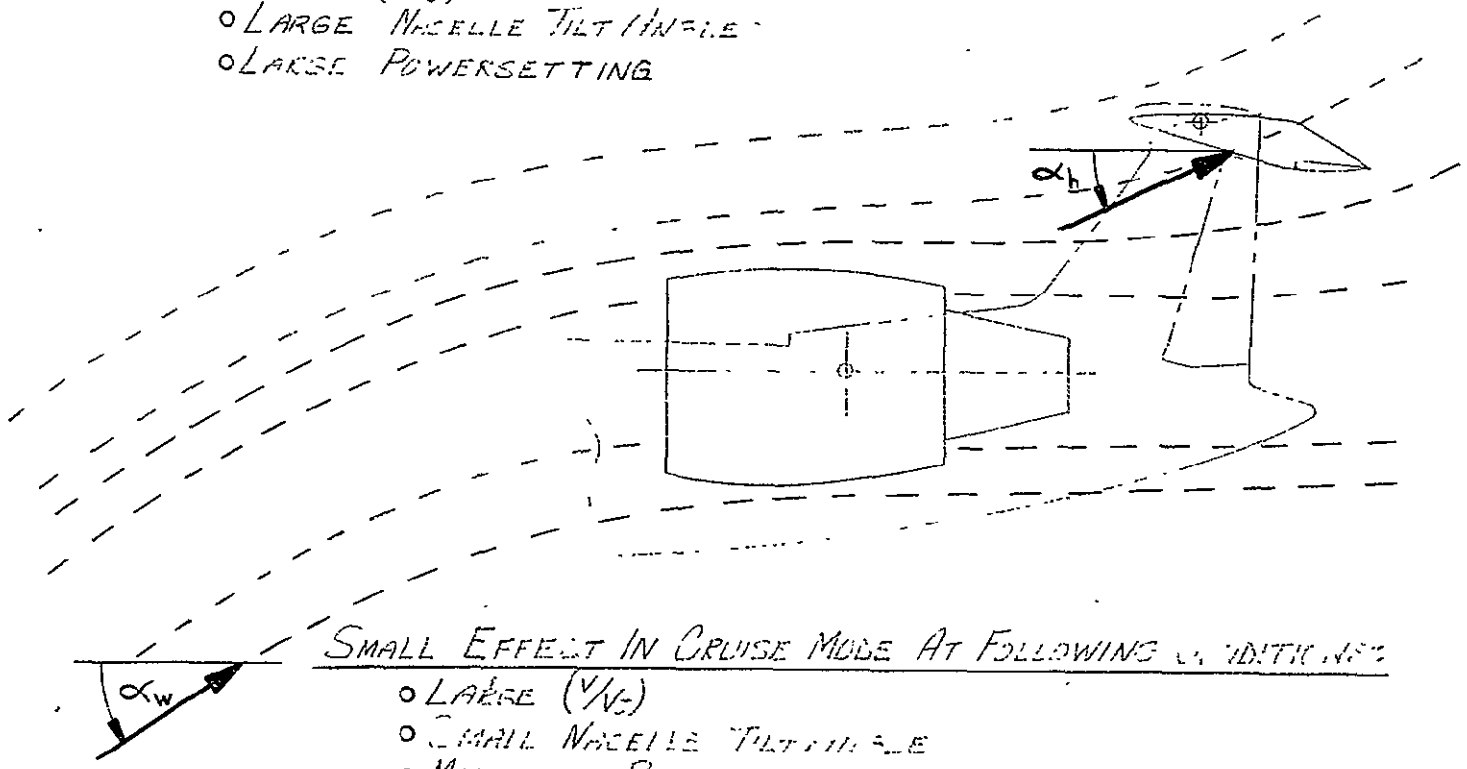

SMALL EFFECT IN CRUISE MODE AT FOLLOWING CONDITIONS:

- LARGE (V/V_T)
- SMALL NACELLE TILT ANGLE
- MODERATE POWERSETTING

ENGR	L. L. . .	. . .	REVISED	DATE	POWER EFFECT ON HORIZONTAL TAIL	
CHECK						FIGURE 3.10
APR						
APR						37

EXTRAPOLATED FROM NASA TN D 7191

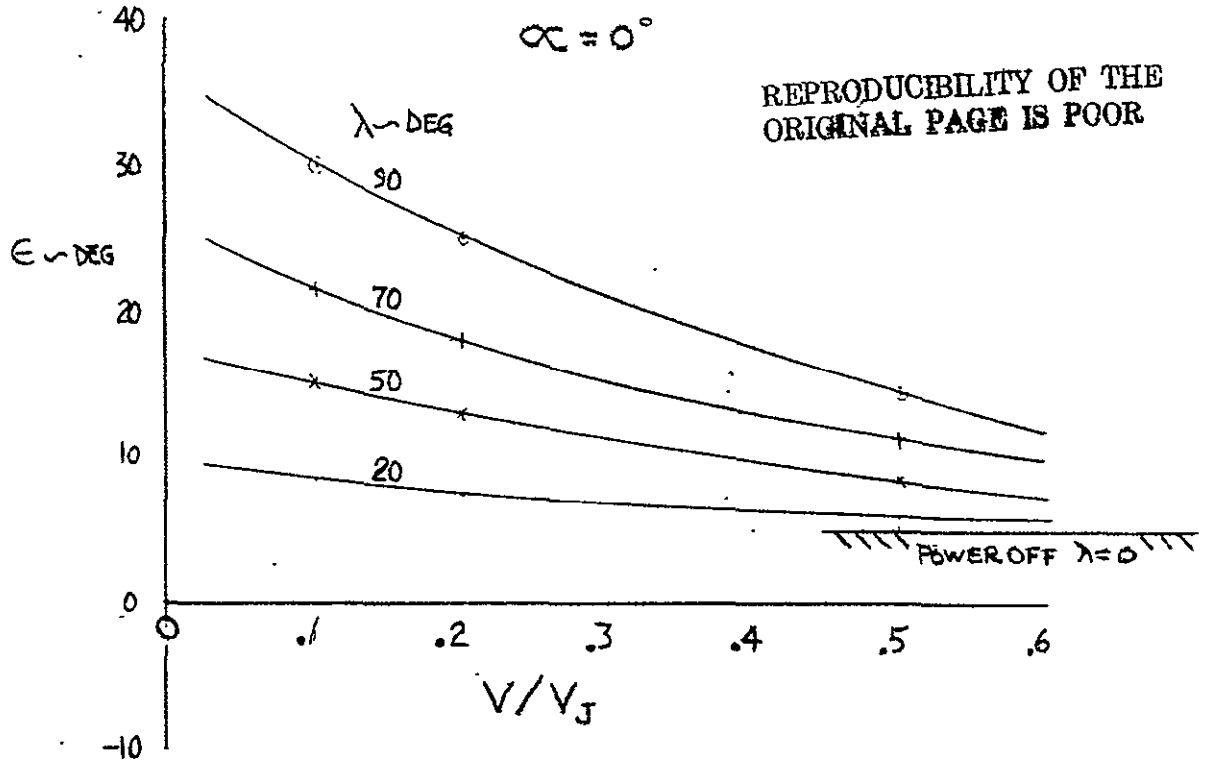

REPRODUCIBILITY OF THE ORIGINAL PAGE IS POOR

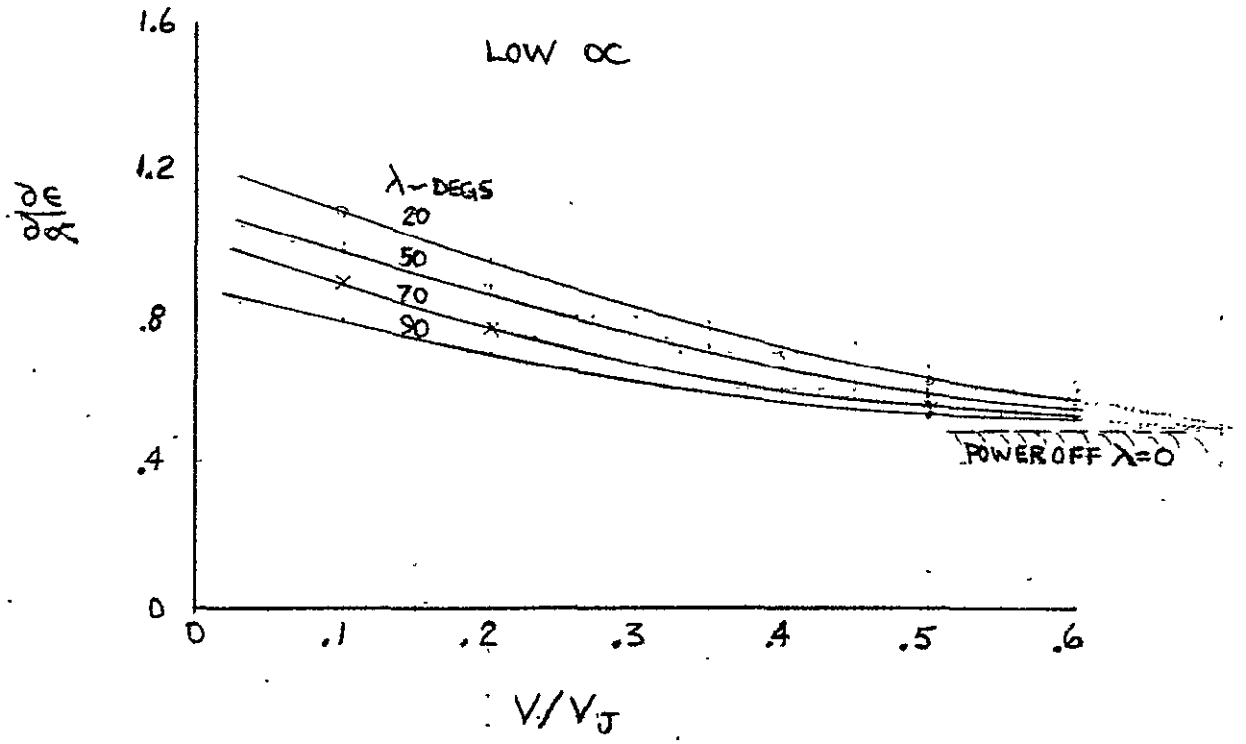

CALC	PG	2/1976	REVISED	DATE	MODEL 1041-135-2A FLOW FIELD AT HORIZONTAL TAIL ESTIMATED DATA
CHECK					
APR					FIGURE 3.11
APR					
					PAGE 38

The lateral-directional power effects are accounted for by predicting the effect of the tilting nacelle on the vertical fin. The flow field at the fin is schematically illustrated on Figure 3.12. The stabilizing effect of the fin is adversely affected by the propulsive induced flow field at high tilt angles and high power settings. The sideslip angle of the vertical fin is approximated by the following relationship:

$$\beta_{fin} = \beta_{airplane} - \sigma$$

The sigma term is analogous to the downwash parameter but its behavior is much more complex and difficult to estimate because of sensitivity to fuselage geometry. In general, sigma has a positive sign for a low wing/T-tail arrangement for power off. The derivative of sigma with respect to airplane sideslip angle is directly related to the weathercock static stability. The power off estimate for this derivative is greater than one. The fin's stabilizing contribution decays as the power builds up. A term $K\sigma$ is defined as a power effects factor that operates on the flow field factor $(1 - \frac{\partial\sigma}{\partial\beta})$. The K-Sigma factor is evaluated by assuming a trend similar to that exhibited by the downwash derivative. The evaluation for K-Sigma is shown on Figure 3.13.

This factor has been applied to fin contribution to the derivatives Y_β, L_β, and N_β. The equations for the power effects derivatives are shown in Section 2.0 in matrix form.

The order of magnitude and the data trends used in this report are illustrated on Figure 3.14.

3.4 Gyroscopic Moments

The gyroscopic effects of the relatively large propulsion system are fully represented, including the variation with nacelle tilt angle. For example,

FIN SIDE SLIP ANGLE
AND STABILIZING
DERIVATIVES ARE AFFECTED

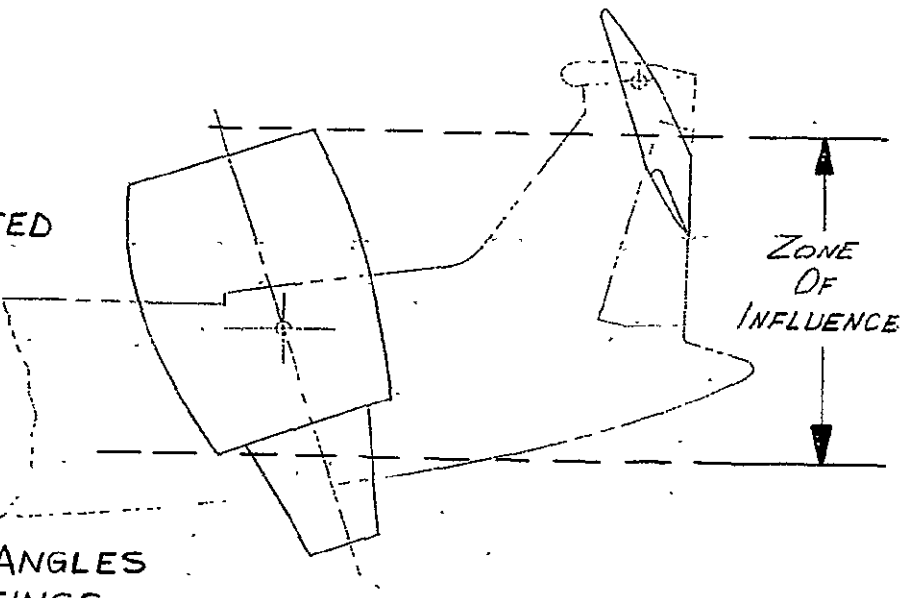

LARGE EFFECT

- SMALL V/V_J
- LARGE NACELLE TILT ANGLES
- LARGE POWER SETTINGS

NOTE : AT CRUISE ZONE OF INFLUENCE IS REDUCED

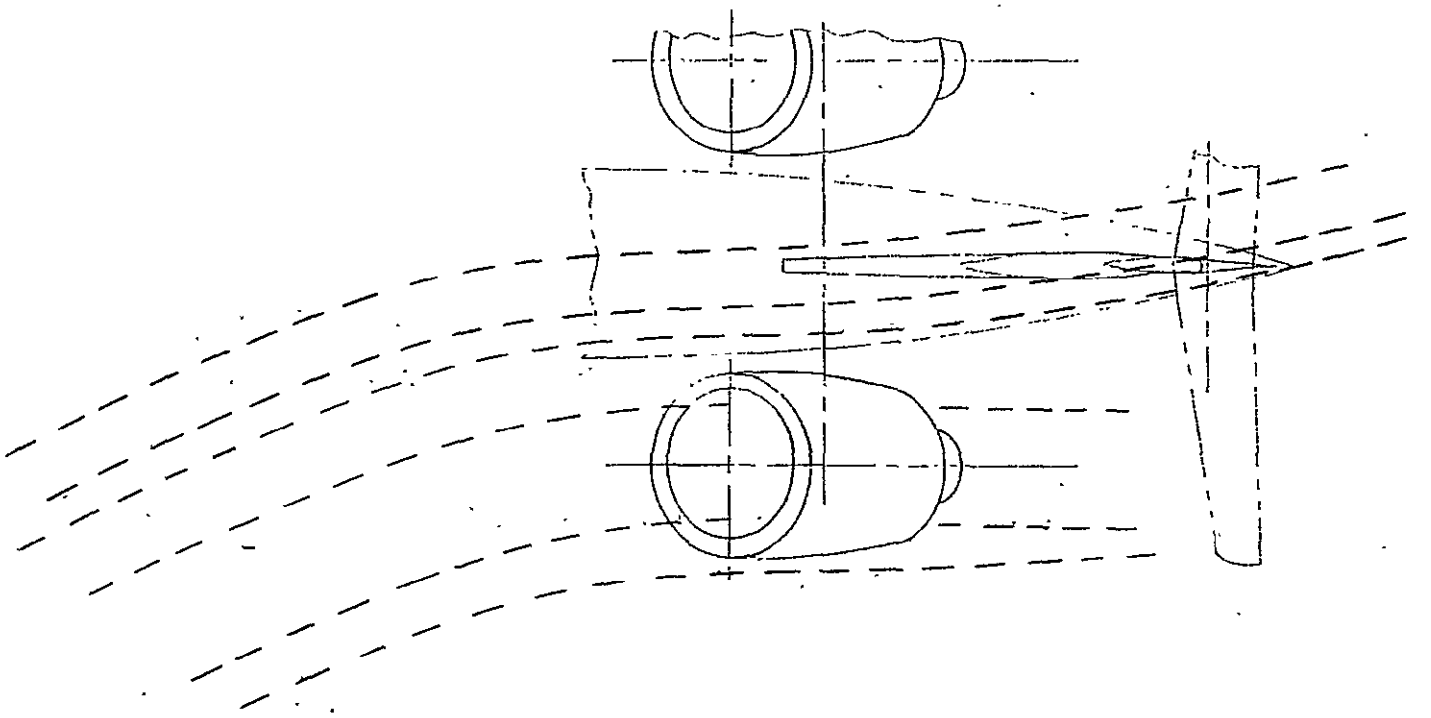

ENGR.	L. Lemke		REVISED	DATE
CHECK				
APR				
APR				

POWER EFFECTS ON FIN

FIGURE 3.12

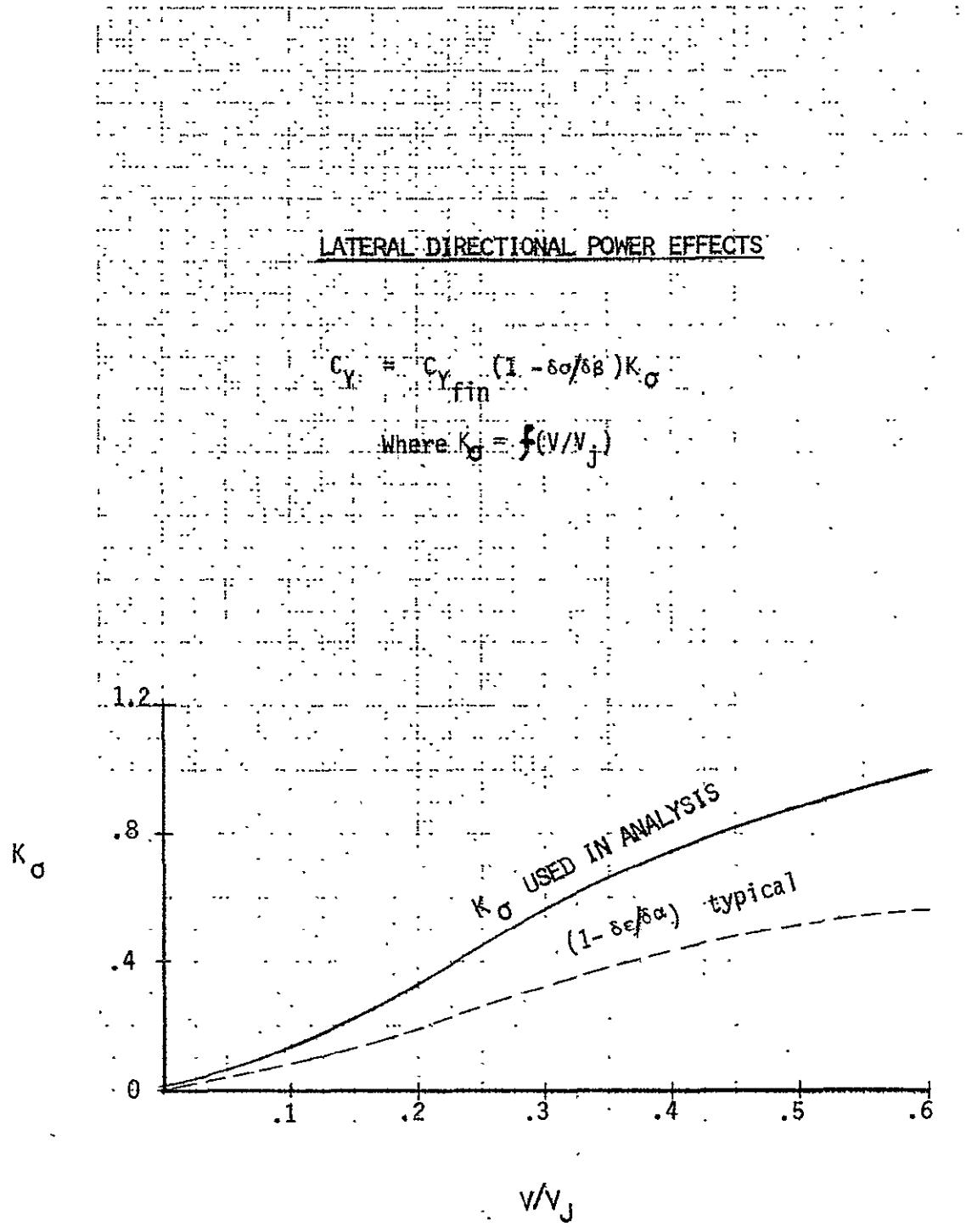
LATERAL DIRECTIONAL POWER EFFECTS
$C_Y = C_{Y_{fin}} (1 - \delta\sigma/\delta\beta) K_\sigma$
Where $K_\sigma = f(V/V_J)$
1.2
.8
.4
0
K_σ
K_σ USED IN ANALYSIS
$(1 - \delta\epsilon/\delta\alpha)$ typical
.1
.2
.3
.4
.5
.6
V/V_J

FIGURE 3.13

VARIATION OF STATIC STABILITY WITH AIRSPEED

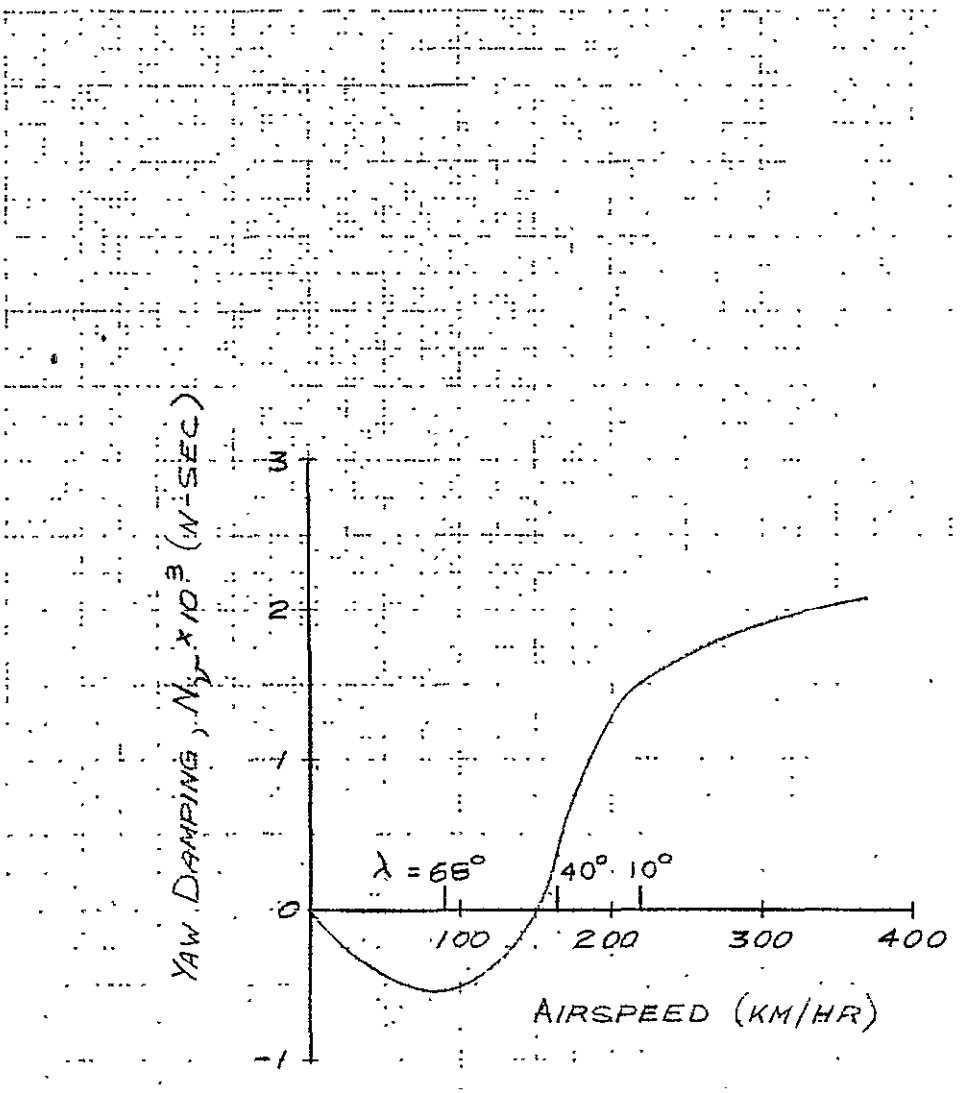

FIGURE 3.14

in hover the gyroscopic coupling is predominately from pitch rate to rolling moment (see Figure 3.15). In cruise (nacelles at zero tilt) the coupling is predominately from pitch rate to yawing moment. Figure 2.10 defines the equations used to predict the gyroscopic effects (shown in matrix form). An insert in the figure defines the physical values to estimate the propulsion system angular momentum vectors. The shaft system operates at constant speed. The small variation in momentum due to changes in gas generator speed have been neglected. The X and Z axis angular momentum vectors for several tilt angles are graphically shown on Figure 3.16.

3.5 Flight Control and Stick Sensitivity

The airplane has eight different control elements in the V/STOL flight regime. They are as follows:

- Fan blade roll
- Fan blade pitch
- Vane yaw
- Aileron
- Stabilizer
- Rudder
- Height control
- Nacelle tilt angle

This section evaluates the control power and shows the pilot control sensitivities that can be used. The data of references 4 and 5 were used as a guide to define the level of sensitivity for good handling qualities. The selected sensitivities are shown on Figure 3.17. Maximum travel of the control surfaces used in this study are tabulated in Figure 3.18. The aerodynamic controls are active throughout the airplane flight envelope. The fan controls are phased out as speed builds up. The stick sensitivities, in terms of angular acceleration for full stick travel, are given as a function of speed on Figure 3.19. Figures 3.20 and 3.21 show the response of the airplane

PROPULSION SYSTEM ANGULAR MOMENTUM $\left(H \sim kg\text{-}m^2/sec\right)$

FIGURE 3.15

VARIATION OF GYROSCOPIC COUPLING WITH NACELLE TILT

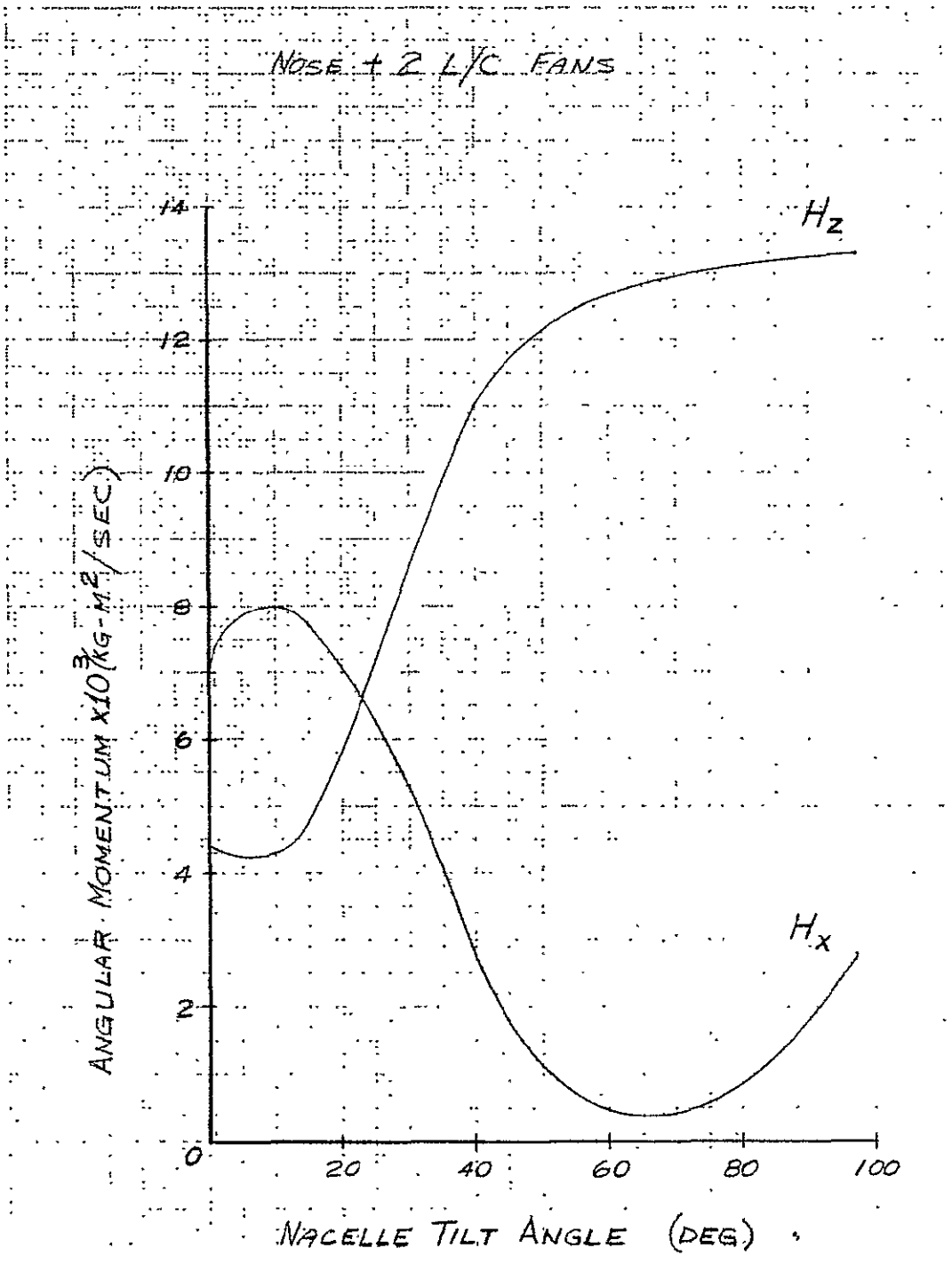

FIGURE 3.16

CONTROL SENSITIVITY

CONTROL AXIS	ALLOWABLE RANGE SPECIFICATIONS	SELECTED SENSITIVITY
ROLL $^{\Delta}$	.20 to .89 Rad/Sec^2/In	0.20 Rad/Sec^2/In
PITCH$^{\Delta}$	.08 to .16 Rad/Sec^2/In	0.10 Rad/Sec^2/In
YAW$^{\Delta}$	.05 to .20 Rad/Sec^2/In	0.15 Rad/Sec^2/In
HEIGHT*	30 to 230 MPM/In (100 to 750 FPM/In)	105 MPM/In (344 FPM/In)

* MIL F 83300

$^{\Delta}$ AGARD-R577

FIGURE 3.17

CONTROL DEFLECTIONS

AERODYNAMIC SURFACES	
AILERON, δ_A	$\pm$ 16 Degrees
STABILIZER, δ_S	+ 30 to -10 Degrees
RUDDER, δ_r	$\pm$ 25
POWER CONTROLS	
FAN PITCH, $\delta^*_{\beta\theta}$	ΔBETA = $\pm$ 6 Degrees
FAN ROLL, $\delta^*_{\beta\phi}$	ΔBETA = $\pm$ 6 Degrees
YAW VANE, $\delta_{V\psi}$	$\pm$ 8 Degrees

* DEFLECTION OF NUMBER 2 FAN.

Control elements have the following slave relationships:

$\delta_{V_3} = 2\,\delta_{V_2}$ $\qquad$ $\delta_{\beta\theta_1} = \delta_{\beta\theta_2}$

$\delta_{\beta\phi_1} = \delta_{\beta\phi_2}$ $\qquad$ $\delta_{\beta\theta_3} = -2\delta_{\beta\theta_2}$

FIGURE 3.18

INTEGRATED ROLL CONTROL POWER

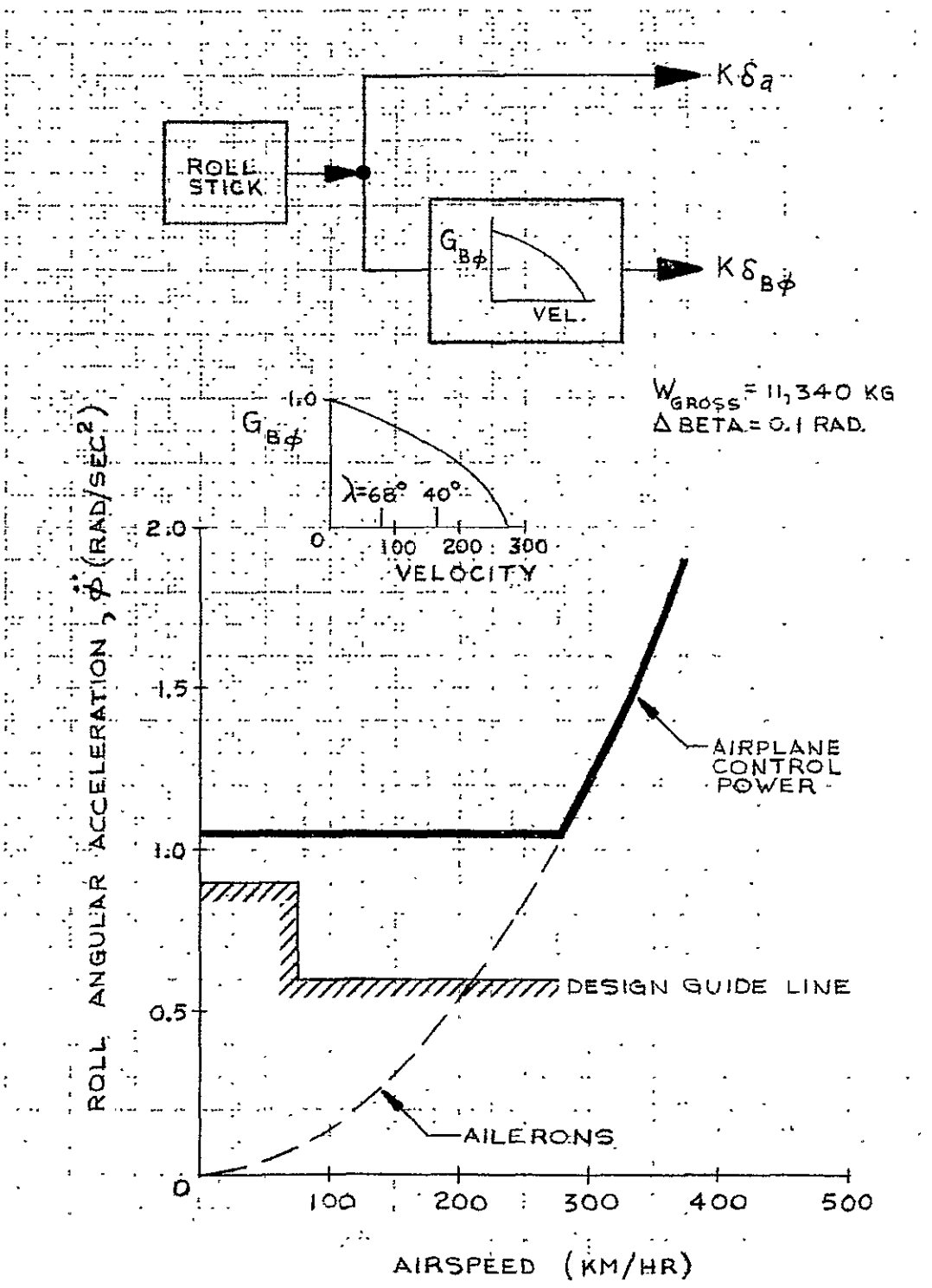

FIGURE 3.19

INTEGRATED PITCH CONTROL POWER

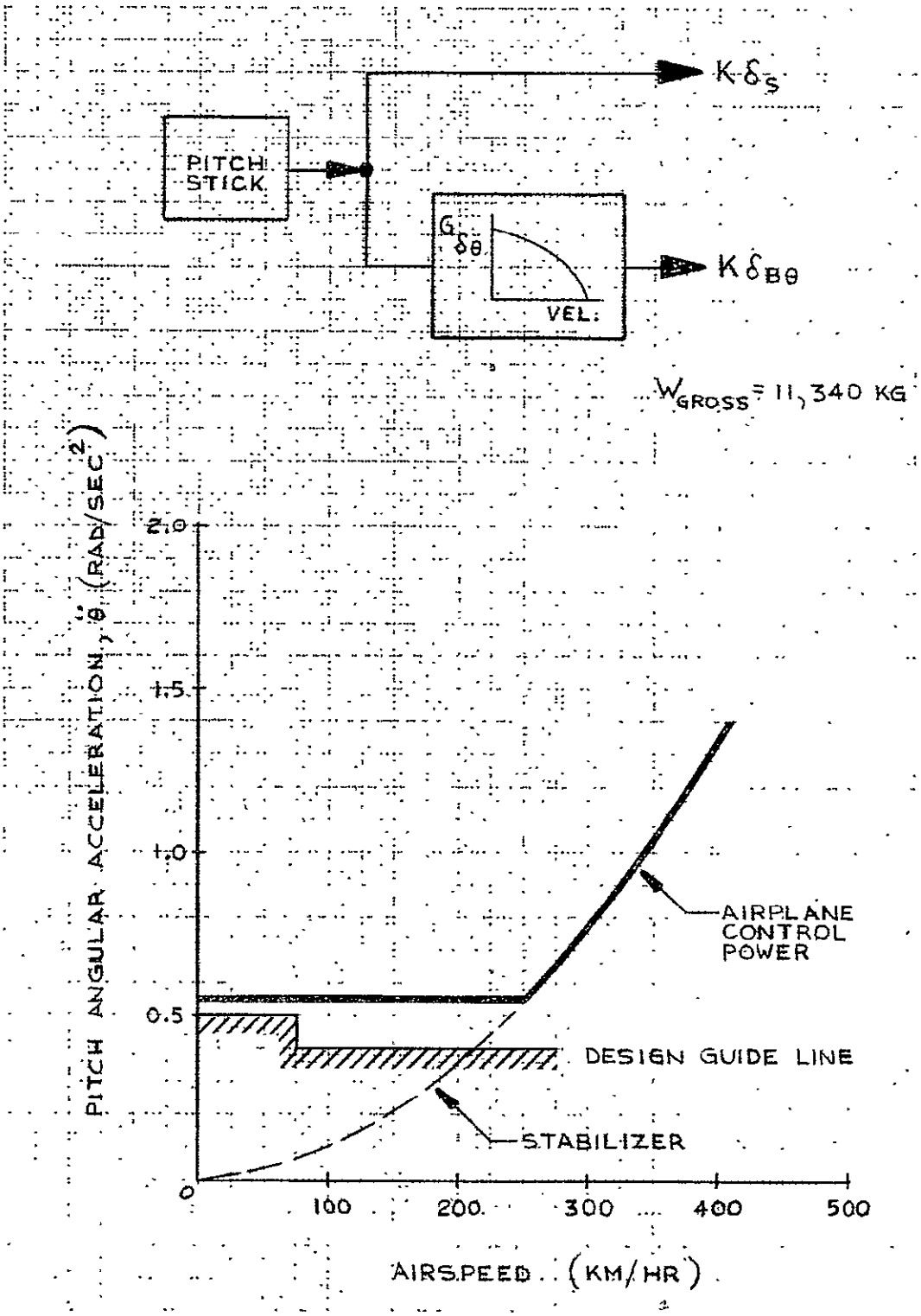

FIGURE 3.19

INTEGRATED YAW CONTROL POWER

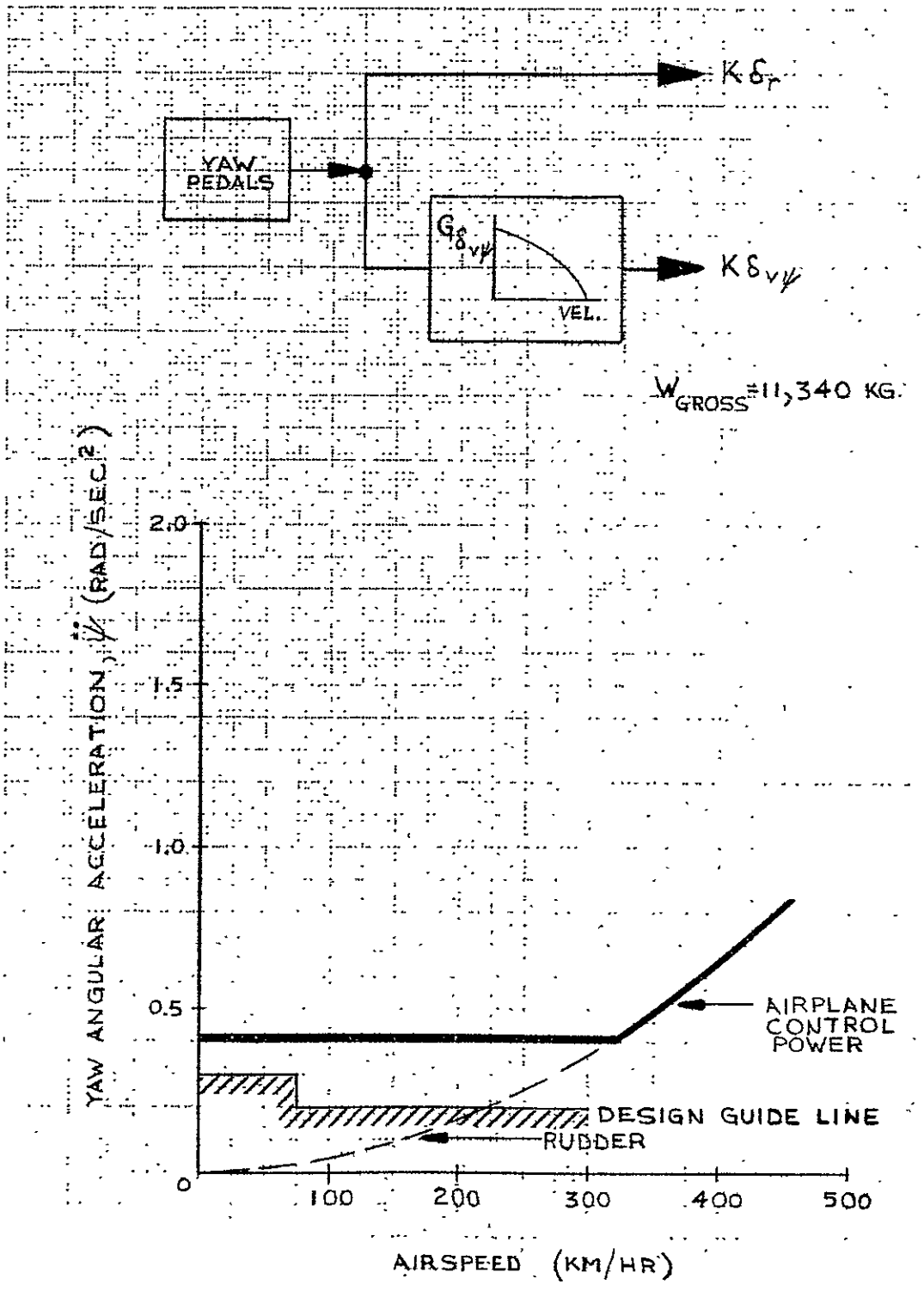

FIGURE 3.19

HEIGHT RESPONSE

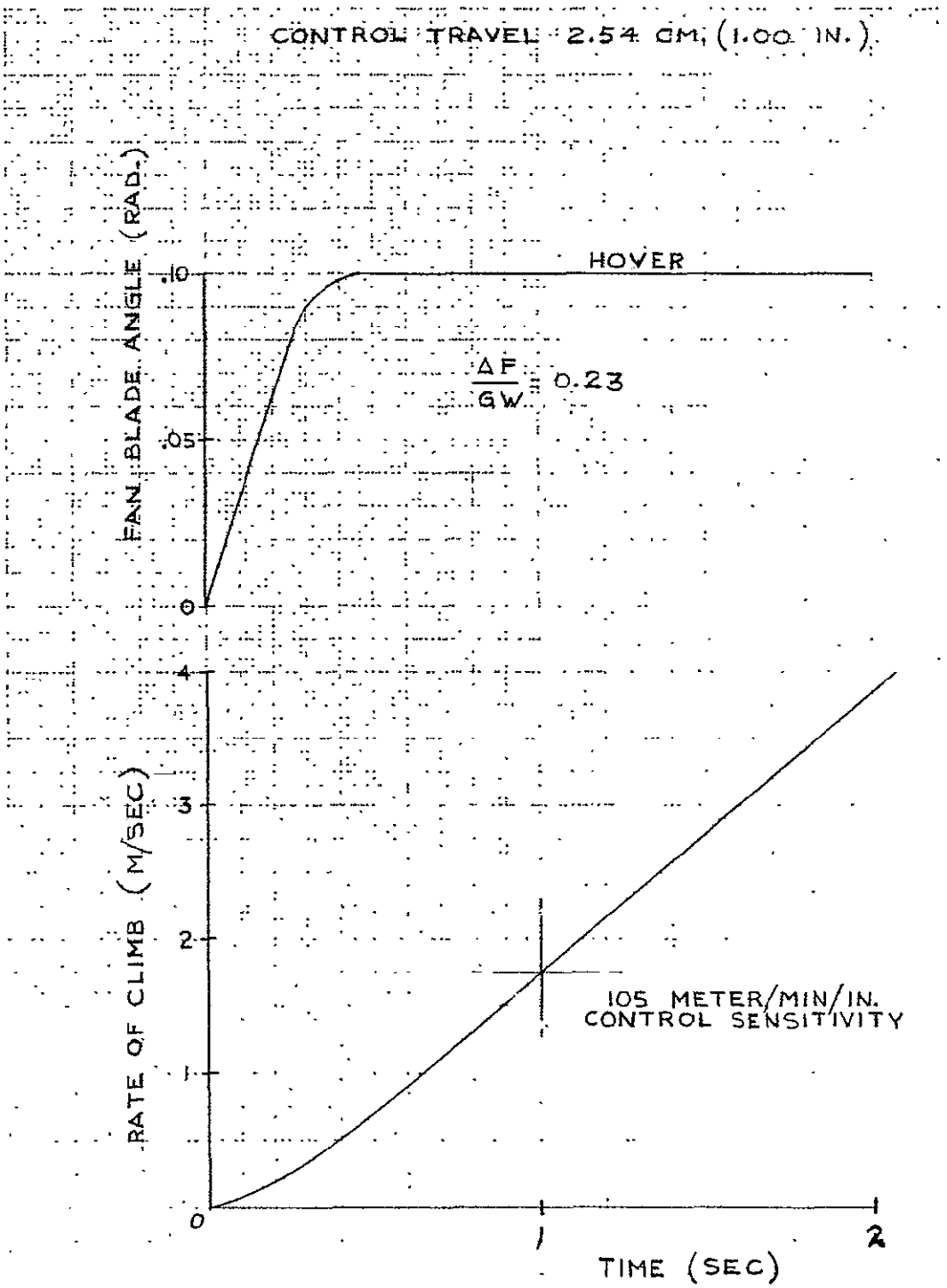

FIGURE 3.20

BANK ANGLE RESPONSE

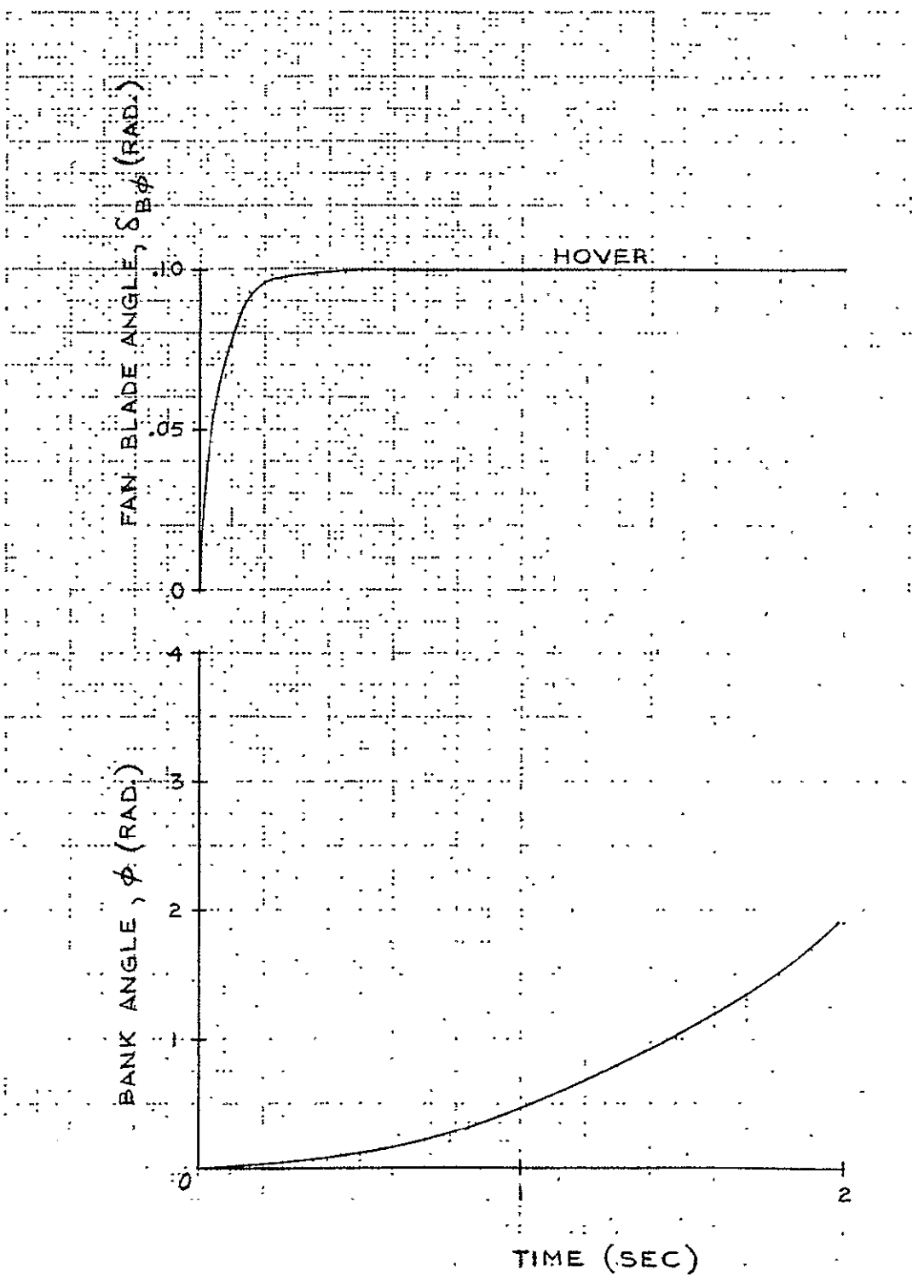

FIGURE 3.21

PITCH ATTITUDE RESPONSE

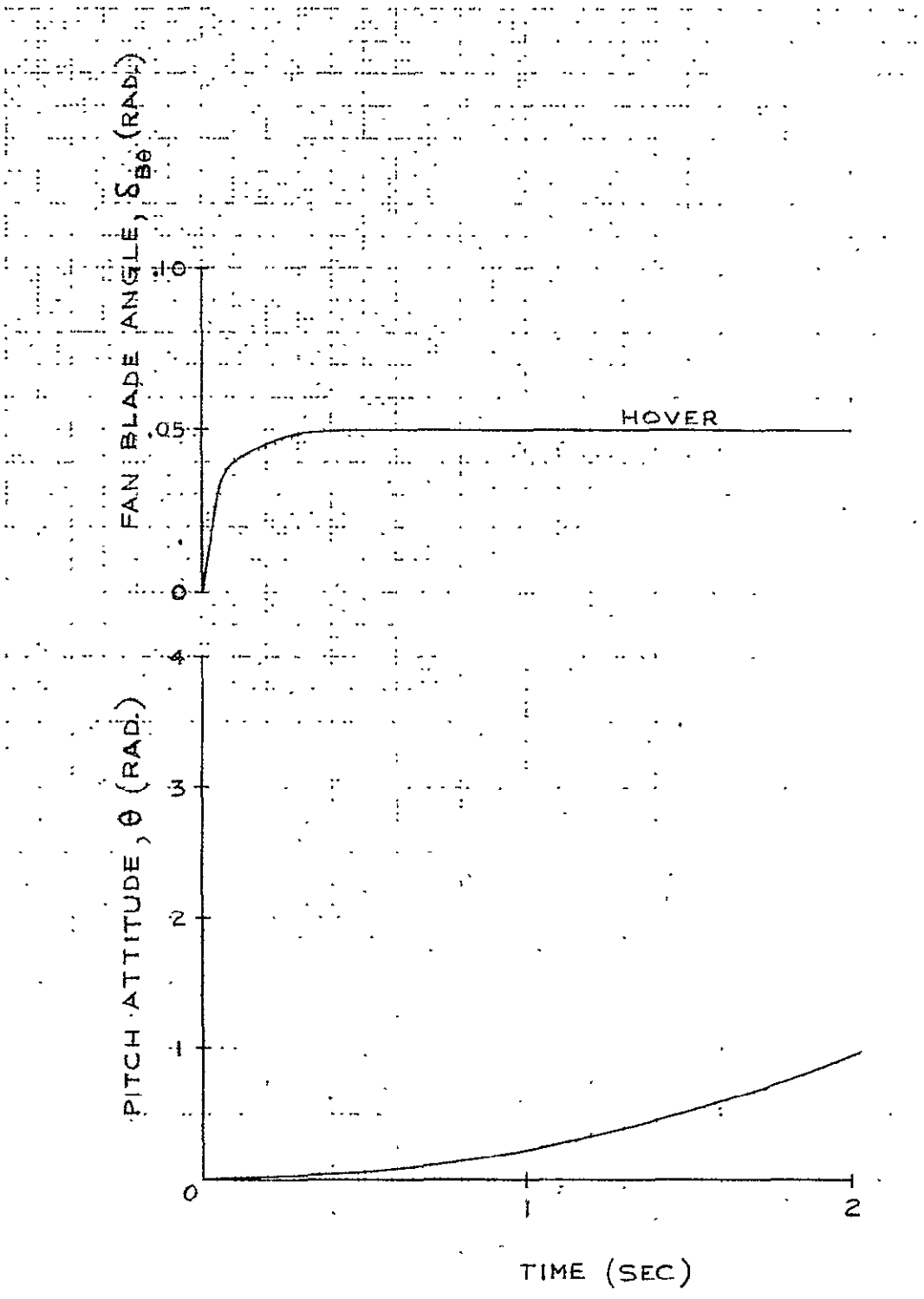

FIGURE 3.21

YAW ANGLE RESPONSE

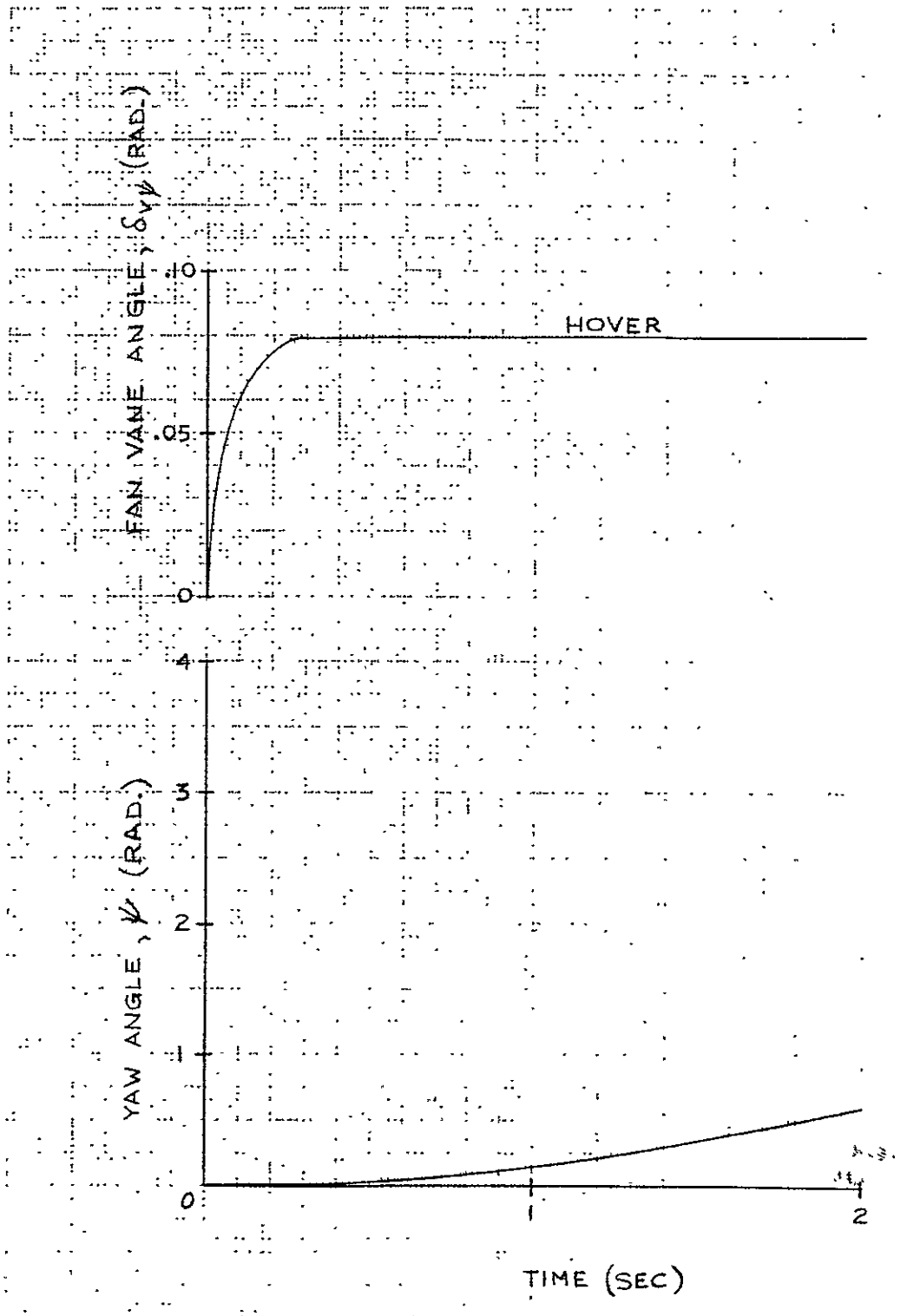

FIGURE 3.21

to a step input of maximum control. The airplane responses are shown with the stability augmentation system disengaged. Thrust response is represented by a first order lag for the data shown. Time constants for thrust response are discussed in the next section.

Fan thrust is very sensitive to blade angle. Figure 3.22 shows the general trend from zero to maximum thrust. It has been scaled up from the Hamilton Standard "Q" fan to illustrate blade effectiveness, and was not used in the study. A representative value of 1490 newtons/degree (335 lbs/deg) was used.

3.6 Propulsion System Data

The propulsion system of the Model 1041-135-2A is a fundamental element of the airplane's control system. Fan thrust is modulated by variations in fan blade angle to produce pitching and rolling moments. Yawing moments are generated by vectoring fan thrust with the yaw vanes. Height control is achieved by the modulation of the airplane net thrust through a single lever similar to a throttle. The fan speed is governed at about 3600 rpm. A preliminary schematic of the propulsion system control is shown on Figure 3.23.

Thrust response for attitude control is different than the response to height control commands. The response to attitude control demands is at constant system horsepower. The estimated response is given on Figure 3.24. Response to height control demands is not quite as crisp as attitude control, but still very fast. Estimated height control response is shown on Figure 3.25. Response to this type of command is slower than to attitude commands because it requires gas generator speed change (Figure 3.26) in addition to blade angle response. A flyup command has the longest time constant because the system horsepower must be increased to match the increase in thrust. The initial increase in thrust droops slightly

FAN THRUST SENSITIVITY

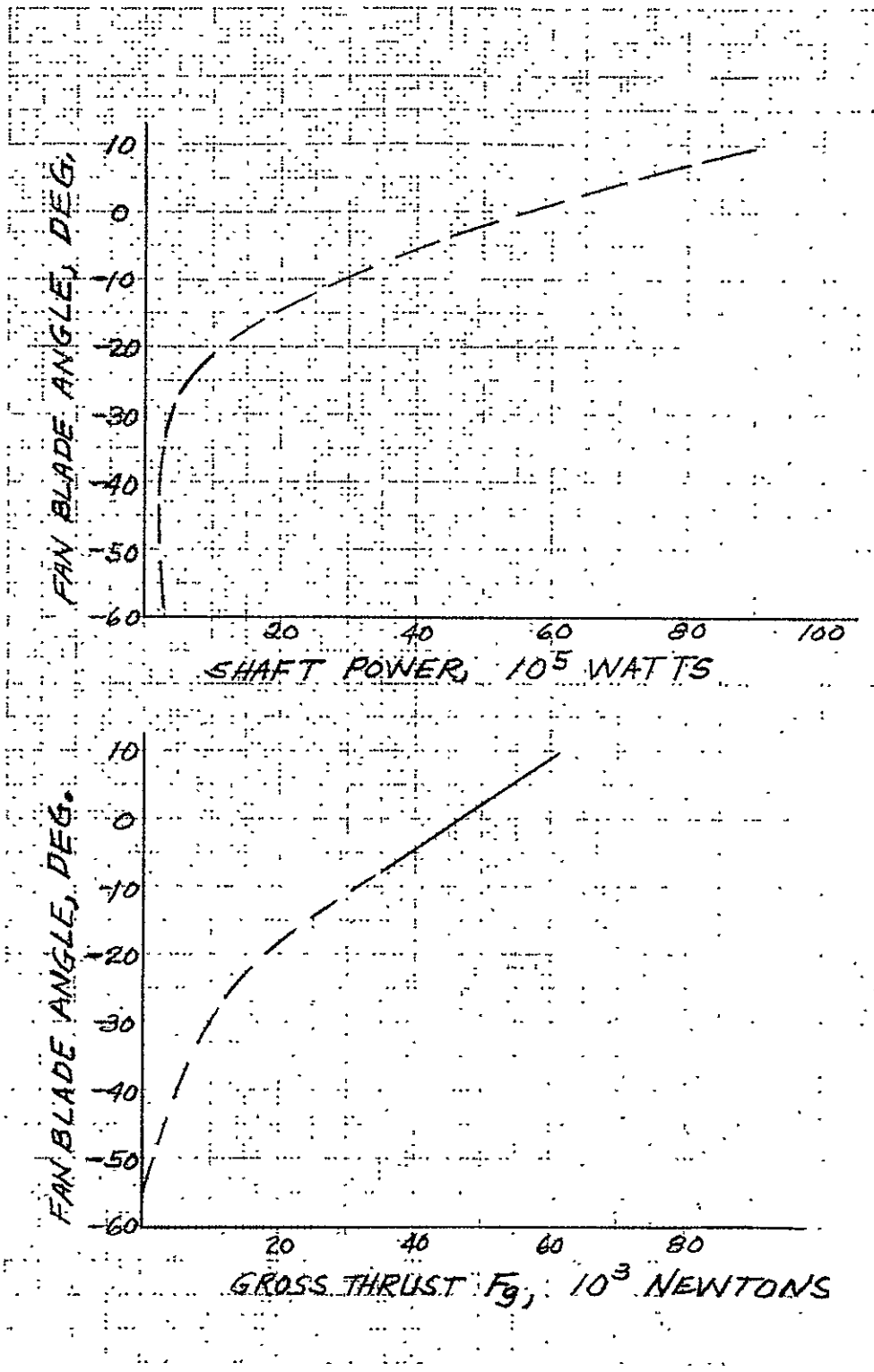

FIGURE 3.22

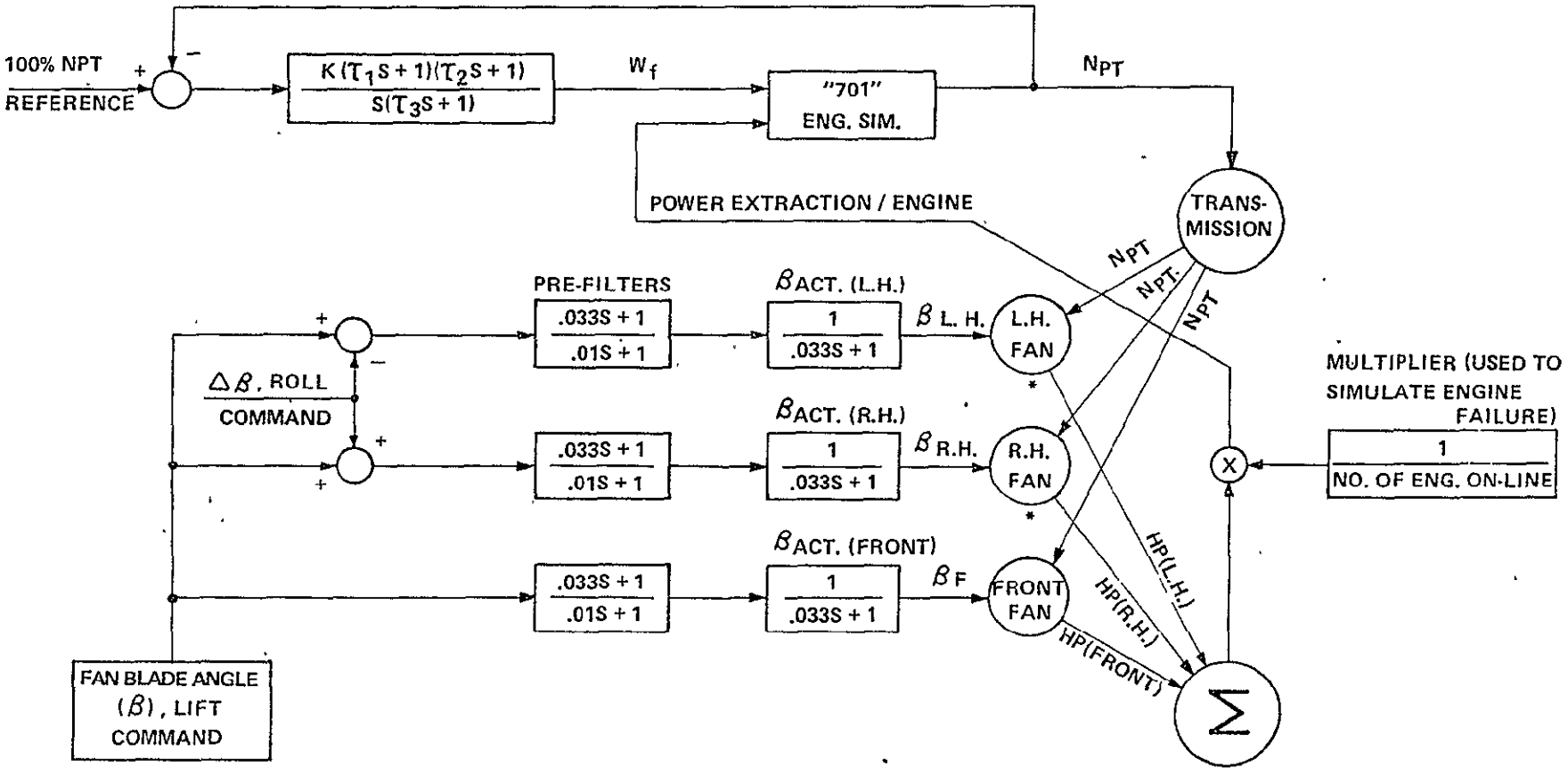

*ALLISON "701" / NAVY FAN LIFT CONTROLS STUDY (PRELIMINARY *)*

**EFFECT OF FAN NOT INCLUDED IN "701" CYCLE SIMULATION DYNAMICS*

FIGURE 3.23

CONTROL BLOCK DIAGRAM – CLOSED LOOP ON POWER TURBINE SPEED (OPEN LOOP LIFT COMMAND)

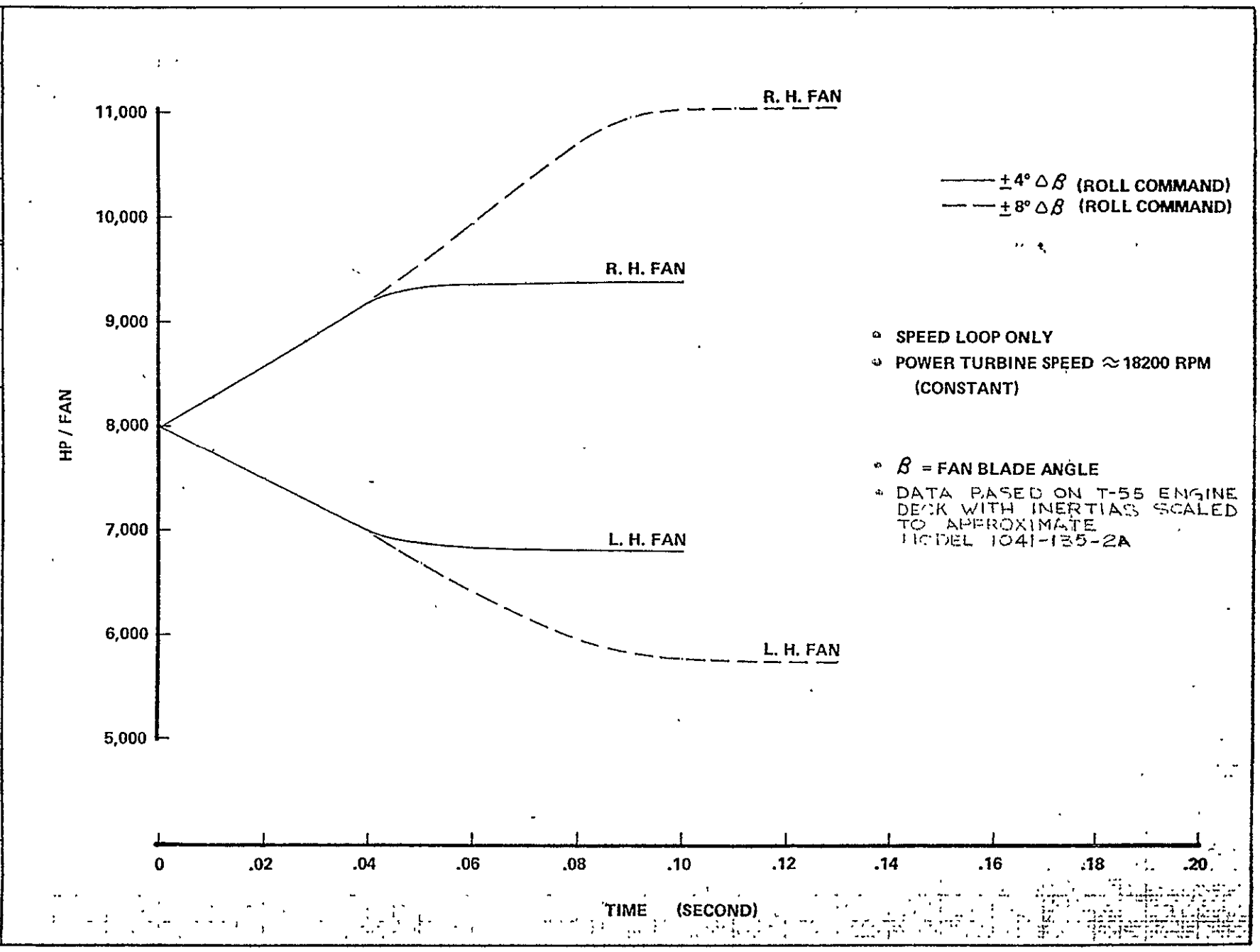

CALC	CHECK	APR	APR
REVISED			
DATE			

FAN RESPONSE TO ATTITUDE COMMAND INPUT

FIGURE 3.24

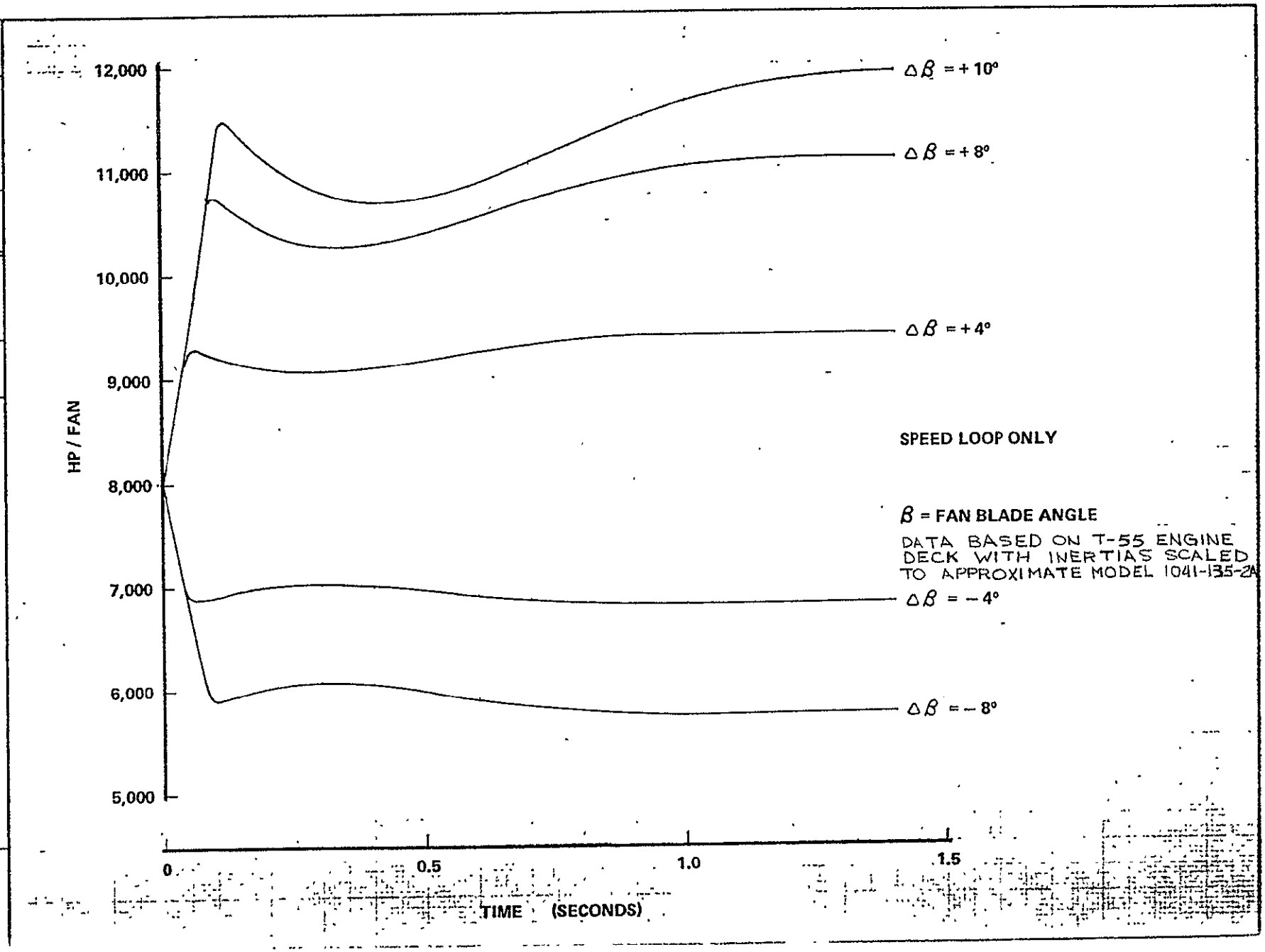

CALC | CHECK | APR | APR

REVISED | DATE

FAN RESPONSE TO LIFT COMMAND INPUT

FIGURE3.25

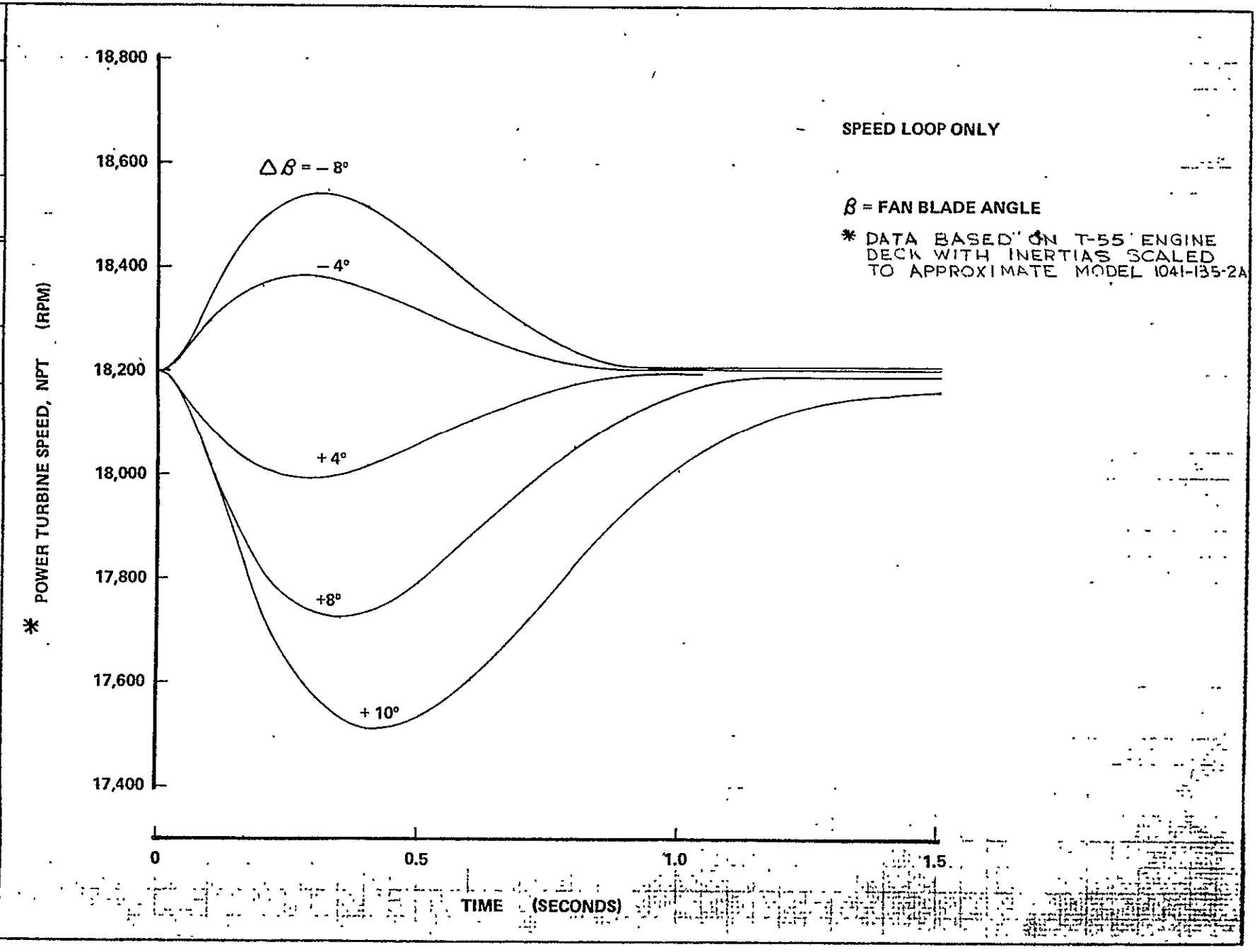

POWER TURBINE RESPONSE TO LIFT COMMAND INPUT

FIGURE 3.26

PAGE 60

	CALC	CHECK	APR	APR
REVISED				
DATE				

DI 4100 3240

K+E ALBANENE 1061 MADE IN U.S.A.

until the gas generator comes up to speed to balance horseposer requirements. Flydown commands are similar to flyup commands in that an engine speed change is required. A flydown command reduces the thrust on all three fans and the fan speed governor maintains equilibrium by commanding a slowdown in engine speed to balance system power. The curves on Figure 3.25 ($\Delta\beta = -8^{o}$) show the system responding to a flydown command. There is some ballooning of system power as the engines respond.

The propulsion system performance parameters of gross thrust, fan inlet airflow, fan power, fan blade angle and gas generator speed are shown on Figure 3.27. The data represent the system operation at constant fan RPM.

PROPULSION SYSTEM PERFORMANCE PARAMETERS

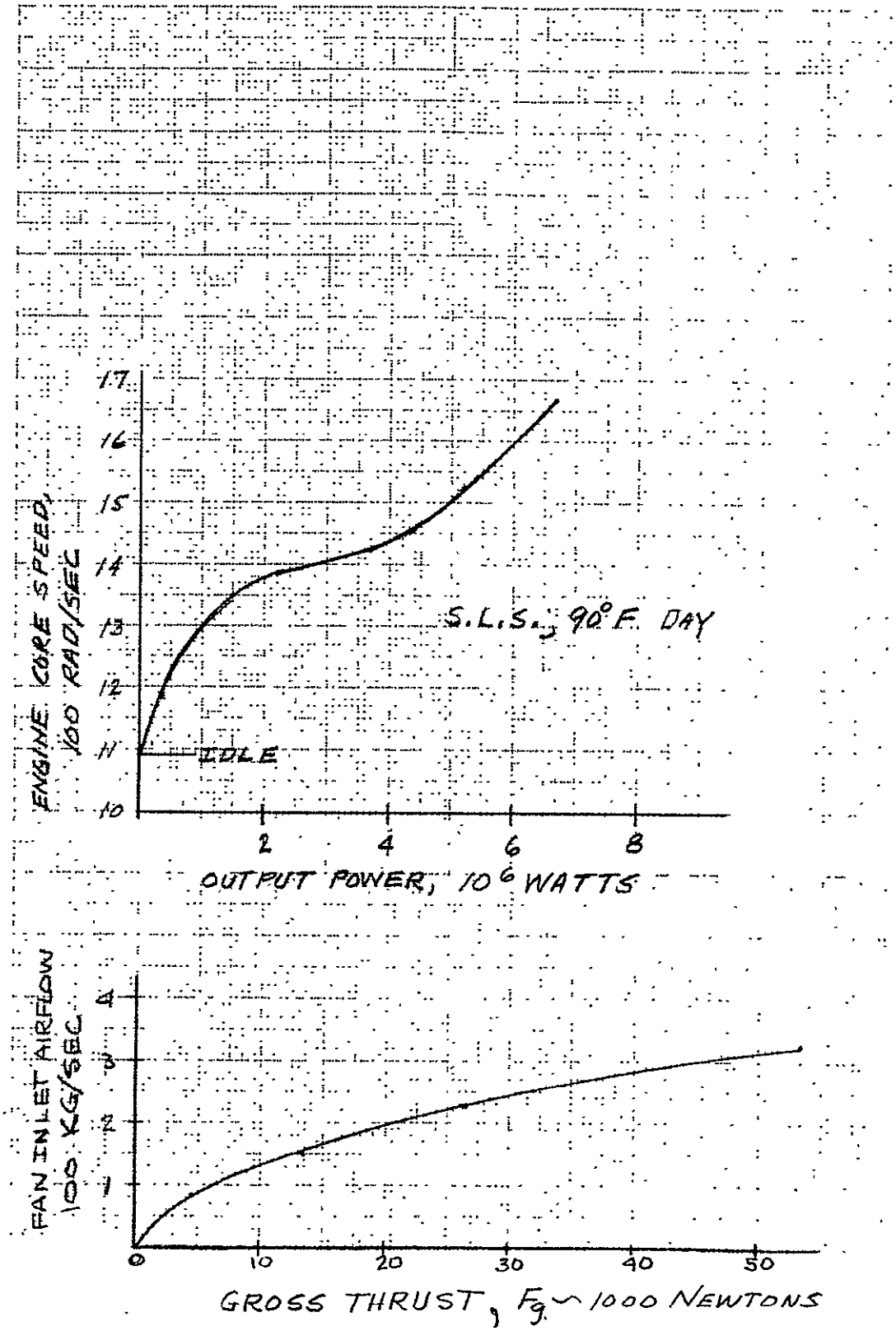

FIGURE 3.27

4.0 STABILITY AUGMENTATION SYSTEM DEVELOPMENT

4.1 Unaugmented System

The loci of the eigenvalues representing the characteristics of the unaugmented aircraft are shown in Figures 4.1 and 4.2 over the transition range from 97 degrees fan tilt at hover to zero degrees fan tilt at 240 km/hr. Although some coupling exists between the lateral-directional and longitudinal modes from gyroscopic fan moments and fan induced flow effects, the magnitude was not sufficient to significantly affect the values of either the open or closed loop eigenvalues. Figure 4.3 compares the poles of the airplane modeled for 6 degree of freedoms with 2 separated 3 degree of freedom models using the classical split between the longitudinal and lateral-directional axis. Comparisons of the roll mode, the spiral mode and the periodic modes shows only a small migration of the roots. Therefore, in all further discussion and control law development, the classical split between longitudinal and lateral-directional modes has been made to simplify the analysis to two 3 degrees of freedom problems. An exception is the failure analysis (Section 5.0), where large unsymmetric moments result from fan blade or vane control failure.

4.2 Augmentation System

A successful stability augmentation system has been designed that produces a dramatic improvement in the airplane handling qualities. A basic problem in achieving the objective, however, was the large shift in the values of the open loop poles and changes in control effectiveness during transition. The pole shift is inherent to V/STOL aircraft.

Although it would be desirable to have the closed loop system characteristics invariant with changes in forward speed, this cannot be accomplished without a complex gain schedule in combination with a sophisticated compensation design. Before selecting the final design, both rate and attitude type systems were evaluated in an attempt to both minimize the number of system elements (i.e., sensors) required and linearize the gain schedules in an effort to achieve maximum system reliability. The

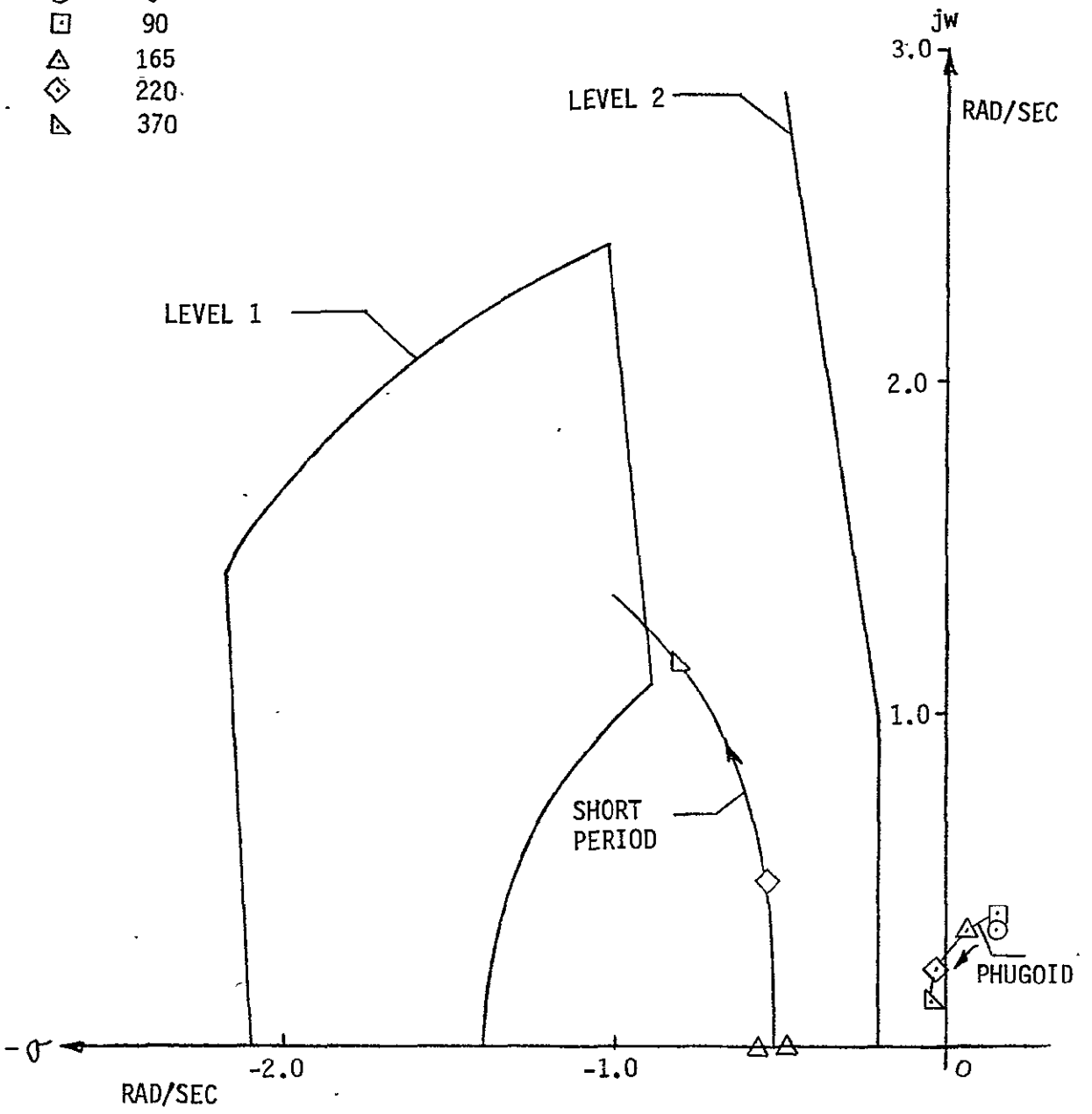

DYNAMIC STABILITY CRITERIA

UNAUGMENTED SYSTEM

LONGITUDINAL

FIGURE 4.1

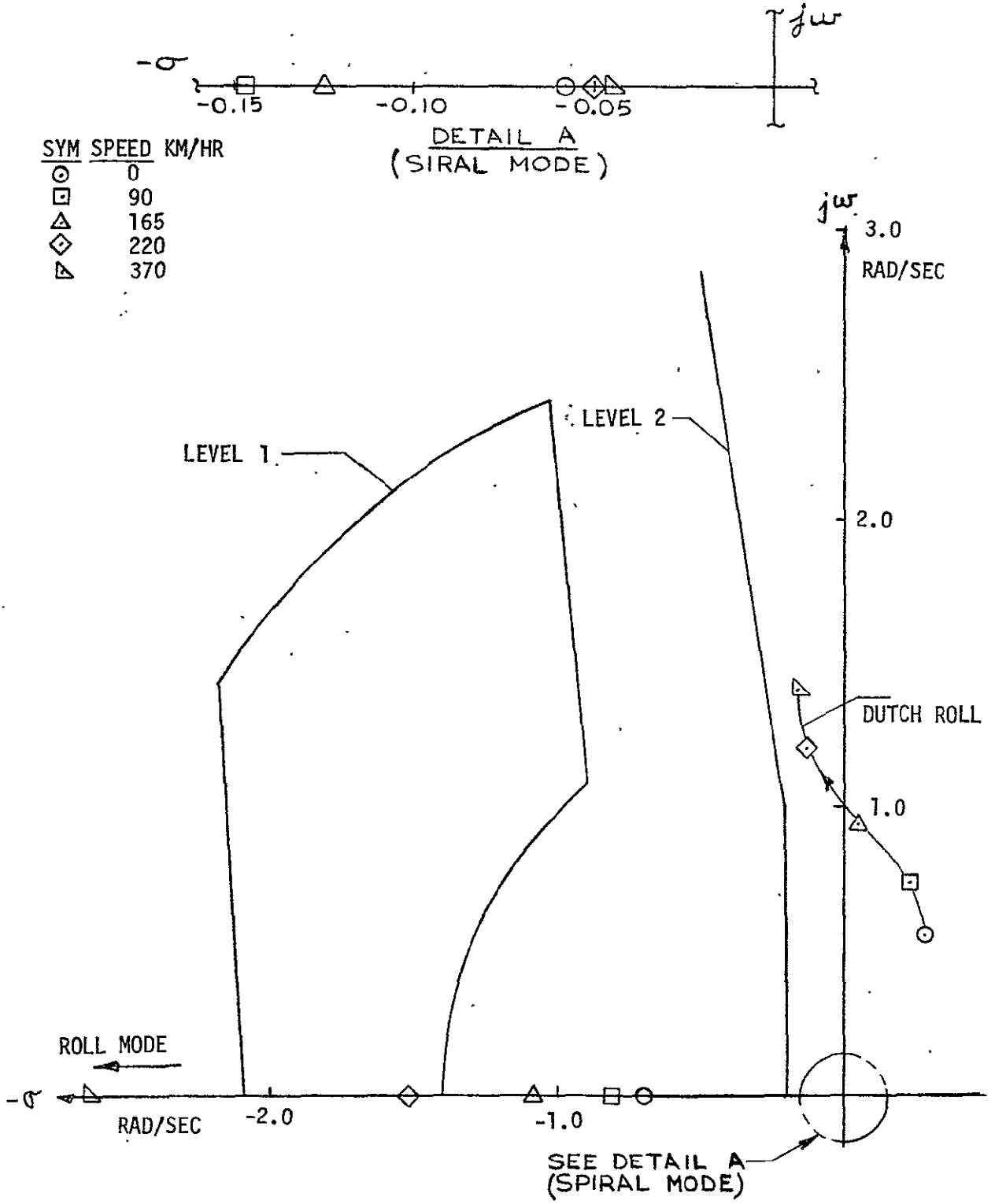

DYNAMIC STABILITY CRITERIA

UNAUGMENTED SYSTEM

LATERAL

FIGURE 4.2

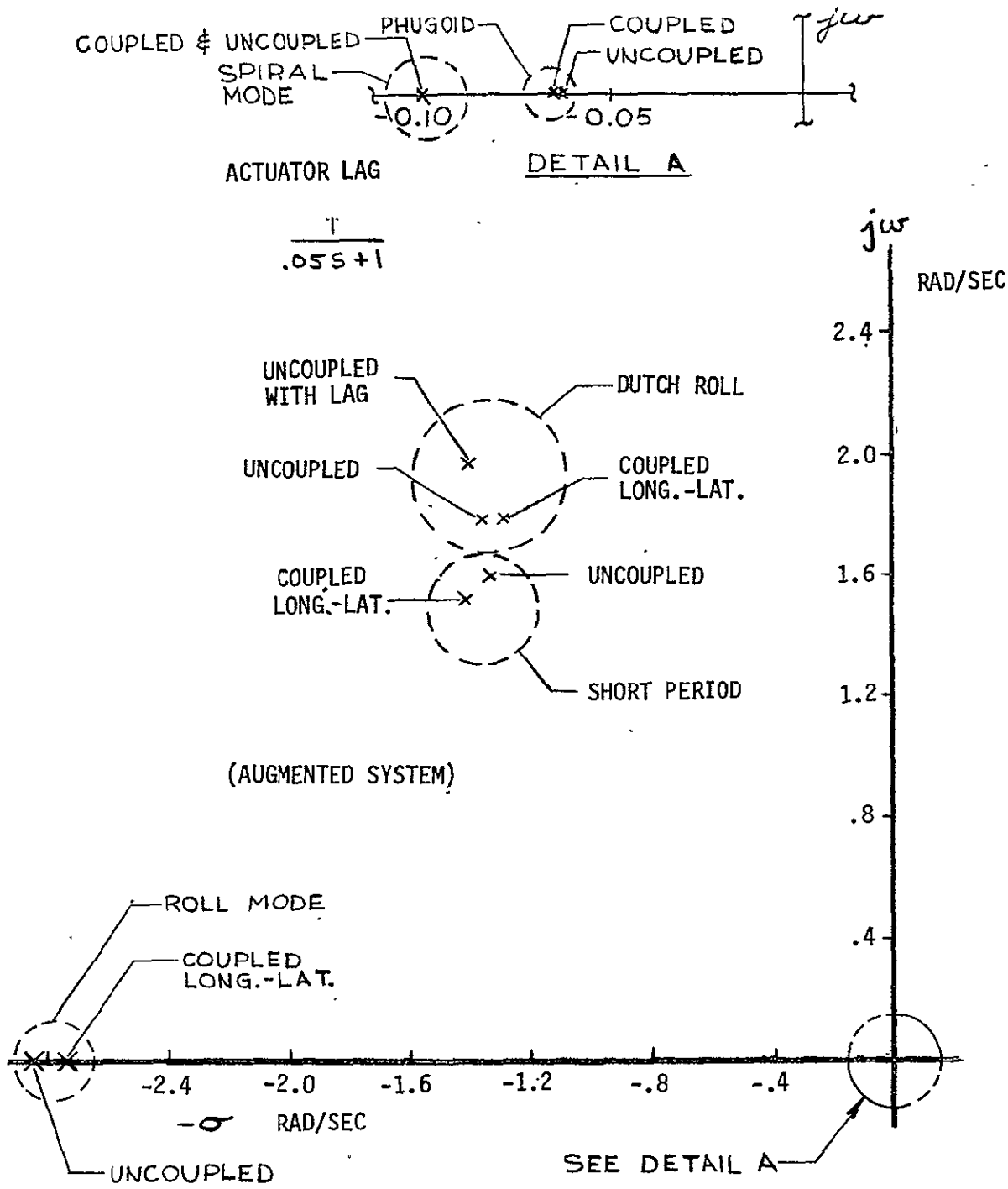

ROOT ANALYSIS - HOVER

ACTUATOR LAG AND LATERAL - LONGITUDINAL COUPLING

FIGURE 4.3

overall stability augmentation system configuration is shown in Figure 4.4. The individual lateral and longitudinal systems are shown in Figure 4.5. The selected gain schedules are shown on Figures 4.6 and 4.7. It was found that a constant gain matrix would not work. However, a simply-scheduled gain matrix is quite successful in meeting flying qualities goals. The gain matrix has 10 elements that account for feedback of pitch rate and attitude to the stabilizer and fan pitch; feedbacks of roll rate and attitude to the aileron and fan roll; and yaw rate to the rudder and yaw vanes. The gain matrix with the corresponding state variables (u, v, ...Ψ) and control vector of fan and aerodynamic control is:

$$\begin{matrix}\text{FAN}\\ \\ \\ \text{AERODYNAMIC}\\ \\ \end{matrix}\left\{\begin{matrix}\delta_{B\phi}\\ \delta_{B\theta}\\ \delta_{B\psi}\\ \delta_a\\ \delta_s\\ \delta_r\end{matrix}\right\} = \begin{bmatrix} 0 & 0 & 0 & K_p & K_\phi & 0 & 0 & 0 & 0\\ 0 & 0 & 0 & 0 & 0 & K_q & K_\theta & 0 & 0\\ 0 & 0 & 0 & 0 & 0 & 0 & 0 & K_r & 0\\ \hdashline 0 & 0 & 0 & K_p & K_\phi & 0 & 0 & 0 & 0\\ 0 & 0 & 0 & 0 & 0 & K_q & K_\theta & 0 & 0\\ 0 & 0 & 0 & 0 & 0 & 0 & 0 & K_r & 0\end{bmatrix} X \begin{bmatrix} u\\ v\\ w\\ p\\ q\\ \theta\\ r\\ \psi\end{bmatrix}$$

The feedback gains for angular rates and attitudes are determined according to either airspeed or cruise fan tilt angle. Aerodynamic surface gains will be scheduled vs dynamic pressure and the fan control gains will be scheduled vs nacelle tilt angle. A summary of the gains is shown in Figures 4.6 and 4.7 for the longitudinal and lateral directions respectively.

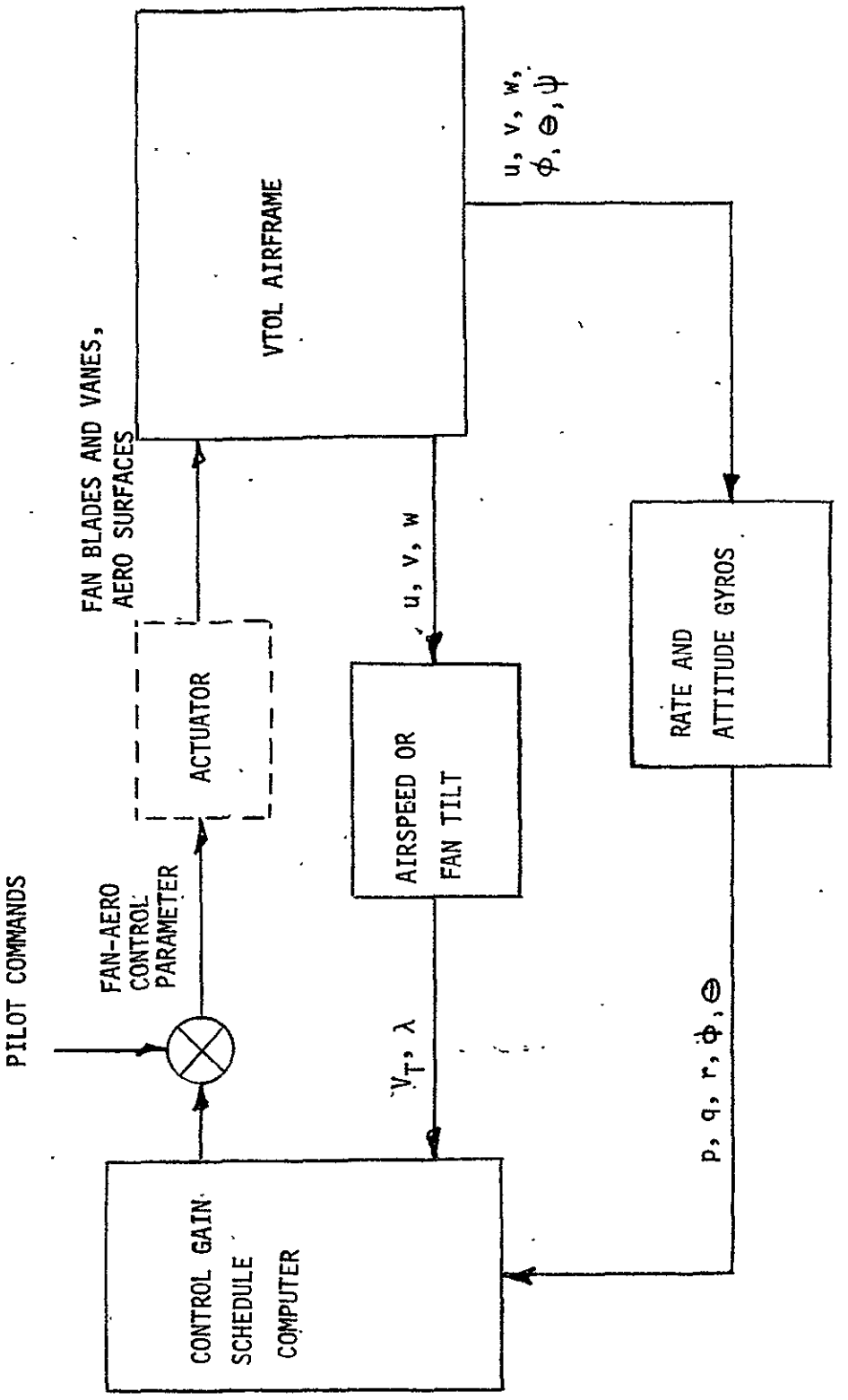

VTOL CONTROL SYSTEM

FIGURE 4.4

LATERAL

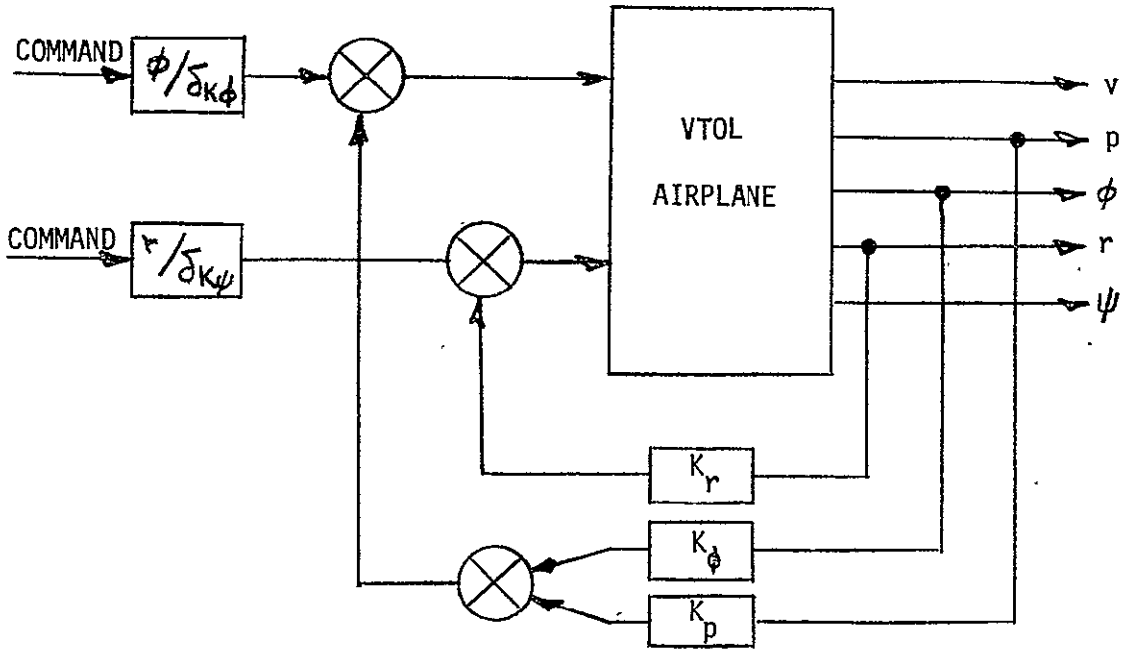

LONGITUDINAL

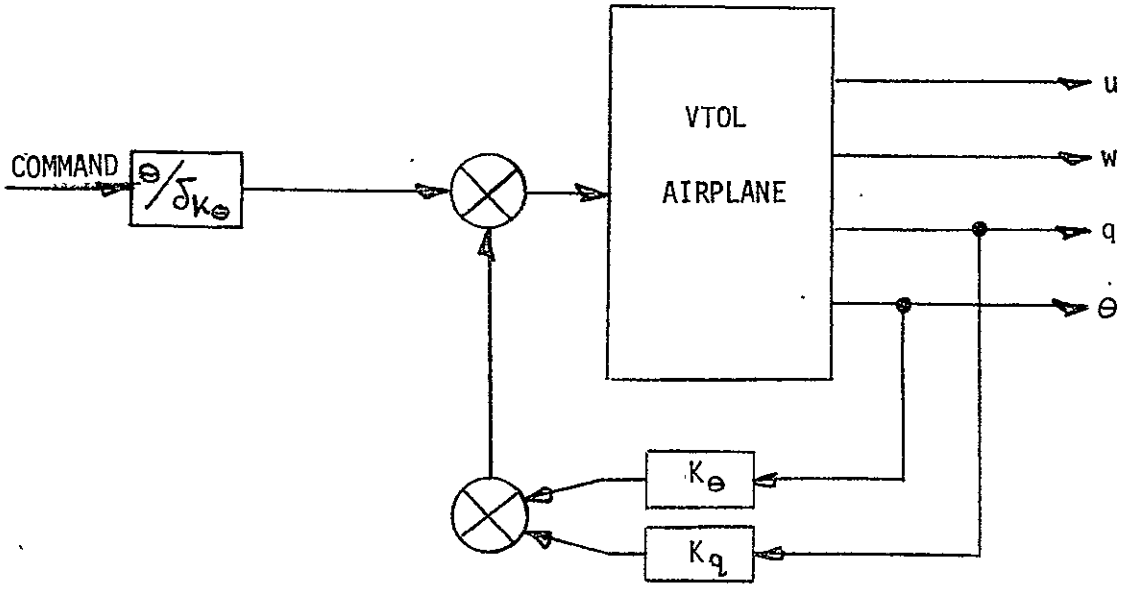

VTOL CONTROL SYSTEMS

FIGURE 4.5

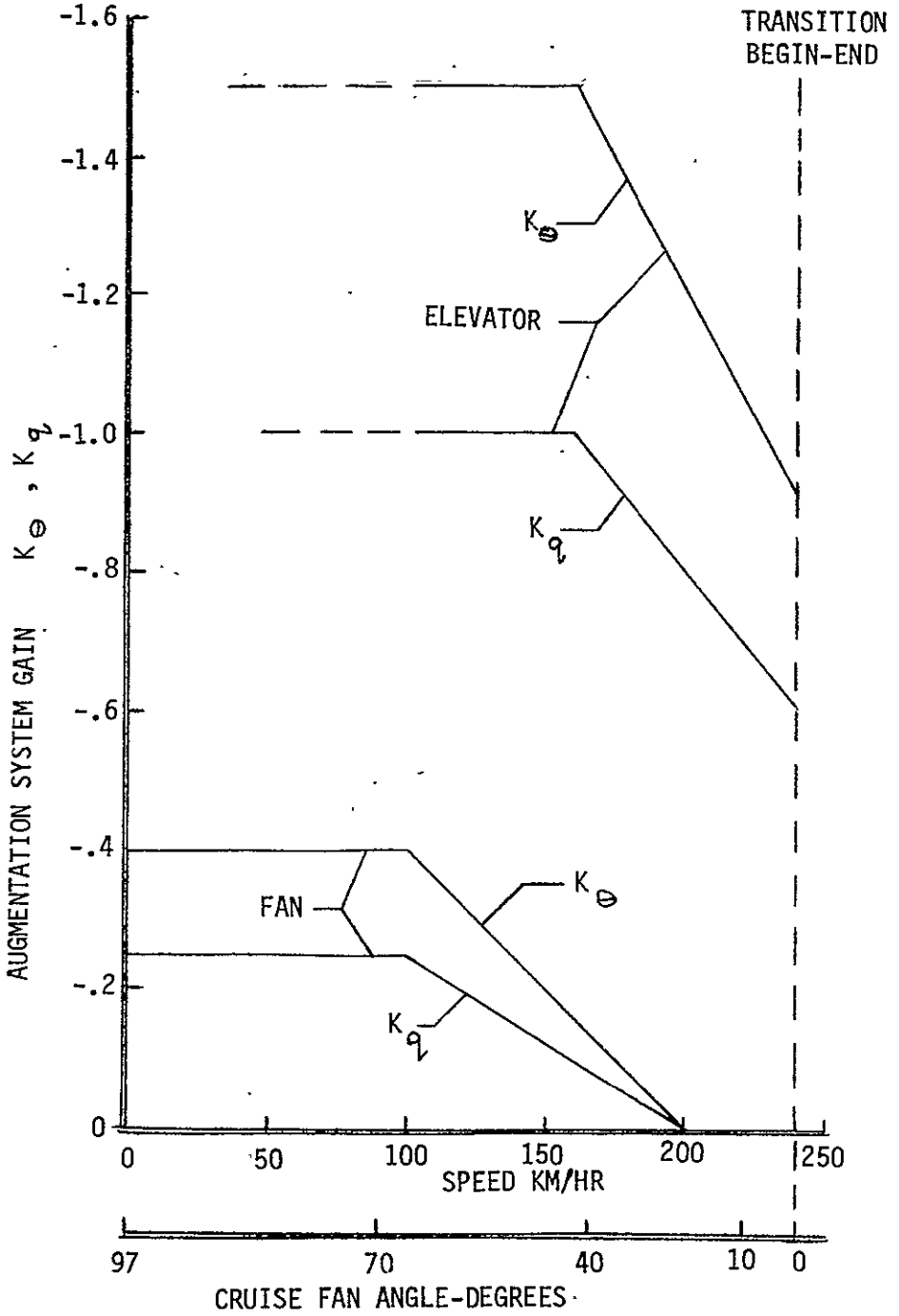

CONTROL GAIN SCHEDULE
LONGITUDINAL

FIGURE 4.6

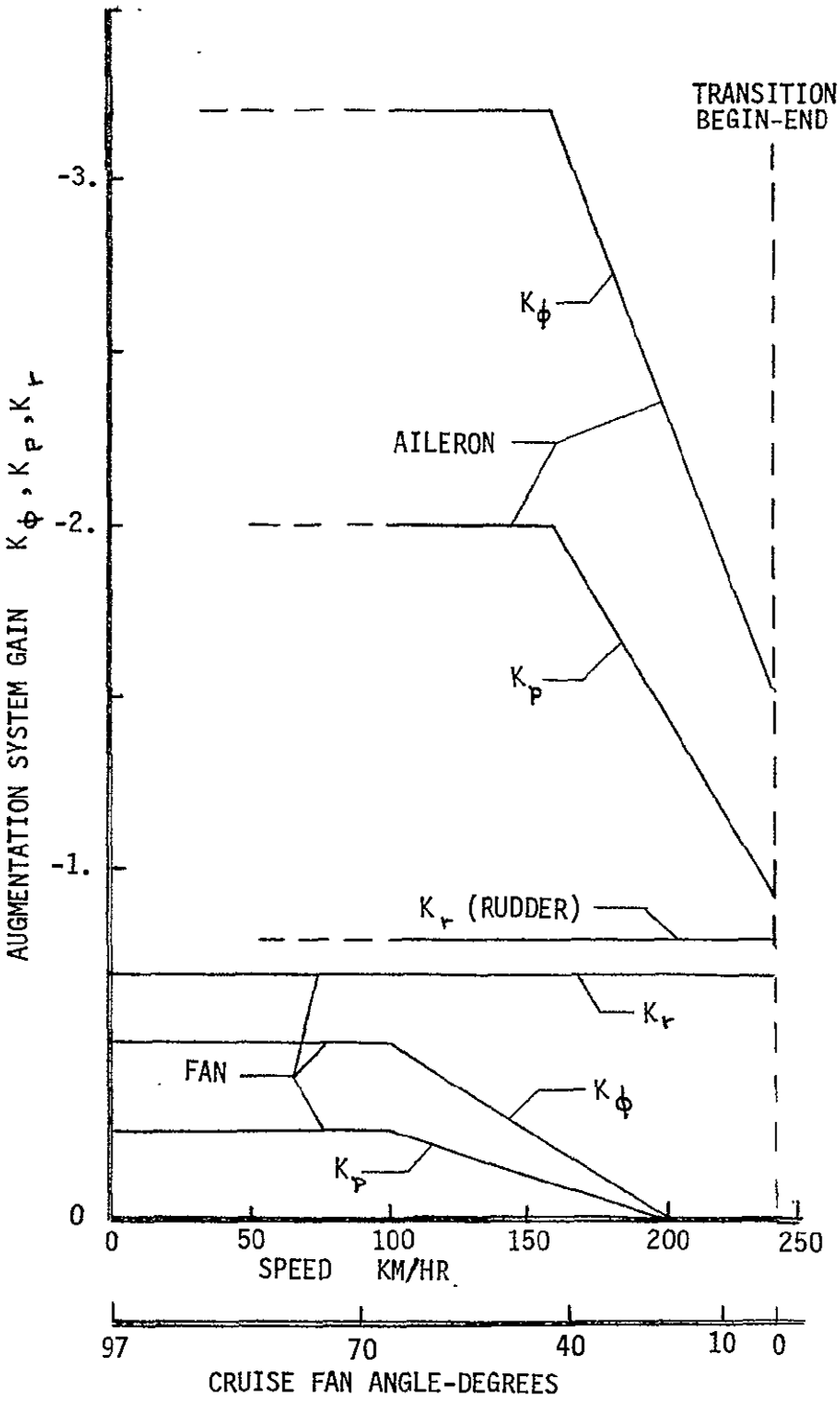

CONTROL GAIN SCHEDULE
LATERAL

FIGURE 4.7

Sufficient design margin was included in the scheduling of the gains to allow for deviations in gain resulting from errors in airspeed measurement and fan tilt angle and the response of the airplane to fan blade angle, nacelle tilt angle and engine power control changes.

As indicated in Figure 4.7, feedback to yaw vane control was used throughout the transition range in order to properly damp the dutch roll mode. At the lower speeds, feedback to the yaw vane is required because of low dynamic pressure. At higher speed yaw rate feedback was needed to help shift the open loop system zeros that were in close proximity to the unaugmented dutch roll eigenvalues. After the zeros were driven from the neighborhood of the poles, the poles were shifted into the desired frequency-damping band through roll and roll rate feedback using conventional aileron control.

The gain schedules shown in Figures 4.6 and 4.7 also correspond to the ability of the fan to control the system as related to fan tilt angle. At the higher speeds with low fan tilt, only marginal fan control can be obtained in pitch and roll due to the rotation of the thrust vector. However, the increase in dynamic pressure is sufficient at these airspeeds to permit transition to normal aerodynamic controls. Consequently at 200 km/hr, the gain schedule essentially, disengages fan blade angle control from the stability augmentation system.

4.3 System Response

The purpose of this section is to discuss the response characteristics of the augmented aircraft to pilot commands. However, it is emphasized that only generalizations can be stated herein inasmuch as the type of control system that will ultimately be used can only be determined with additional work largely oriented toward a pilot controlled flight simulator representation of the aircraft. Therefore, it is sufficient to say that the SAS system specified herein was derived primarily from stability considerations.

The responses that are shown for the hover and 90 km/hr are based on pitch and roll attitude commands and yaw rate commands. Previous studies (Ref. 8) of V/STOL type aircraft have generally indicated that attitude type systems are more desirable than rate systems at the lower speeds. As the V/STOL accelerates to the higher speed end of the transition range, the aircraft should react to stick commands as a rate type system which is typical for normal aircraft control systems.

The effect of a first order .05 second time constant actuator in the fan blade and vane control systems was also investigated and is shown in Figure 4.2 for hover condition root locus plot of system poles. The actuator pole is thus shown to be sufficiently far removed from the other system open loop poles to cause little effect on the eigenvalves. The actuator was not included in any response analyses.

4.3.1 Hover Response

The aircraft responses to control inputs are shown in Figures 4.8. through 4.14 for the SAS on condition. The flight control law equivalency is an attitude command in pitch and roll and a rate command system in yaw. All responses are for a 0.1 unit step stick input to either the fan blades for pitch and roll or fan vanes for yaw.

The longitudinal responses illustrates the effect of an aft stick input. As indicated in Figure 4.8. the airplane reaches and stabilizes at the final attitude in about 2 seconds with minimal overshoot. The resulting aft acceleration and sink rate shown are proportional to the attitude and result from the sine-cosine effect onthe gross thrust term relative to gravity. However, the pilot can be expected to compensate in such a situation by increasing the total fan thrust.

The response of the aircraft to a roll attitude command is shown in Figure 4.9. The roll attitude reaches a maximum of about 0.2 radians

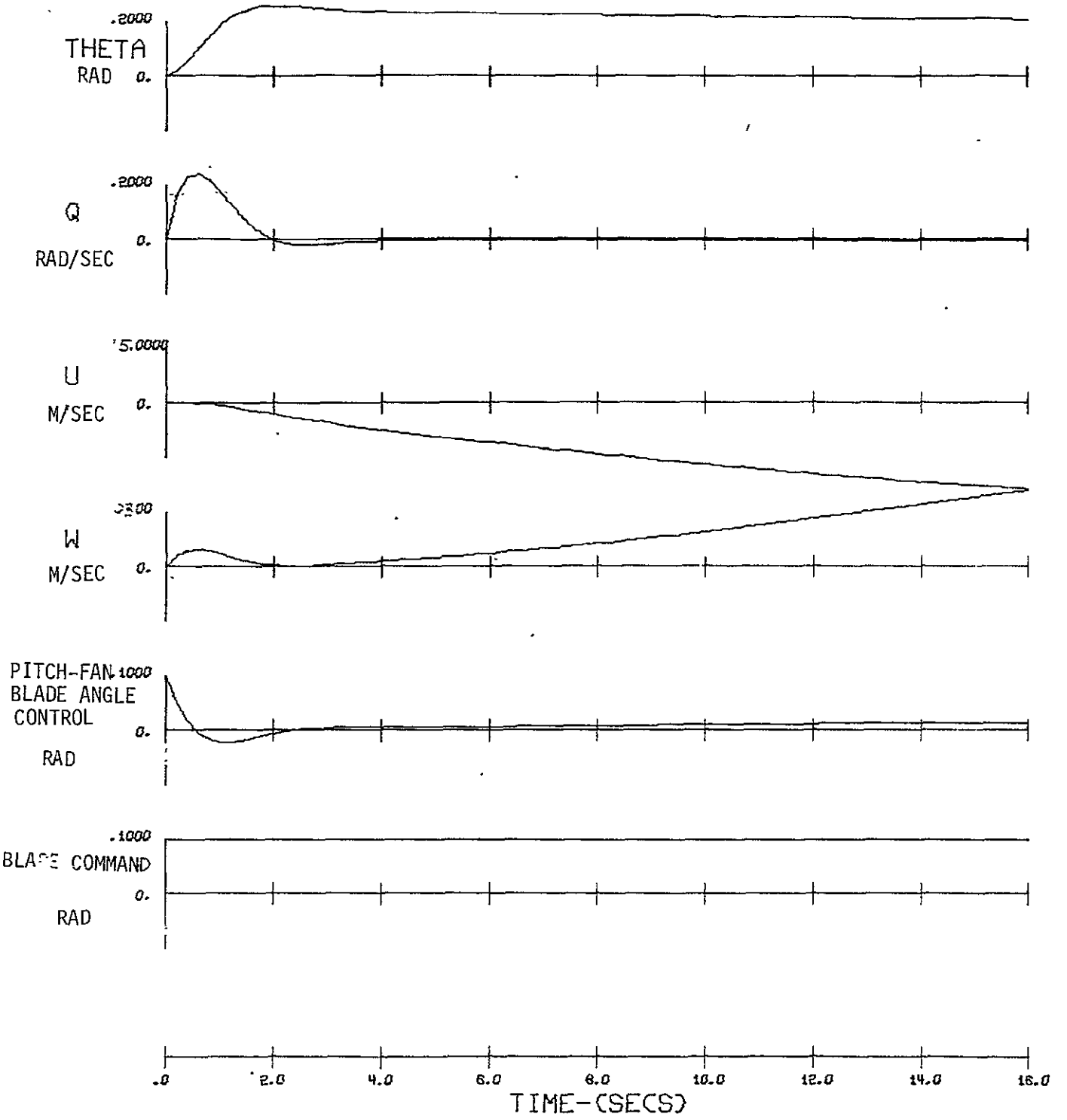

LONGITUDINAL RESPONSE

HOVER-SAS ON

PITCH-FAN BLADE COMMAND

FIGURE 4.8

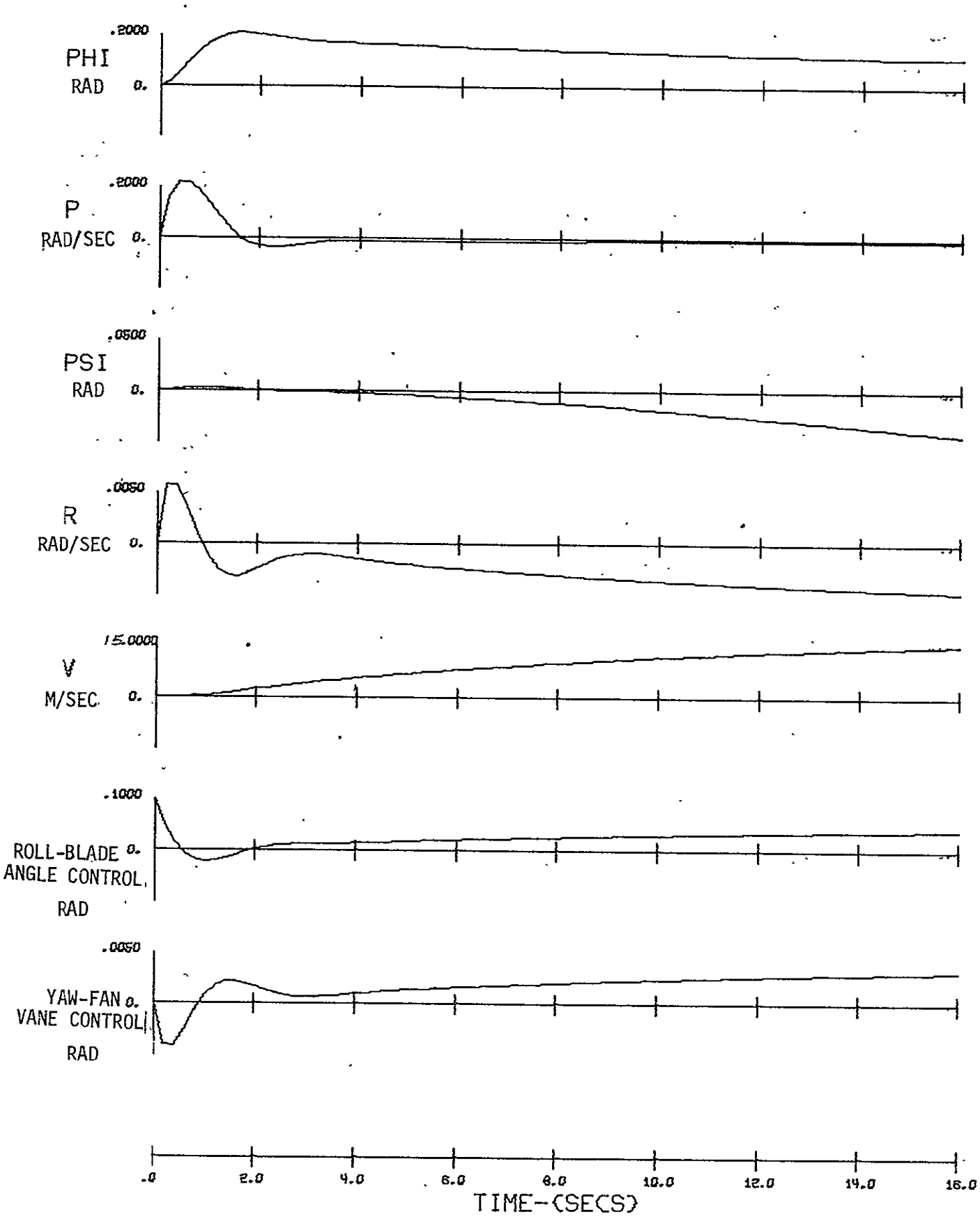

LATERAL RESPONSE

HOVER-SAS ON
ROLL-FAN BLADE COMMAND

FIGURE 4.9

in 1.5 seconds following which the roll attitude decreases until a final roll attitude that is 60 percent of the maximum is reached. However, the pilot response to this characteristic would be to increase the roll stick input if the roll attitude is to be maintained for more than a few seconds. Some sideslip occurs due to both cross axis coupling from fan inlet momentum and control coupling from the fan geometry. Unless the roll is maintained for a long time the sideslip characteristic should not be undesirable.

Compensation was added to the fan blade control system to improve the roll attitude response performance as shown in Figure 4.10. The improvement was achieved by using a lead-lag filter to shift the pole responsible for the decrease in roll attitude to a location further out along the $-\sigma$ axis to both decrease the time constant and amplitude of the pole. The new pole representing the filter response characteristic does not have a significant component in the aircraft response. This exercise was performed to demonstrate the possible improvement that can be achieved by special tailoring of the control system. However, the improvement obtained must be balanced against the additional problems introduced for designing either a phase out schedule or method of shifting the filter poles and zeroes with airspeed.

Figure 4.11 shows the response of the aircraft to a command to the yaw vanes. A rapid yaw rate response occurs with a minimal amount of roll coupling and a low lateral velocity response. The roll coupling that exists is due to the vertical offset of thrust of the yaw vane reaction point in all three fans. The side velocity that then occurs is due to the roll attitude as the vane deflections for yaw control have been designed to produce a net zero side force. Both the roll and side velocity are sufficiently small that a pilot correction would not be required.

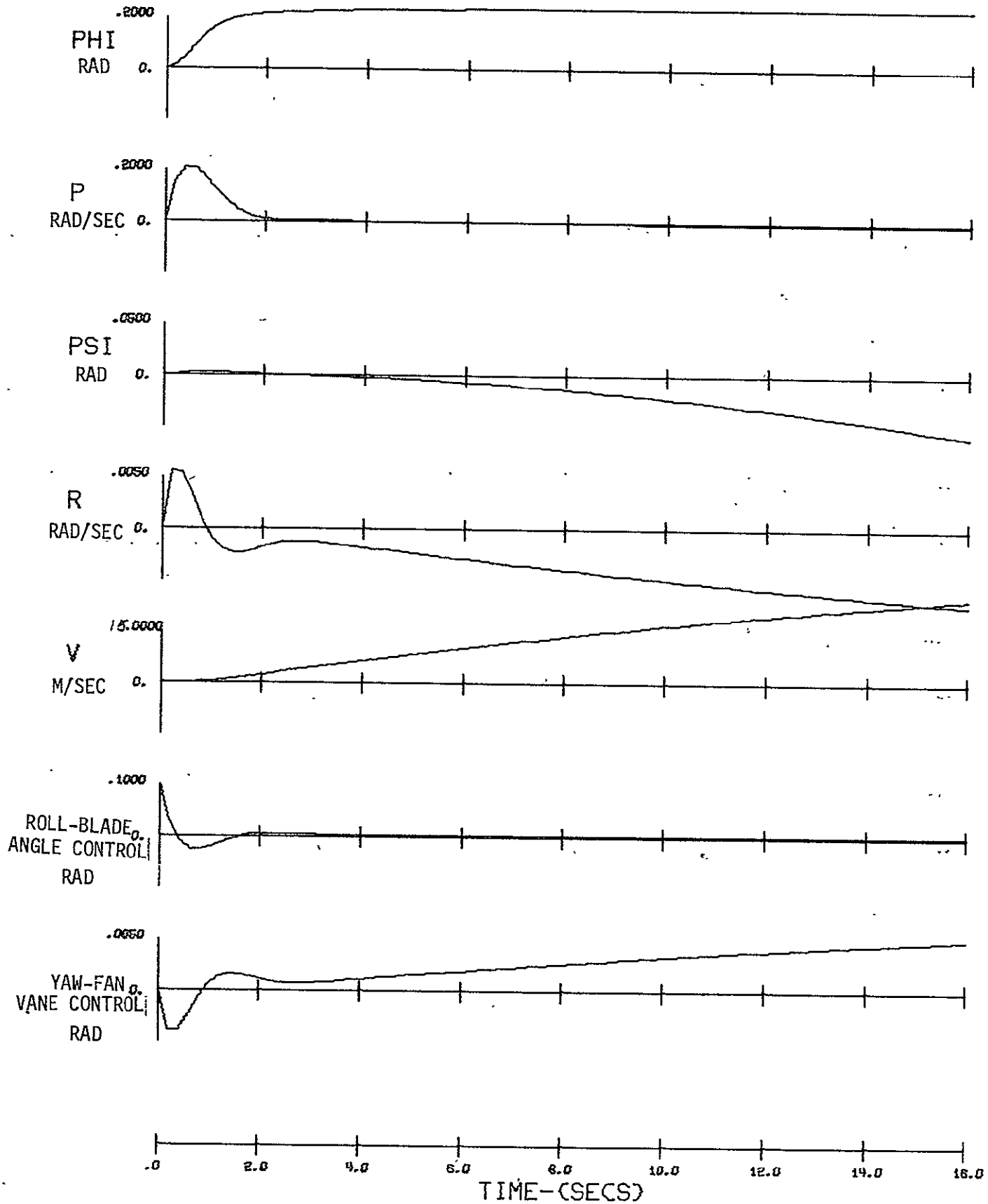

LATERAL RESPONSE
HOVER-SAS ON
ROLL-FAN BLADE COMMAND

FIGURE 4.10

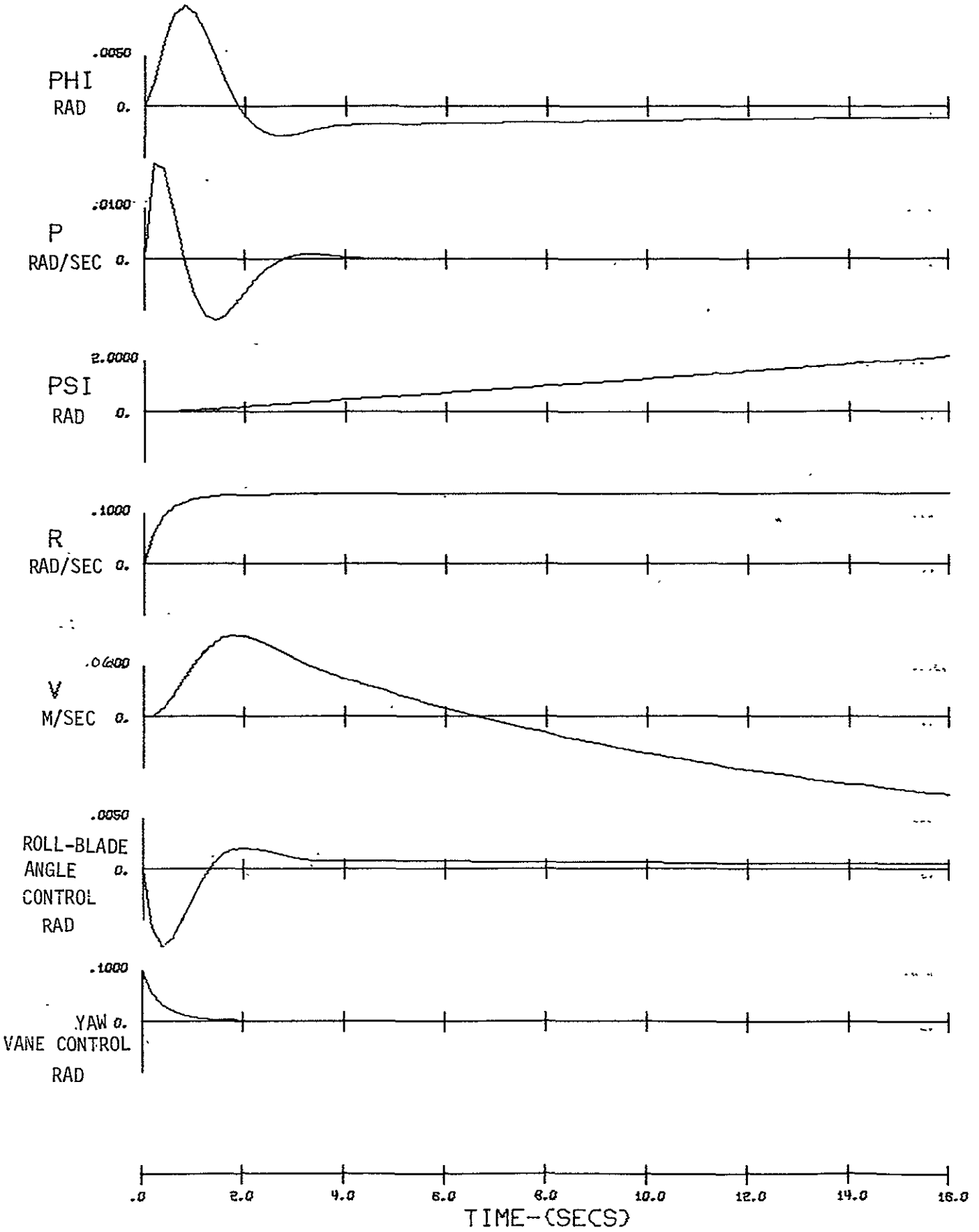

DIRECTIONAL RESPONSE

HOVER-SAS ON
YAW-FAN VANE COMMAND

FIGURE 4.11

4.3.2 90 Km/Hr Responses

The responses at 90 km/hr are similar to the responses at hover with the exception that the aerodynamics on the aircraft are beginning to contribute to the overall response. However, insufficient control authority exists through the aircraft rudder, stabilizer and ailerons to permit any effective control or stability augmentation using these surfaces. Therefore, the same control inputs are used here as were used for the hover response analysis. Time histories of airplane longitudinal, lateral and directional responses are shown on Figures 4.12, 4.13, and 4.14 respectively.

The longitudinal response to step command at 90 km/hr results in a response having characteristics very similar to the hover condition as shown by comparing Figure 4.12 with Figure 4.8. The major difference is the change in the aircraft body axis velocity components. In the inertial reference frame, the incremental velocity differences between the two conditions are small.

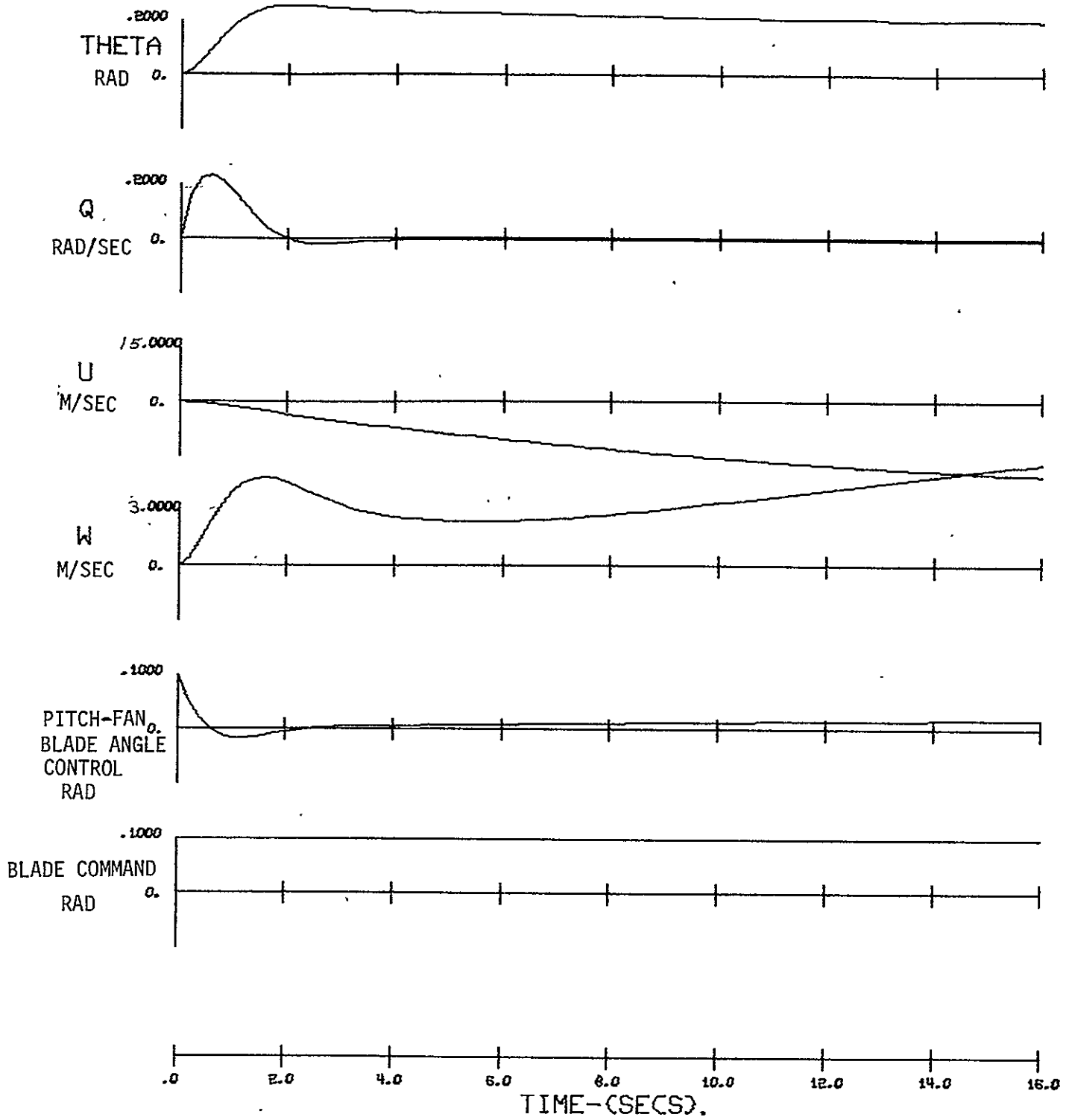

LONGITUDINAL RESPONSE

90 Km/Hr - SAS ON
PITCH-FAN BLADE COMMAND

FIGURE 4.12

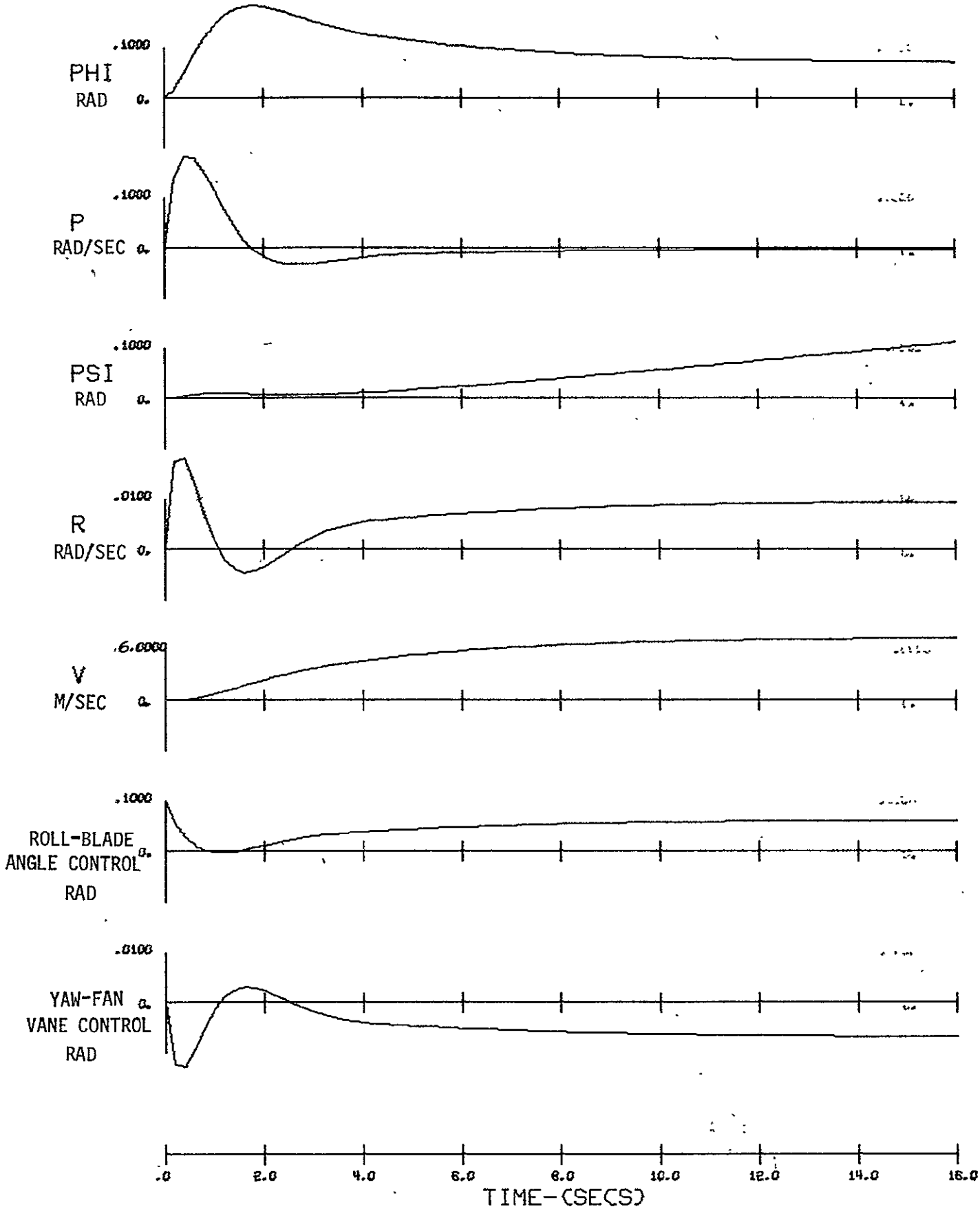

LATERAL RESPONSE

90 Km/Hr - SAS ON

ROLL-FAN BLADE COMMAND

FIGURE 4.13

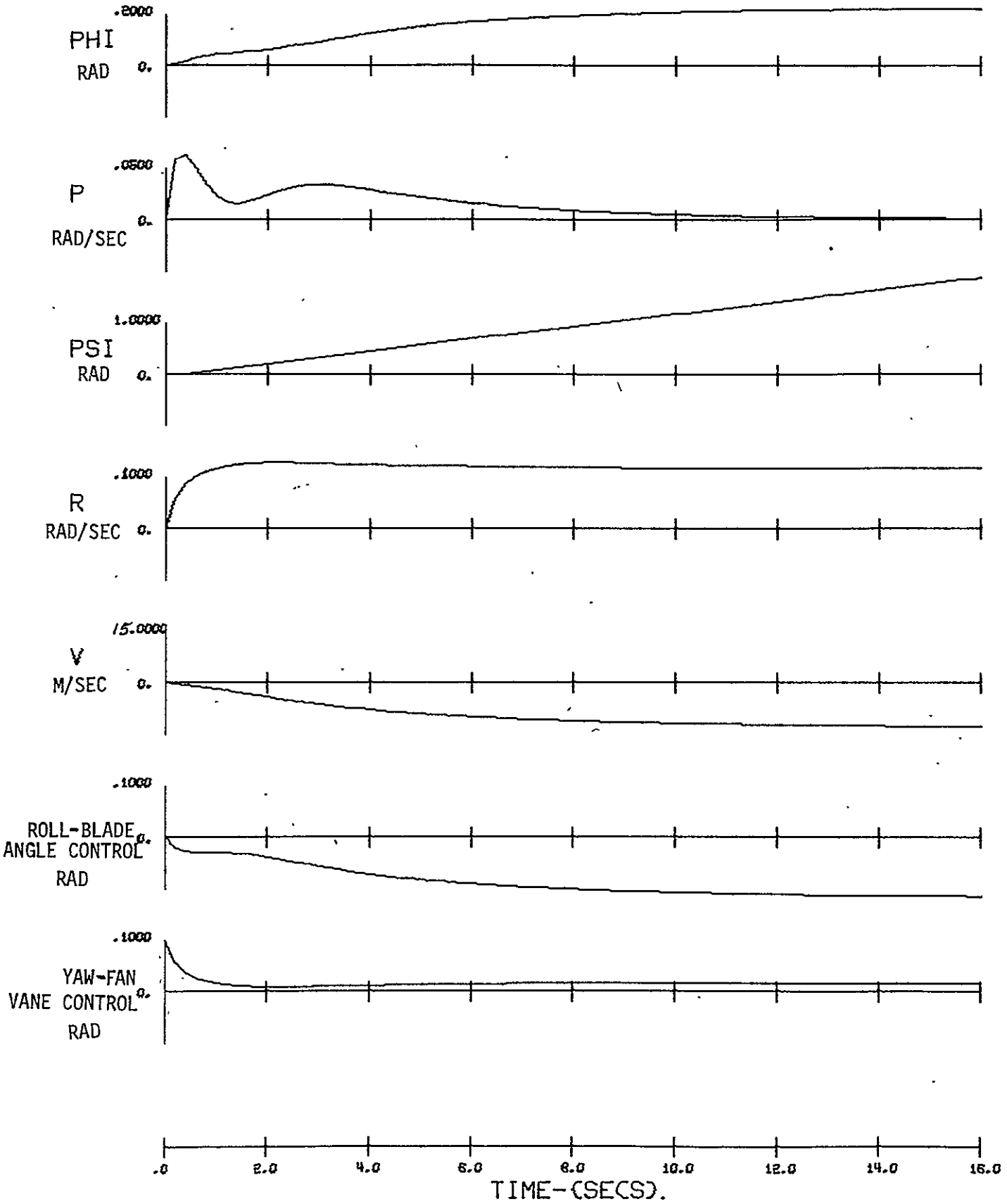

DIRECTIONAL RESPONSE

90 Km/Hr - SAS ON
YAW RATE-FAN VANE COMMAND

FIGURE 4.14

5.0 FAILURE ANALYSIS

The purpose of the failure analysis is to determine the criticality of a particular control system element. The analysis will point out those elements which must be designed fail safe or where back-up systems are required, and those elements where failure will cause only a marginal increase in pilot work load. The failure conditions examined in the following sections were all for the hover condition which is most critical for the following reasons: (1) All control power must be applied through the fans as there is no forward velocity for aerodynamic controls, (2) the airplane has either just taken off or is about to land and is in an attitude where a severe control or power transient may cause large aircraft excursions resulting in impact with the ground. For the analysis, only single failure occurences were considered.

5.1 Engine Failure

Failure of a single engine was investigated assuming an engine control system with both engine RPM feedback and total fan power feedback that controls the fan blade angle. The control system response characteristics for the engine failure condition are shown in Figure 5.1. The dominant feature of the response is that as the fan slows down, the fan blade angle increases and partially compensates for the loss in fan thrust with fan RPM decrease. The inertia of the propulsion system effectively helps drive the fans immediately after the failure until power is increased sufficiently on the remaining two engines to restore full RPMs. The net change in total fan thrust is shown in Figure 5.2.

The net effect of the RPM decrease and blade angle increase on the VTOL response is indicated in Figure 5.3. The net response is small as the impulse that is equivalent to the engine failure is only approximately 2500 Newtons-sec with a resulting peak vertical acceleration of .02g. The response does not affect airplane attitude since the distribution

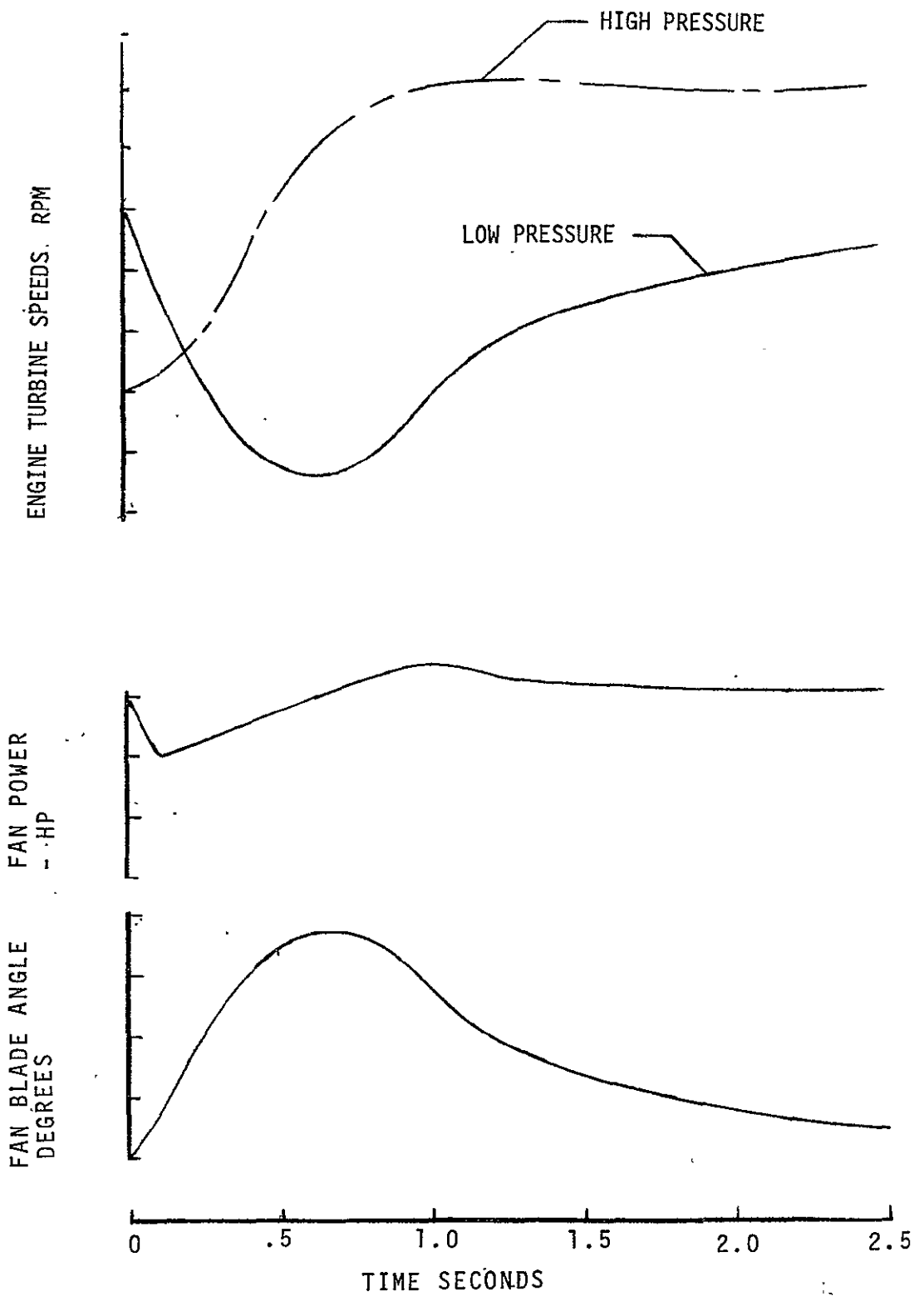

FAN AND POWER TURBINE RESPONSE
TO GAS GENERATOR FAILURE

FIGURE 5.1

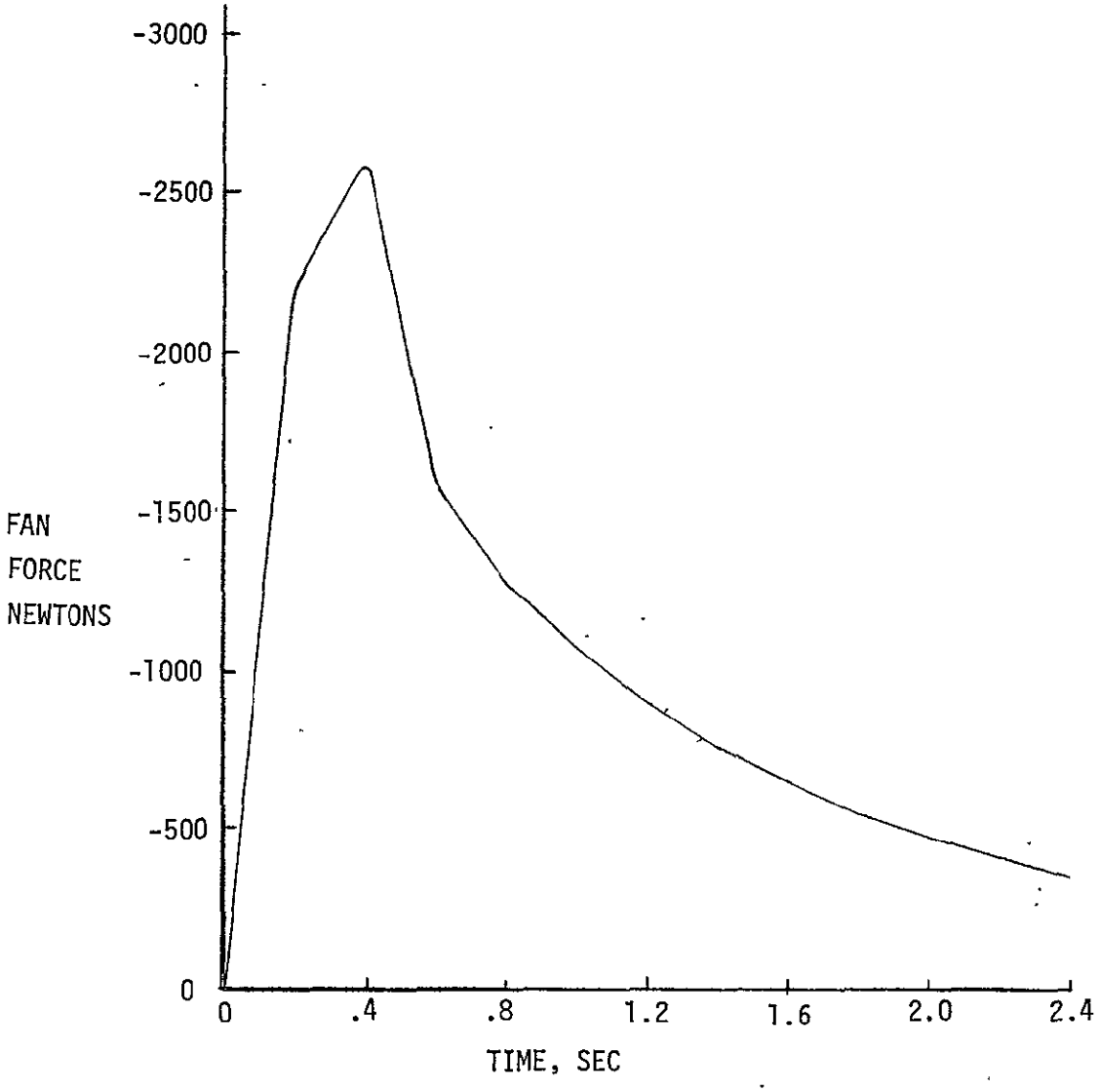

CHANGE IN TOTAL
FAN THRUST DUE TO
ENGINE FAILURE

FIGURE 5.2

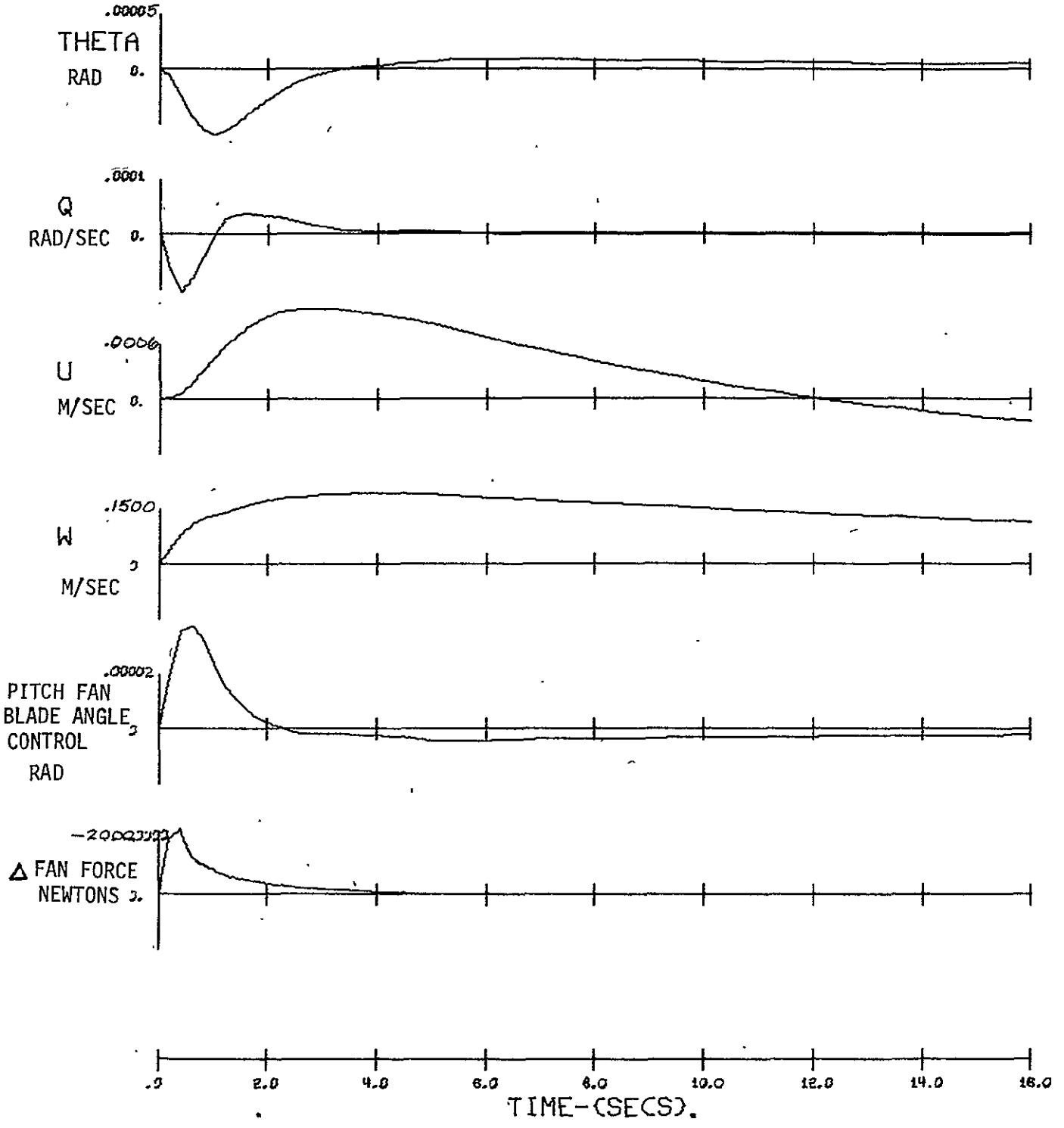

SINGLE ENGINE FAILURE
LONGITUDINAL RESPONSE

FIGURE 5.3

of power to the individual fans is maintained thereby preventing any non-symmetric response.

5.2 Cruise Fan Blade Lockup - Roll and Pitch Control

Both the roll and pitch axis control are affected by lockup in either cruise fan. For the SAS on condition with fan lockup, the two pairs of complex poles move towards the origin. The damping of the poles remains the same. The handling characteristics or VTOL response will experience dome degradation, but will remain flyable. Figure 5.4 shows the nominal system poles for the SAS on and the poles for the blade lockup condition (on the number one fan).

5.3 Nose Fan Vane Lockup - Yaw Control

The most severe condition for failure that effects the yaw axis is a lockup of the nose fan vanes. Control is then affected by the cruise fan vanes, without a compensating side force from the nose fan vanes to prevent a side velocity. Yaw control sensitivity at hover is reduced from 0.15 RAD/SEC^2/IN to 0.05 RAD/SEC^2/IN and maximum control power is reduced from 0.4 RAD/SEC^2 to 0.2 RAD/SEC^2. The reduced levels of control sensitivity and power are still adequate and meet level 2 design guidelines (see Reference 19). The nose fan vane jam effect on the dynamic modal qualities is indicated by the values of the poles as shown in Figure 5.4. Of somewhat less significance than the nose fan vane lockup is the lockup of the yaw vane on either cruise fan.

5.4 Sensor Failure - System Stability

The most critical condition results from failure of either the pitch rate gyro or roll rate gyro for the hover condition. The failures will produce a very low damped oscillation at 2.4 rad/sec (Figure 5.5) until the VTOL speed increases to around 90 km/hr. The handling properties for this failure condition are not satisfactory inasmuch as damping is less than that required for Level 2 operation.

Failure of the pitch and roll attitude gyros will also produce a lightly damped oscillation, but at a sufficiently low frequency that the pilot will

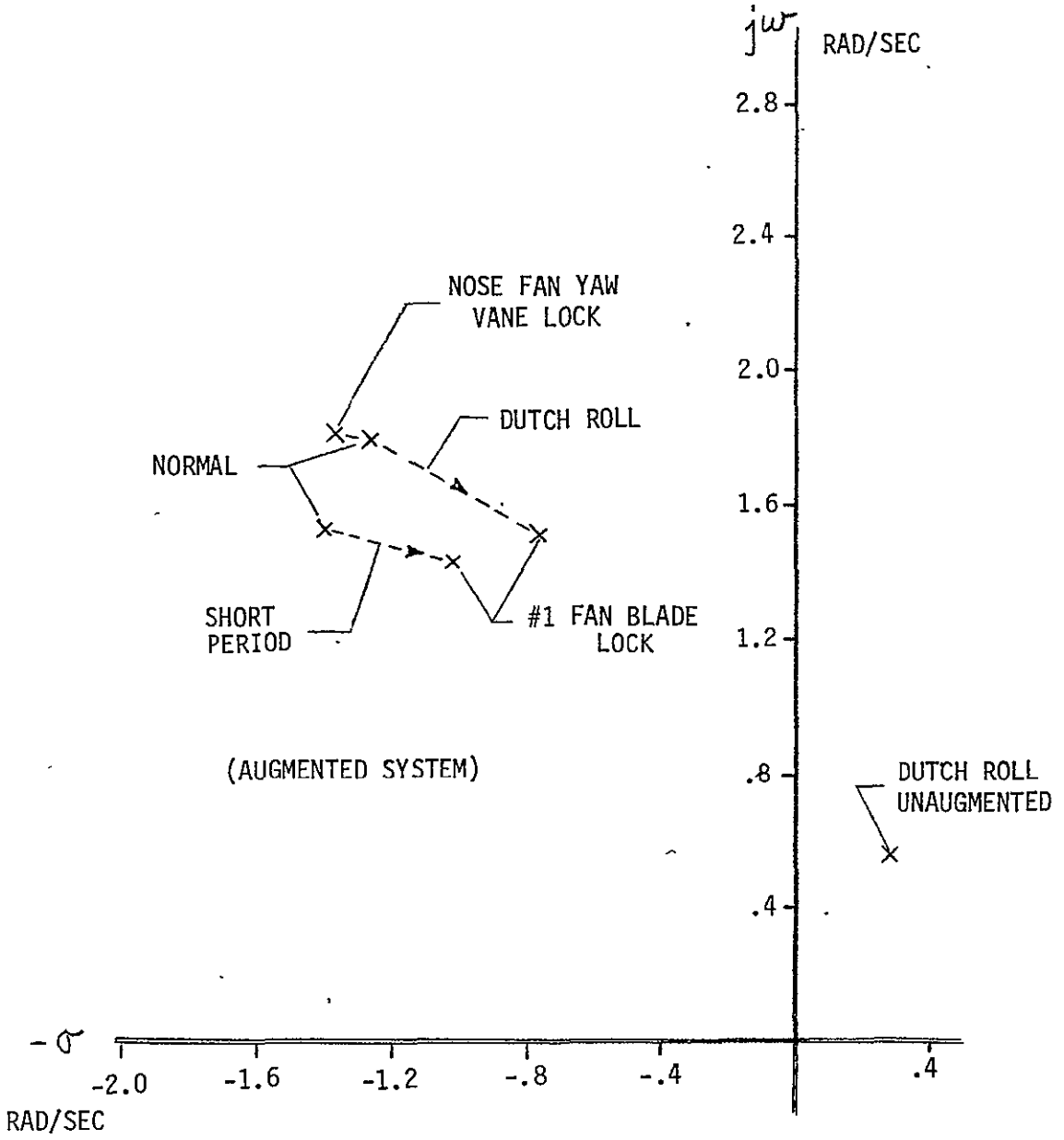

NOTE: POLES LOCATED ALONG AXIS
DO NOT SHOW SIGNIFICANT
SHIFT ON BLADE OR VANE LOCK

FAN BLADE AND VANE LOCK
ROOT ANALYSIS - HOVER

FIGURE 5.4

be able to satisfactorily control the airplane. The attitude gyro failures also become less critical as speed increases, except for the one root for the longitudinal condition as shown in Figure 5.5. This mode is easily controllable due to the low rate of divergence. The effect of yaw rate gyro feedback was also investigated but was found to have only a minor effect on the oscillatory roots.

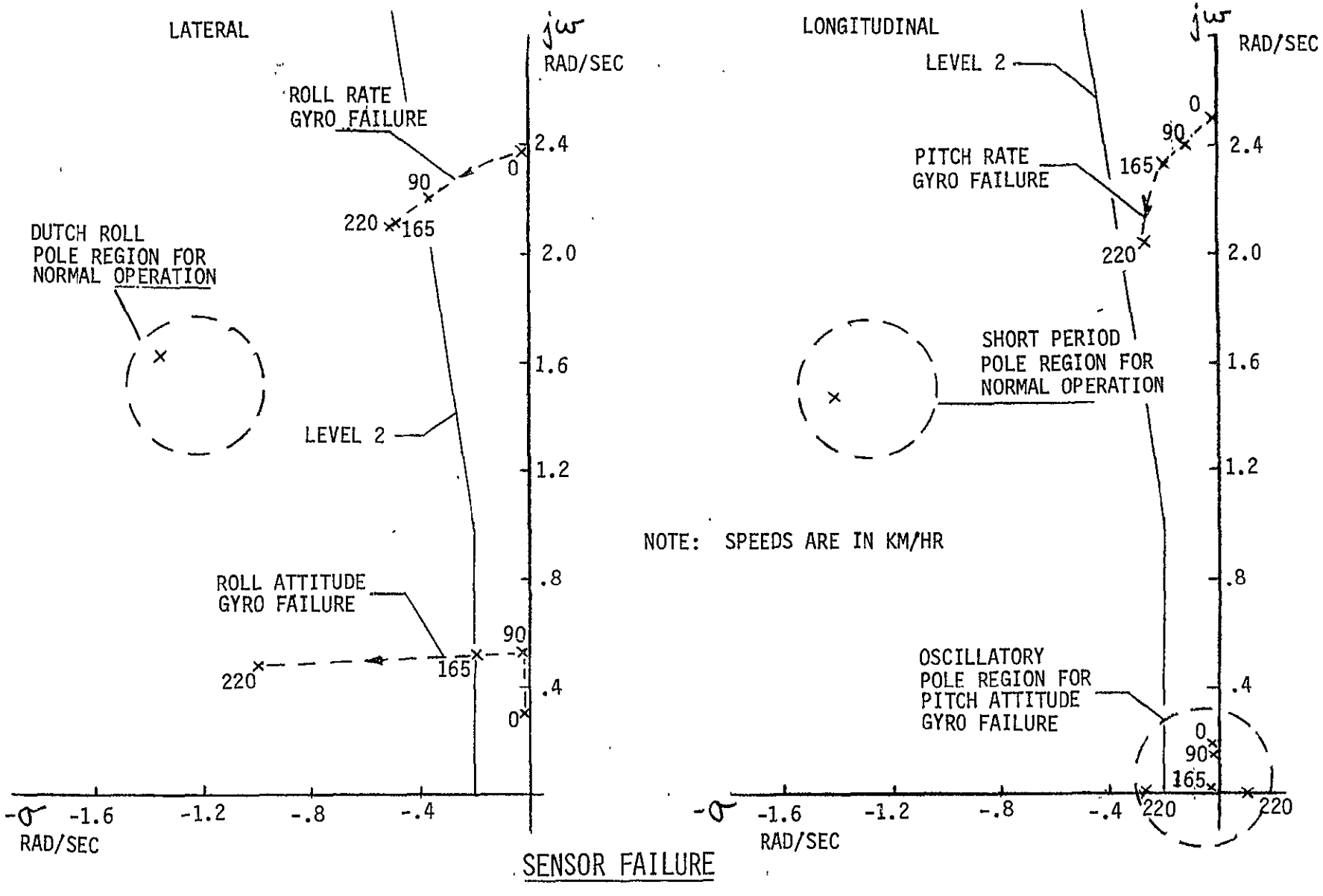

SENSOR FAILURE

FIGURE 5.5

6.0 REFERENCES, SYMBOLS AND DEFINITIONS

6.1 References

1. USAF Stability and Control DATCOM, Oct. 1960, Revised Jan. 1975.

2. Dynamics of Flight, B. Etkin, John Wiley & Sons, 1959.

3. NACA TR921, Theoretical Symmetric Span Loading at Subsonic Speeds for Wings Having Arbitrary Plan Form, J. DeYoung and C. W. Harper

4. Agard Report No. 577 Part II, "V/STOL Handling Documentation, June 1973.

5. MIL F-83000, Military Specification - Flying Qualities of Piloted V/STOL Aircraft, Dec. 1970.

6. AFFDL TR-70-88, Background Information and Users Guide for MIL F-83300 Military . . . . . March 1971.

7. NASA TN D 7191; Aerodyanmic Characteristics of a Vectored-Thrust V/STOL Fighter in the Transition-Speed Range; May 1973; LRC.

8. NASA CR114557; Piloted Simulation of the Boeing Model R984-33V/STOL Research Aircraft-Vol I - Analysis of the Flight Control System and Flight Characteristics, W. M. Eldridge, A. A. Lambregts, R.E. Spitzer. Feb. 73

9. Gambucci, B. J., Aoyagi, K., and Rolls, L.S.: Wind Tunnel Investigation of a Large-Scale Model of a Lift/Cruise Fan V/STOL Aircraft., May 1976 (NASA TMX 73, 139).

10. Aoyagi, K., Hickey, D.H., and DeSavigny, R.A., Aerodynamic Characteristics of a Large-Scale Model with a High Disk-Loading Lifting Fan Mounted in the Fuselage, 1961 (NASA TND-775).

11. Maki, Ralph L., and Hickey, D. H., Aerodynamics of a Fan-In-Fuselage Model, 1961 (NASA TND-789).

12. Grunwald, K. J., and Goodson, K. W., Aerodynamic Loads on an Isolated Shrouded-Propeller Configuration for Angles of Attack from -10^{o} to 110^{o}, 1962 (NASA TND-995).

13. Kirk, J. V., Hickey, D. H., and Hall, L.P., Aerodynamic Characteristics of a Full-Scale Fan-In-Wing Model Including Results in Ground Effect with Nose-Fan Pitch Control, 1964 (NASA TND-2368).

14. Giulianetti, D. J., Biggers, J.C., and Corsiglia, V.R., Wind Tunnel Test of a Full-Scale, 1.1 Pressure Ratio, Ducted Lift-Cruise Fan, 1964 (NASA TND-2498).

15. Davenport, E. E., and Kuhn, R. E., Wind Tunnel-Wall Effects and Scale Effects on a VTOL Configuration with A Fan Mounted in the Fuselage, 1965 (NASA TND-2560).

16. Hall, L. P., Hickey, D. H., and Kirk, J. V., Aerodynamic Characteristics of a Large-Scale V/STOL Transport Model with Lift-Cruise Fans (NASA TND-4092).

17. Mineck, R. E., Aerodynamic Characteristics of a Vectored-Thrust V/STOL Fighter in the Transition - Speed Range, 1973 (NASA TND-7191).

18. Dr. Hoad, C. L. Gentry, Jr., Longitudinal Aerodynamics of a Low Wing Lift Fan Transport Including Hover Characteristics In and Out of Ground Effects.

19. NASA CR137976 (D180-20213-1), Follow-on Studies for Design of a Lift Cruise Fan Technology V/STOL Airplane, A. Arnold et al., Dec. 1976.

6.2 List Of Symbols and Definitions

SYMBOL	DEFINITION
A	state variable dynamic matrix
B	fan blade angle state/variable controls matrix
C_D	drag coefficient (non dimensional)
C_{D_α}	drag due to α (1/rad)
C_{D_q}	drag due to q (1/rad/sec)
C_{D_u}	drag due to u (non-dimensional)
C_{L_α}	lift coefficient due to α (1/rad)
C_L	Lift coefficient (non dimensional)
$C_{l_q}, C_{l_r}, C_{l_p}$	rolling moment coefficient due to pitch, yaw, and roll rate (1/rad/sec)
C_m, C_n	pitching and yawing moment coefficient
g	acceleration due to gravity (980.665 cm/sec^2)
G	control gear ratio
F_g	gross thrust (Newtons)
$F_{g_x}, F_{g_y}, F_{g_z}$	resultant x,y, and z components respectively of fan gross thrust Newtons
H	angular momentum ($kg\text{-}m^2/sec$)
Ix,Iy,Iz	vehicle inertias about x,y, and z body axes (kilogram-m^2)
jw	imaginary axis component of complex root (rad/sec)
K_r	augmentation gain in yaw (non dimensional)

K_{σ}	power effects factor for the fin
K_{ϕ}	augmentation gain in roll (non dimensional)
K_p	augmentation gain in roll rate (sec)
K_{θ}	augmentation gain in pitch (non dimensional)
K_q	augmentation gain in pitch rate (sec)
L_p	$\partial L / \partial p$
L,M,N	moments exerted on the vehicle about boyd x,y, and z axes respectively (Newton-M)
p,q,r	airplane roll, pitch, and yaw rate. Angular velocity about body x,y, and z axis, respectively (rad/sec)
NF,3	nose fan
LF,2	left fan
RF,1	right fan
S_W	wing area (M^2)
s,S	Laplace transform operator (1/sec)
Ts	static thrust
X,Y,Z	forces exerted on airplane along the x,y,z body axes (Newtons)
V_h	tail volume coefficient
V_J	jet-exit velocity (M/sec)
V	airspeed km/hr
WB	wing-body
ω_a	inlet airflow
α	airplane angle of attack (rad)
θ	airplane pitch angle (rad)
ρ	atmosphere density (kg/m^3)
β	sideslip angle (rad) & fan blade angle

σ	sidewash angles
δ	control element deflection (rad)
ϕ	airplane roll angle (rad)
ψ	airplane yaw angle (rad)
ϵ	downwash angle (rad)
Ω	angular speed rad/sec
τ	real axis component of complex root (rad/sec)
δ_a	aileron deflection (rad)
δ_s	stabilizer deflection (rad)
δ_r	rudder deflection (rad)
$\delta_{B\theta}$	fan pitch, powered pitch attitude control deflection (rad)
$\delta_{B\phi}$	fan roll, powered roll attitude control deflection (rad)
$\delta_{v\psi}$	vane yaw, powered yaw attitude control deflection (rad)
$\delta_{\dot{\lambda}}$	nacelle tilt angle control deflection
δ_{HP}	height control deflection

7.0 APPENDIX

7.1 Airplane Trim Conditions for Level Flight

The operating condition of the airplane at five flight speeds is described in this section. The operating conditions are computed by solving the 3 degrees of freedom equations of motion (axial force, normal force and pitching moment). The equations were solved for the independent variables listed below.

- Nose fan gross thrust
- Lift cruise fan gross thrust
- Nacelle tilt angle

The three equations of motion are non-homogeneous. The equations are not solvable in closed form, consequently they were programmed on a PDP -11 mini-computer and interatively solved using a Newton-Raphson convergence technique.

A force and moment free body diagram of the airplane is shown on Figure 7.1.

The detailed operating condition of the airplane is given on Figures 7.2. through 7.6. In each tabulation values are given for the following fourteen variables:

- Center of gravity
- Gross weight
- Airspeed
- Angle of attack
- Tail incidence
- Nacelle tilt angle
- Nose fan thrust
- l/c fan thrust

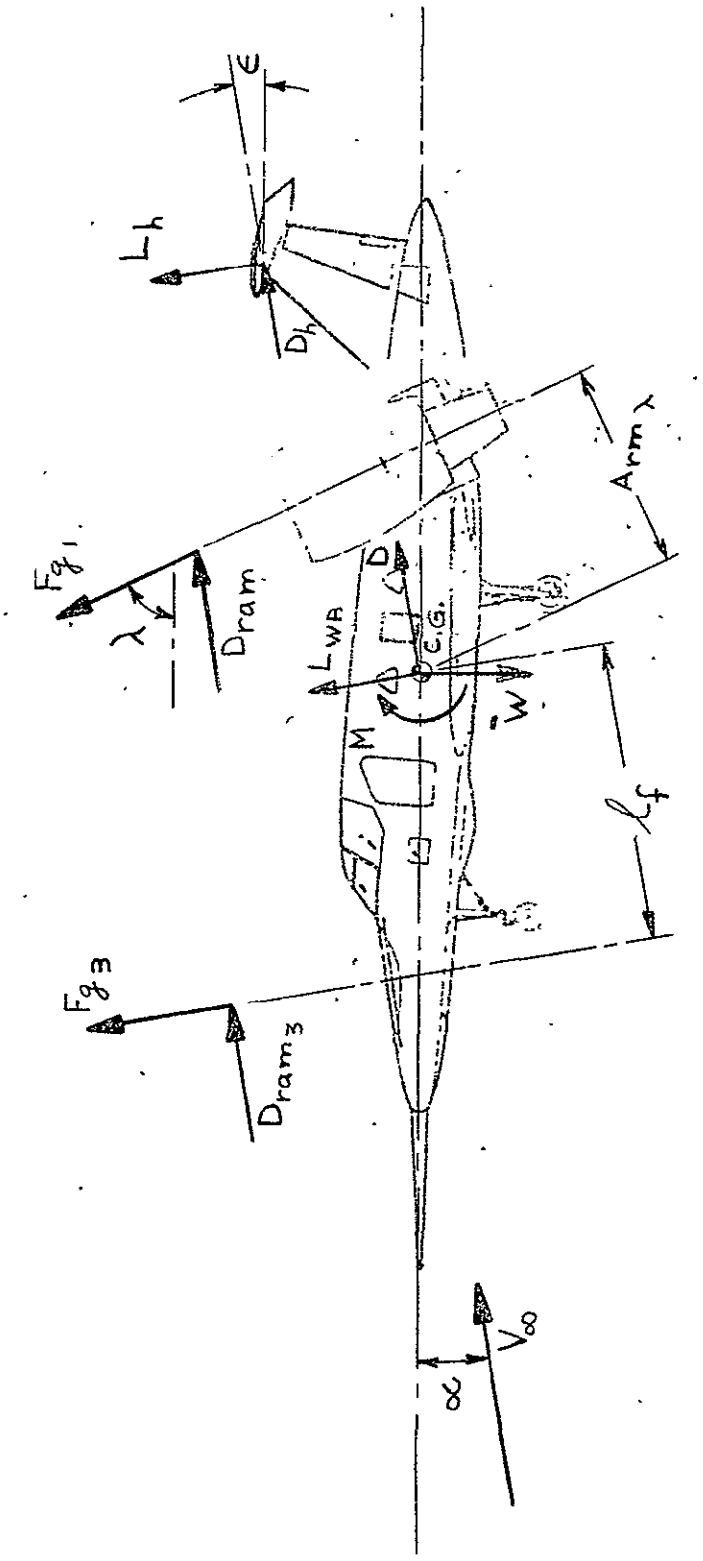

FREE BODY DIAGRAM

FIGURE 7.1

- o System shaft horsepower
- o Average engine speed
- o Fan blade angle
- o Fan exhaust velocity
- o Speed ratio v/vjet
- o Fan inlet airflow

7.2 Effect of Nacelle Tilt Rate on Aircraft Deceleration

Engine tilt rate requirements for deceleration have been examined. The tilt rates encountered flying a constant flight path angle approach to a vertical landing are shown on Figure 7.7. Data for decelerations levels from .05 to .20 g"s are shown. Peak tilt rates in the order of 6 degrees per second are encountered at the high speed end of the approach. The effect of deceleration on the tilt rate is shown as an inset on the figure.

BOEING MODEL 1041 - 135 -2A
VTOL TRIM VTOL TRIM VTOL TRIM VTOL TRIM

CG POSTION	WATERLINE 95.0 FUSE. STATION 255.3		
GROSS WEIGHT		11340 KG 25000 LBS	
AIRPEED		0 M/S 0 KNOTS	
ANGLE OF ATTACK		0 DEG	
TAIL INCIDENCE		0 DEG	
NACELLE TILT ANGLE =		96.2276 DEG	
L/C FAN GROSS THRUST =		39745.3 NEWTONS 8935.55 LBS	
NOSE FAN GROSS THRUST =		33313.4 NEWTONS 7489.53 LBS	
SYSTEM SHAFT POWER =		9500.2 KILOWATTS 12734.9 HORSEPOWER	
AVE. ENGINE SPEED		13475.3 RPM 14155.1 RPM	3 ENG.OPERATION 2 ENG. OPERATION
FAN BLADE ANGLE	NOSE FAN L/C FAN	-11.1789 DEG -9.15661 DEG	
FAN EXHAUST VELOCITY	NOSE	133.132 M/S 436.784 F/S	
	L/C FAN	141.856 M/S 465.866 F/S	
V/VJET	NOSE L/C FAN	0 0	
FAN INLET AIRFLOW	NOSE	251.225 KG/S 552.133 LB/S	
	L/C FAN	280.149 KG/S 617.613 LB/S	

FIGURE 7.2

BOEING MODEL 1041 - 135 -2A
VTOL TRIM VTOL TRIM VTOL TRIM VTOL TRIM

CG POSTION	WATERLINE	95.0
	FUSE. STATION	255.3
GROSS WEIGHT		11340 KG 25000 LBS
AIRPEED		25.72 M/S 50 KNOTS
ANGLE OF ATTACK		7 DEG
TAIL INCIDENCE		0 DEG
NACELLE TILT ANGLE =		69.4998 DEG
L/C FAN GROSS THRUST =		39572.4 NEWTONS 8896.68 LBS
NOSE FAN GROSS THRUST =		25565.7 NEWTONS 5747.68 LBS
SYSTEM SHAFT POWER =		8718.42 KILOWATTS 11686.9 HORSEPOWER
AVE. ENGINE SPEED		13407.7 RPM 3 ENG.OPERATION 13923.8 RPM 2 ENG. OPERATION
FAN BLADE ANGLE	NOSE FAN	-12.9347 DEG
	L/C FAN	-9.22642 DEG
FAN EXHAUST VELOCITY	NOSE	118.356 M/S 388.307 F/S
	L/C FAN	141.639 M/S 465.153 F/S
V/VJET	NOSE	.217483
	L/C FAN	.181553
FAN INLET AIRFLOW	NOSE	216.867 KG/S 476.621 LB/S
	L/C FAN	279.358 KG/S 615.869 LB/S

FIGURE 7.3

BOEING MODEL 1041 - 135 -2A

VTOL TRIM	VTOL TRIM	VTOL TRIM VTOL TRIM
CG POSTION	WATERLINE	95.0
	FUSE. STATION	255.3
GROSS WEIGHT		11340 KG 25000 LBS
AIRPEED		46.296 M/S 90 KNOTS
ANGLE OF ATTACK		9 DEG
TAIL INCIDENCE		0 DEG
NACELLE TILT ANGLE =		46.7387 DEG
L/C FAN GROSS THRUST =		33851.5 NEWTONS 7610.51 LBS
NOSE FAN GROSS THRUST =		15732 NEWTONS 3536.87 LBS
SYSTEM SHAFT POWER =		6789.5 KILOWATTS 9101.21 HORSEPOWER
AVE. ENGINE SPEED		13224 RPM 3 ENG.OPERATION 13538.8 RPM 2 ENG. OPERATION
FAN BLADE ANGLE	NOSE FAN	-18.2259 DEG
	L/C FAN	-11.0472 DEG
FAN EXHAUST VELOCITY	NOSE	92.8811 M/S 304.728 F/S
	L/C FAN	133.833 M/S 439.518 F/S
V/VJET	NOSE	.498839
	L/C FAN	.345856
FAN INLET AIRFLOW	NOSE	170.052 KG/S 373.734 LB/S
	L/C FAN	252.91 KG/S 557.561 LB/S

FIGURE 7.4

BOEING MODEL 1041 - 135 -2A
VTOL TRIM VTOL TRIM VTOL TRIM VTOL TRIM

CG POSTION	WATEPLINE	95.0
	FUSE. STATION	255.3
GROSS WEIGHT		11340 KG 25000 LBS
AIRPEED		61.728 M/S 120 KNOTS
ANGLE OF ATTACK		10 DEG
TAIL INCIDENCE		0 DEG
NACELLE TILT ANGLE =		14.3318 DEG
L/C FAN GROSS THRUST =		28031.5 NEWTONS 6302.06 LBS
NOSE FAN GROSS THRUST =		8304.9 NEWTONS 1867.11 LBS
SYSTEM SHAFT POWER =		5058.82 KILOWATTS 6781.25 HORSEPOWER
AVE. ENGINE SPEED		12960.1 RPM 3 ENG.OPERATION 13307.3 RPM 2 ENG. OPERATION
FAN BLADE ANGLE	NOSE FAN	-29.4551 DEG
	L/C FAN	-12.3376 DEG
FAN EXHAUST VELOCITY	NOSE	71.9088 M/S 235.921 F/S
	L/C FAN	123.529 M/S 405.677 F/S
V/VJET	NOSE	.8591
	L/C FAN	.49961
FAN INLET AIRFLOW	NOSE	115.952 KG/S 254.834 LB/S
	L/C FAN	226.898 KG/S 500.217 LB/S

FIGURE 7.5

BOEING MODEL 1041 - 135 -2A
VTOL TRIM VTOL TRIM VTOL TRIM VTOL TRIM

CG POSTION WATERLINE 95.0
FUSE. STATION 255.3

GROSS WEIGHT 11340 KG
25000 LBS

AIRSPEED 102.88 M/S
200 KNOTS

ANGLE OF ATTACK 6 DEG

TAIL INCIDENCE -4 DEG

NACELLE TILT ANGLE = 0 DEG

L/C FAN GROSS THRUST = 39104.5 NEWTONS
8791.48 LBS

NOSE FAN GROSS THRUST = 0 NEWTONS
0 LBS

SYSTEM SHAFT POWER = 6599.68 KILOWATTS
8847.02 HORSEPOWER

AVE. ENGINE SPEED 13201.6 RPM 3 ENG.OPERATION
13511.7 RPM 2 ENG. OPERATION

FAN BLADE ANGLE NOSE FAN -56.5061 DEG
L/C FAN -9.41048 DEG

FAN EXHAUST VELOCITY NOSE 0 M/S
0 F/S

L/C FAN 141.049 M/S
462.214 F/S

V/VJET NOSE 0
L/C FAN .729253

FAN INLET AIRFLOW NOSE 6.02267 KG/S
13.2364 LB/S

L/C FAN 277.21 KG/S
611.134 LB/S

FIGURE 7.6

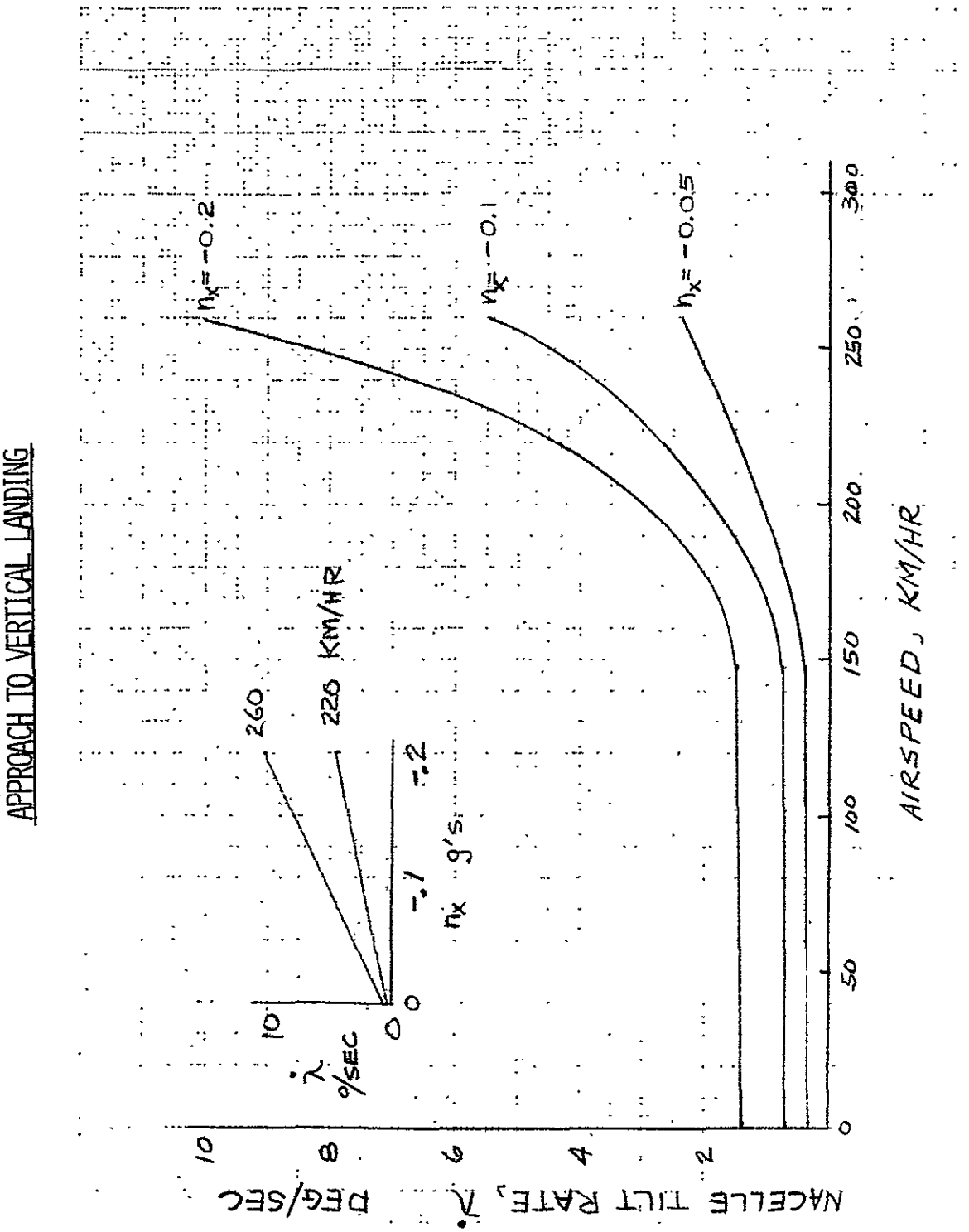
APPROACH TO VERTICAL LANDING
NACELLE TILT RATE, $\dot{\lambda}$, DEG/SEC
AIRSPEED, KM/HR
$n_x = -0.2$
$n_x = -0.1$
$n_x = -0.05$
260
220 KM/HR
$\dot{\lambda}$ °/SEC
n_x g's
0
-.1
-.2
10
0
2
4
6
8
10
50
100
150
200
250
300

FIGURE 7.7